This is the peer reviewed version of the following article: Mohammadzadehmoghadam, S. and Dong, Y. and Davies, I. 2015. Recent Progress in Electrospun Nanofibres: Reinforcement Effect and Mechanical Performance. Journal of Polymer Science, Part B : Polymer Physics. 53 (16): pp. 1171–1212, which has been published in final form at http://doi.org/10.1002/polb.23762. This article may be used for non-commercial purposes in accordance with Wiley Terms and Conditions for Self-Archiving at http://olabout.wiley.com/WileyCDA/Section/id-820227.html#terms

Recent Progress in Electrospun Nanofibres: Reinforcement Effect and Mechanical Performance

Soheila Mohammadzadehmoghadam, Yu Dong, Ian Jeffery Davies

Department of Mechanical Engineering, Curtin University, GPO Box U1987, Perth, WA 6845, Australia

Correspondence to: Y. Dong (Email: Y.Dong@curtin.edu.au)

ABSTRACT

Composite materials are becoming increasingly important as structural materials for aeronautical and space engineering, naval, automotive and civil engineering, sporting goods and other consumer products. Fibre-based reinforcement represents one of the most effective manufacturing strategies for enhancing the mechanical strength and other properties of composite materials. Electrospinning has gained widespread interest in the last two decades due to its ability to fabricate continuous ultrafine nanofibres with unique characteristics. The impact of electrospinning on fibre synthesis and processing, characterisation and applications in drug delivery, nanofiltration, tissue scaffolding and electronics has been extensively studied in the past. In this paper, the authors have focused on a comprehensive review of the mechanical performance and properties of electrospun nanofibres as potential reinforcements as well as their advanced nanocomposites.

KEYWORDS: electrospinning; nanofibre; nanocomposite; reinforcement; mechanical property

Reference: S. Mohammadzadehmoghadam, Y. Dong and I. J. Davies, "Recent progress in electrospun nanofibres: Reinforcement effect and mechanical performance", *J. Polym. Sci. Part B: Polym. Phys. (ISSN 0887-6266) in press (accepted May 15th 2015)*.

TABLE OF CONTENTS

INTRODUCTION

The lack of strength and stiffness for structural application involving plastics entails the necessity of reinforcing elements with the industrial manufacture of fibre-reinforced polymers (FRPs). This was dated back to 1935 when Owens Corning introduced the first glass fibre.[1] In the 1970s, composite industries began to mature due to the development of better plastic resins and improved reinforcing fibres with composites to optimise various material properties such as mechanical (mainly strength), chemical and/or physical properties.

Due to their remarkable material properties, particularly their high stiffness and strength combined with low density, fibre reinforced composites are very suitable for high-performance components. Since the early 1960s, there has been an increasing demand for stiffer and stronger but light-weight in aeronautics, energy, civil engineering and various structural applications. There exists different textile technologies available that are capable to produce and assemble complex textile structures for this purpose. Novel technologies are necessary to reduce time and cost-consuming processing steps and to increase the structural performance of FRP composites.

Emerging electrospinning technology for the production of nanofibres with specific characteristics has opened a new domain for material selection in advanced composites that could fulfill this demand. The pioneering work in electrospinning has been covered significantly to produce ultrafine continuous nanofibres.[2-5] This innovation, originating from the textile industry, can be transferred to the production of nanofibre reinforced composites. Electrospinning is a simple, low-cost material process that has a unique ability to produce nanofibres of different materials in various fibre assemblies. Since electrospun nanofibres demonstrate higher surface area, higher aspect ratio and better mechanical properties as opposed to conventional microfibres, they could represent a new generation of reinforcement for the fabrication of well-tailored unique nanocomposites.

ELECTROSPINNING PROCESS

The origin of electrospinning can be traced back to 1902 when Morton[6] and Cooley[7] patented methods to disperse fluids with the help of electrostatic forces. In 1934, Formhals[8] patented a method for the fabrication of polymer filaments by electrospinning, which was later improved by Larrondo and Manley[9] in 1981 by spinning polymer melts. These methods were not well recognised until early 1990s at which point they were only known as electrostatic spinning.[10] The method was not well recogonised until early 1990s. However, since then over a hundred synthetic and natural polymers have been electrospun.[11]

The basic criterion for a polymer solution or melt to be electrospinnable is its ability to carry an electric charge and sufficient viscosity to be stretched without breaking up into droplets.[12] There are essentially three components to fulfill the process, namely a high voltage supplier, a capillary tube with a needle of small diameter, and a grounded collecting screen.[11,13] The first stage of processing is polymer melt or solution being introduced into the capillary tube. However, in some cases the polymer may emit harmful odors due to the use of solvents. Thus electrospinning process is normally conducted in a chamber with sufficient ventilation. With an applied high voltage typically in range of 1-30 kV, the pendant drop of polymer solution becomes highly electrified with an electric charge induced on the liquid surface, resulting in the deformation of liquid drops into a conical object, known as Taylor cone. When the electric voltage reaches a critical value, the electostatic force overcomes the surface tension of droplets so that a charged jet of solution is ejected from the tip of the Taylor cone. As this jet travels, the solvent evaporates or solidifies in typically less than a tenth of a second, and a web of small fibres are finally collected.[14,15] During this process, the jet experiences three types of instabilities, namely Rayleigh instability, bending instability and whipping instability, which are beyond the scope of current review. More details about these instabilities can be found elsewhere.[11,16,17] A typical set up for electrospinning is shown in Figure 1.

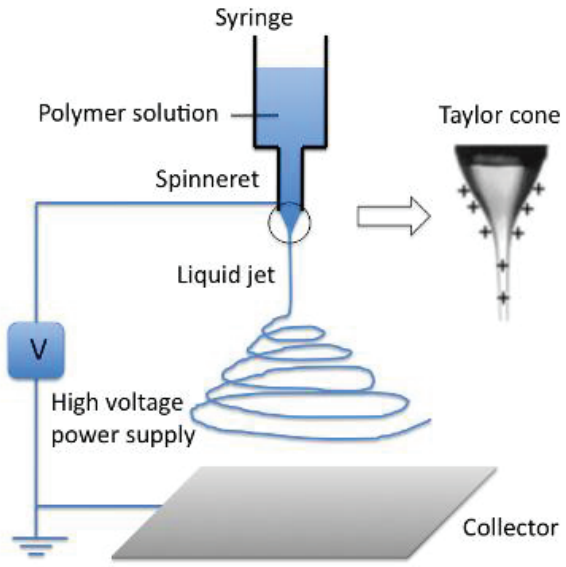

FIGURE 1 Schematic of a basic electrospinning apparatus. Reproduced from Ref. 18, with permission from InTech.

Several other methods exists for fabricating nanofibres including self assembly[19], phase separation[20], melt-blowing[21] and template[22]. Nevertheless, electrospinning has proven to be the most promising emerging technique for manufacturing continuous ultrafine nanofibres. The popularity of electrospinning can be ascribed to its simple, versatile and single-step process to produce well tailored fibres from the microscaled to nanoscaled level based on a variety of precursors such as synthetic and natural polymers, polymer blends, composites with metal or ceramic particles, nanocomposites and ceramics.[11,23,24] Electrospun nanofibres are formed without any further treatment except for ceramics and metallic nanofibres that require post spinning treatment.[25] Electrospun nanofibres exhibit unique characteristics like extraordinarily high specific surface area (typically 1-100 m^2/g) , high porosity (typically 90%), light weight, tunable pore size, flexibility in surface functionalities, relatively high mechanical strength, high permeability, high aspect ratio up to 1000 together with a length up to several centimeters.[11,16,26] Unlike many nanostructures produced in a bottom-up way, electrospinning offers a top-down process, resulting in cost effectiveness and easy processibility.[27] The synthesis of composite nanofibres is another merit of electrospinning and one of the biggest breakthroughs in this field in that small insoluble particles can be added to polymer solutions or encapsulated in dry nanofibres.[23,28]

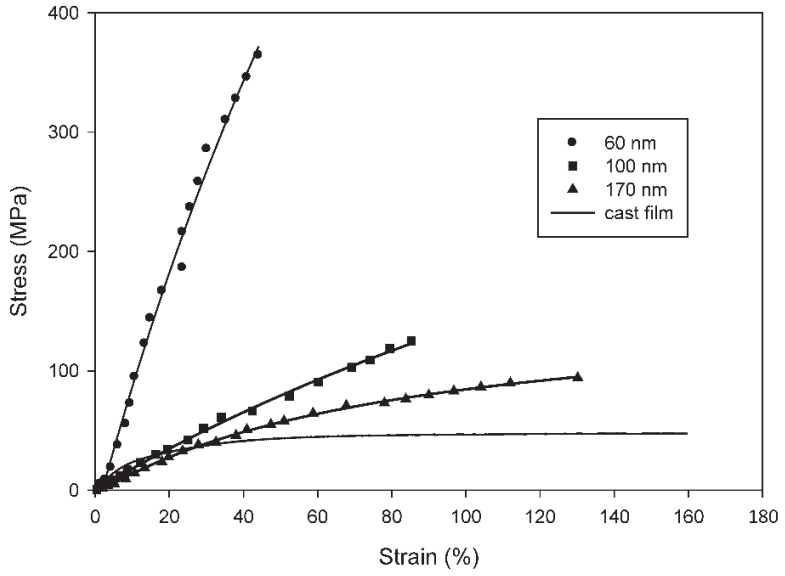

FIGURE 2 Stress–Strain curves of nylon 6 nanofibres with different diameters and bulk forms. Reproduced from Ref. 29, with permission from Elsevier.

Generally speaking, mechanical properties of electrospun nanofibres appear to be moderately high as compared to their bulk material counterparts due to less material defects and higher molecular orientation (Figure 2).[29] In the spinning process, electrospun nanofibres undergo a huge elongation

(draw ratio up to 10^4) and drawing with a strain rate of 10^5 s^{-1}. [17,30] The large shear force and high elongation strain may result in highly aligned molecular chains along the fibre axis. However, during and after the solvent evaporation, the chains are relaxed with the moderate molecular orientation in the fibres.[16,27,31] Moreover, electrospun nanofibres are found to be birefringent, which is indicative of molecular alignment.[26]

Morphology, density and diameter of electrospun nanofibres depend on different parameters, which are classified in three groups[11,14,24] as follows:

- Solution parameters: solution viscosity, solution concentration, molecular weight, surface tension, electrical conductivity, dipole moment and dielectric strength
- Processing parameters: feed (flow) rate, electric field strength, tip-to-collector distance, needle (tip) shape, collector composition and geometry
- Ambient parameters such as temperature, humidity and air flow.

The proper manipulation of these parameters results in desirable morphology and fibre diameter.[10] Accordingly, the effects of these parameters on electrospun nanofibres have been widely investigated to achieve improvements in fibre quality, structures and properties.[11,14,24,28,32]

In order to expand the resulting nanofibrous structure, orientation and its mass production ratio, significant efforts have been made to modify the electrospinning apparatus, particularly its syringe and collector. In general, as-spun fibres are deposited randomly on the surface of a flat collector, leading to randomly oriented nonwoven structures.[15] To obtain well-aligned fibres, collectors have been modified into different types such as rotating drum collector, rotating disk collector, frame collector, and auxiliary electrode/electrical field.[10,11,15,16,33]

There are usually two standard set-ups for electrospinning, namely vertical and horizontal configurations based on the directions of jet ejection. Electrospun micro and nanofibres are usually monolithic and circular-shaped. Thanks to recent development in this technology, several electrospinning system such as coaxial electrospinning, co-electrospinning, multi-jet electrospinning, emulsion electrospinning and side-by-side electrospinning have been introduced. Consequently, nanofibres with specific structures like core/shell, porous, hollow and side-by-side structures can also be prepared.[10,15,34]

The main disadvantage of electrospinning process is its low productivity (only a few grams of fibre mats per hour).[35] To overcome this issue, multi-spinneret electrospinning has been implemented in which the nanofibre productivity is proportional to the number of installed spinnerets.[36] However, some technical barriers exist in this method like spinneret clogging due to solvent evaporation near the outlets.[37] In 2003, a research group at Technical University of Liberec, Czech Republic patented a new technology for the industrial production of nanofibres, which led to a needleless electrospinning device Nanospider™, under the successful commercialisation of Elmarco Inc.[34,38] The technology was based upon the discovery that it is possible to create Taylor cones, and thus the subsequent material flow can be obtained not only from the tip of a capillary but also from a thin film of polymer solution**.** Nanospider™ used a rotating drum partially submerged in a polymer solution for the production of fibres instead of jets or nozzles.[39] Rotating spinnerets such as cylinders, balls, coils and cones are commonly used in this approach, in which the jets are ejected from the spinneret surfaces. Such a process can be set up based on loading a thin layer of polymer solution by the rotation of spinneret onto the spinneret surface. The rotation and perturbance create conical spikes on the surface of this solution layer. When a high voltage is applied to the spinneret, these spikes tend to concentrate charges and amplify the perturbance and the fluid around the spikes is drawn to these spikes under high electric forces, resulting in Taylor cones. Fine solution jets are then ejected from the tips of these Taylor cones with the sufficient electrical forces.[40-42] Rotary jet-spinning is an alternative technology for high-rate spinning. Instead of using electrostatic force as a driving force to generate fibres, a centrifugal force is employed, which is induced by the high speed rotation of a polymer solution or melt.[43]

Modeling and simulations can give a better understanding for the mechanism of electrospinning jets. Geoffrey Taylor, a pioneer in studying electrospinning initially proposed the theory of formation of Taylor cone.[44] For nozzle-based electrospinning, several theoretical models have been proposed to specifically treat one or two individual stages of the process, consisting of the formation of the Taylor cone, jet initiation, thinning, whipping[44-50], solvent evaporation and drying[51].

In recent years, research interest on electrospinning has shifted from fabrication at the laboratory level to applications. The extremely small diameter of electrospun nanofibres, coupled with the high surface area and interconnected fibrous networks, make them desirable for a wide range of applications.[45] Figure 3 categorises the potential applications of nanofibres.[11,12,15,24,34,52-55]

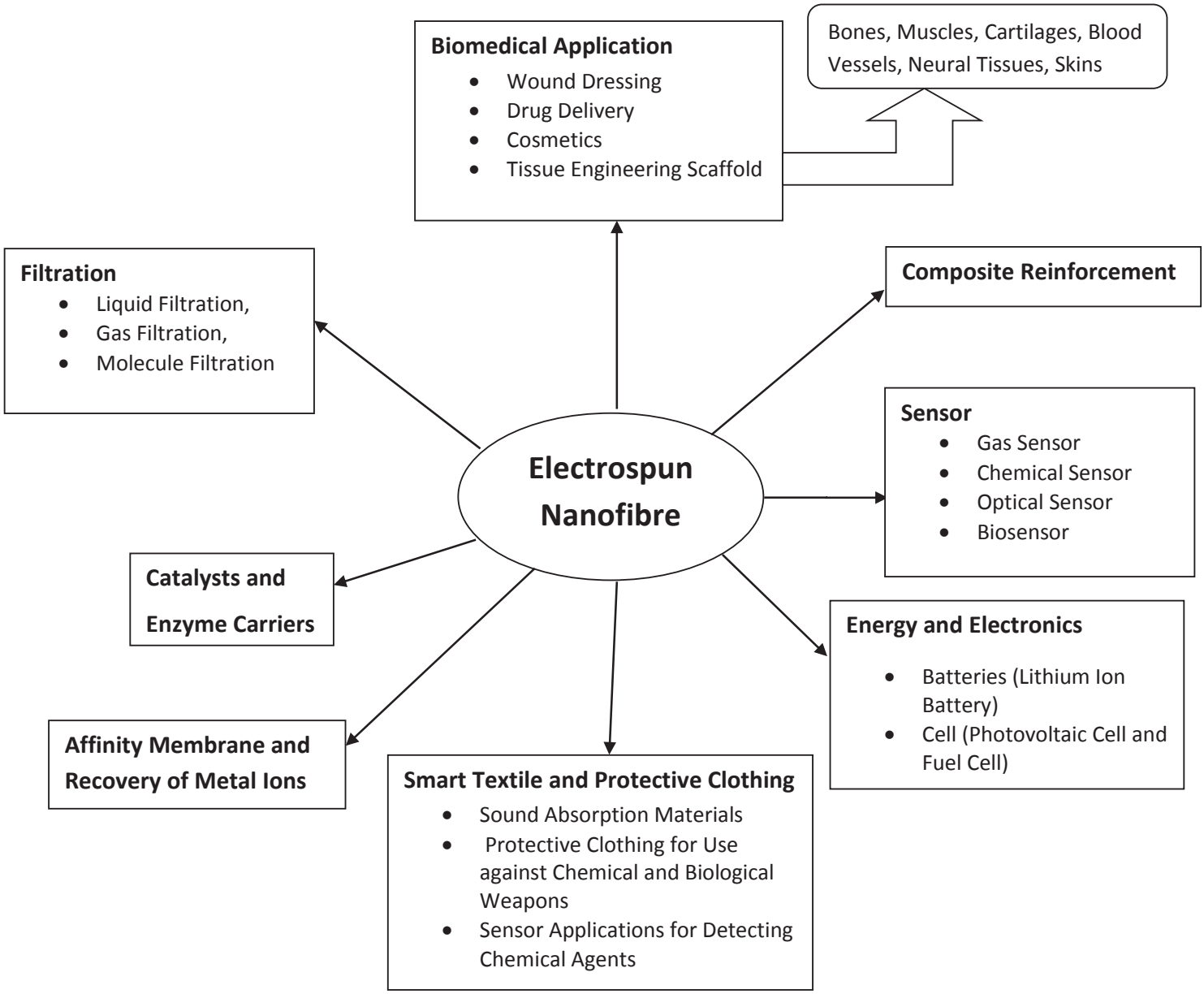

FIGURE 3 Potential applications of electrospun nanofibres

MECHANICAL CHARACTERISATION OF ELECTROSPUN NANOFIBRES

Electrospun nanofibres are integrated in advanced nanomaterials and microstructural components with a wide range of applications such as tissue engineering, filter media, reinforcing elements in composite materials, nanosensors, airborne structures, etc. In most of these applications, they are subjected to

stress and strain from surrounding media during their service life. Hence, they have to possess sufficient mechanical properties in order to perform their targeted functionalities in the above-mentioned applications. Mechanical properties of individual nanofibres dominate their deformations, dynamic and static responses, contacts and friction in nanofibrous networks.[56,57] Therefore, it is critical to measure and understand the properties of single electrospun nanofibres since their mechanical performance is relevant in determining the overall mechanical properties of structural materials incorporated with nanofibres.

Mechanical testing of an individual nanofibrous sample is expected to be the most direct method for examining its mechanical behaviour. However, electrospun fibres are generally too thin and fragile, and thus they are usually collected in a non-woven bundle. Hence, the measurement of mechanical properties of single electrospun fibre encounters great challenges[56-60] to overcome with the availability of following instruments : (1) Manipulation system to precisely isolate, align, and grip single nanofibre on the test frame without slipping or breakage; (2) Suitable mode of observations to ensure that nanofibres are not damaged by characterisation instruments such as scanning electron microscope (SEM) or transmission electron microscope (TEM); (3) Sensitive force transducer that can measure the applied force in the n/μN range, and has a low n/μN resolution and (4) Actuator that can load the nanofibres untill the failure with a high resolution (load unit: μN).

Many researchers have tried to characterise the mechanical property of electrospun nanofibres based on the tensile testing of nanofibrous mats using a universal testing machine.[61,62] This method cannot be deemed appropriate because such a tension test greatly depends on nanofibre diameters, alignment and effects of fibre conglutination and entanglements inside nanofibrous mats.[63] In order to tackle this issue, considerable investigation and techniques for the mechanical characterisation of continuous nanofibres have been performed.[56] Among these, atomic force microscopy (AFM) has rapidly emerged as a general characterisation tool for this purpose since such an instrument incorporates both force and distance sensors, and can be operated in air, liquids and vacuum. It is also coupled with the capability of surface imaging with a nanometer resolution. Since then, a variety of methods have been developed for the mechanical testing of individual polymeric nanofibres. However, a broad range of approaches depend primarily on the AFM for all measurements. These techniques are mainly based on tensile, stretching, bending, nanoindentation, resonance frequency and shear modulation frequency of fibres (Figure 4).[38,56,57,64,65]

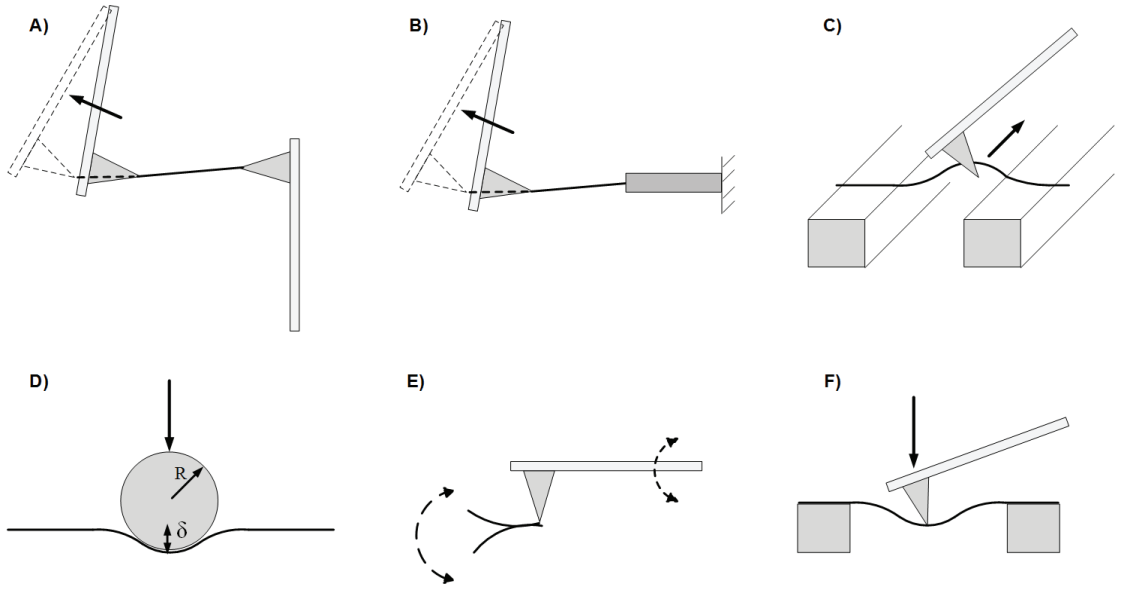

FIGURE 4 Schematic of different techniques for mechanical characterisation of nanofibres: A) and B) tensile testing, C) stretching, D) nanoindentation, E) resonance excitation and F) bending. Reproduced from Ref. 65, with permission from the author S. Makaremi.

Tensile Test Method

Since polymeric nanofibres are mainly used to carry axial loads, as compared to other methods such as bending tests[66], nanoindentation[67] and in situ resonance[68], tensile tests[57,58,69] would appear to be most appropriate for studying mechanical properties of individual electrospun nanofibres. A typical tensile test system contains an actuator, load and elongation measurement tool for specimens. Tensile tests can be conducted by a nano/micro tensile apparatus or an AFM based method to establish data such as tensile strength, yield stress, Young's modulus, strain at break, etc, which involves measuring the applied load and fibre elongation for a known cross-sectional area.[57]

AFM Based Method for Tension Test

As mentioned earlier, AFM has been widely used for the tensile testing of nanofibres[69-71] and was pioneered from mechanical characterisation of carbon nanotubes.[72-74] In this technique, typically one end of the nanofibre is fastened onto a substrate (e.g. a silicon wafer) by the adhesive, which serves as a pulling element. The other end is tethered to the AFM tip that works as a force sensing element. In order to attach the nanofibre to the AFM, a glue (eg. epoxy)[58,69,70] or electron-beam induced deposition (EBID)[71] is typically employed. The microscopic tensile force is exerted through the motion of the AFM tip with the stress-strain behaviour being determined from the length of the nanofibre that is

simultaneously imaged by SEM [58,71] or optical microscope.[69,70] The applied tensile force is further determined from the cantilever's deflection and its spring constant.

In 2004, Tan and Lim[74] proposed an AFM based nanoindentaion system for the tensile testing of microscaled or nanoscaled fibre bundles. In their test, the microfibre was clamped between the nanoindenter tip and the base while the stepper motor of the AFM system was used to stretch the fibre. The load and elongation were calculated from the fibre-transducer series configuration (Figure 5).

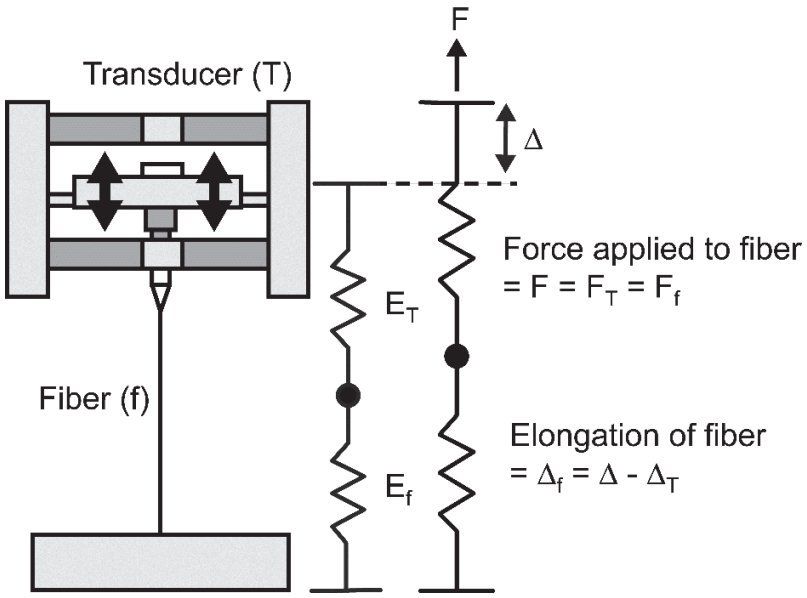

FIGURE 5 Schematic diagram of microfibre-transducer configuration. Reproduced from Ref. 74, with permission from AIP Publishing.

Later, Tan et al.[69] measured the tensile properties of single electrospun polyethylene oxide (PEO) nanofibres in a different manner. A movable optical microscope stage was used as an actuator and an AFM cantilever worked as a load sensor. Resistive strain gauges were integrated into flexible arms of cantilever for higher accuracy. The deflection of cantilever tip resulted in a linear change in resistance that can be easily converted to load by connecting the piezoresistive cantilever tip to a multimeter. Figure 6 illustrates the tensile testing of a PEO nanofibre using a piezoresistive AFM tip. The Young's modulus of such nanofibre with a diameter of 700 nm was found to be approximately 45 MPa.[69]

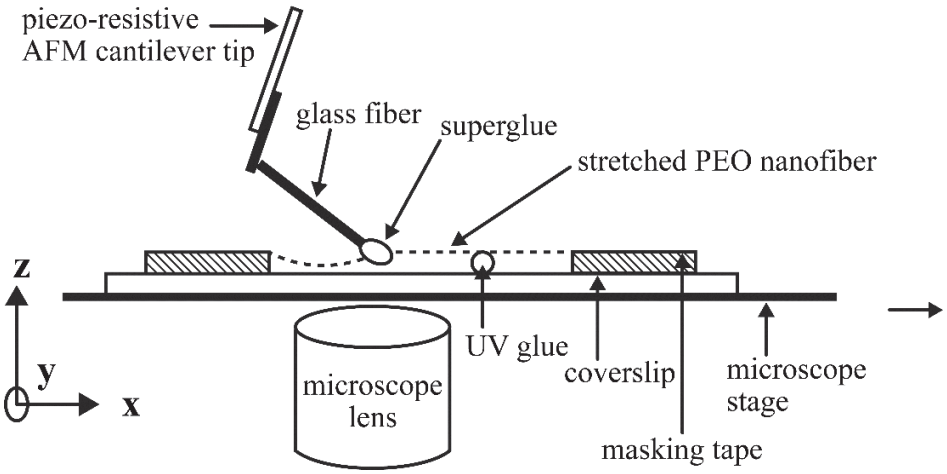

FIGURE 6 Schematic diagram of single PEO nanofibre tensile test using a piezoresistive AFM tip. Reproduced from Ref. 69, with permission from AIP Publishing.

In the other work[70], the tensile properties of electrospun nylon-66 nanofibres with an average diameter of 550 nm were investigated. One end of an electrospun nylon-6,6 nanofibre was mounted to a stainless steel wire and the other end was pulled where it was attached to a cantilever tip (Figure 7). The cantilever deflection and nanofibre elongation were monitored using an optical microscope. The stress-strain curve was then obtained to determine the Young's modulus.

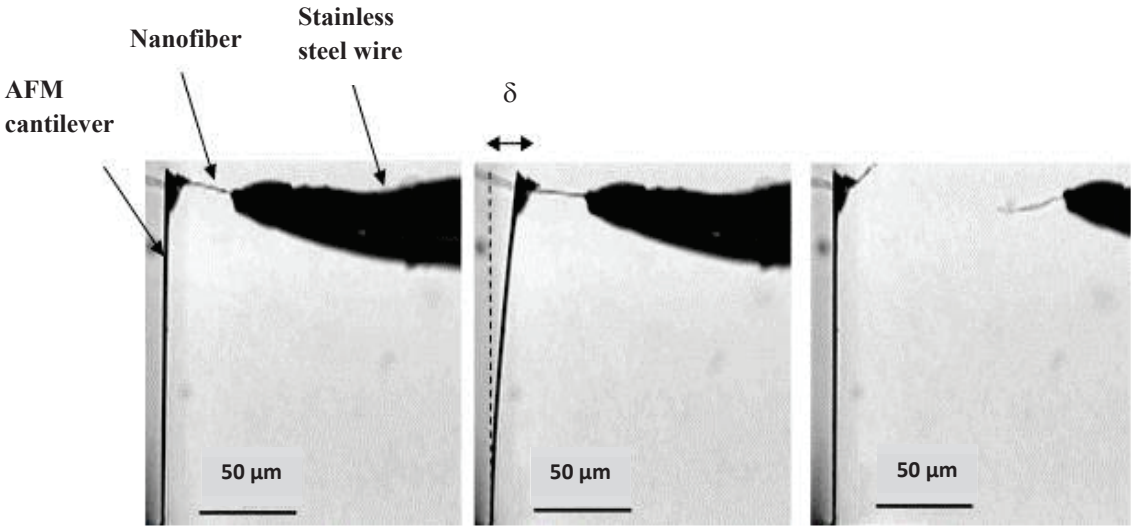

FIGURE 7 Tensile test of single electrospun nylon-6,6 nanofibre up to its fracture. Reproduced from Ref. 70, with permission from Wiley Periodicals, Inc.

Zussman et al.[71] investigated the mechanical behaviour of single electrospun polyacrylonitrile (PAN) derived carbon nanofibres using the same method with the aid of a SEM. To perform the test, an AFM cantilever and tungsten wire were mounted on a nanomanipulator inside the SEM chamber. To bind the nanofibre to the tip of the cantilever, EBID technique was employed. The applied force was obtained from the deflection of AFM observed using SEM. To directly measure the cantilever deflection, Hang et al.[58] used an optical interferometer situated behind the AFM cantilever as an optical sensor. A piezoscanner connected to the AFM head was used for the fine movement of the AFM probe. A piezopositioner underneath the sample stage was in charge of its movement (Figure 8). The whole manipulation was observed by the SEM. The disadvantage of these cantilever-based tensile testing techniques is that they are time-consuming and difficult to manipulate single fibres.

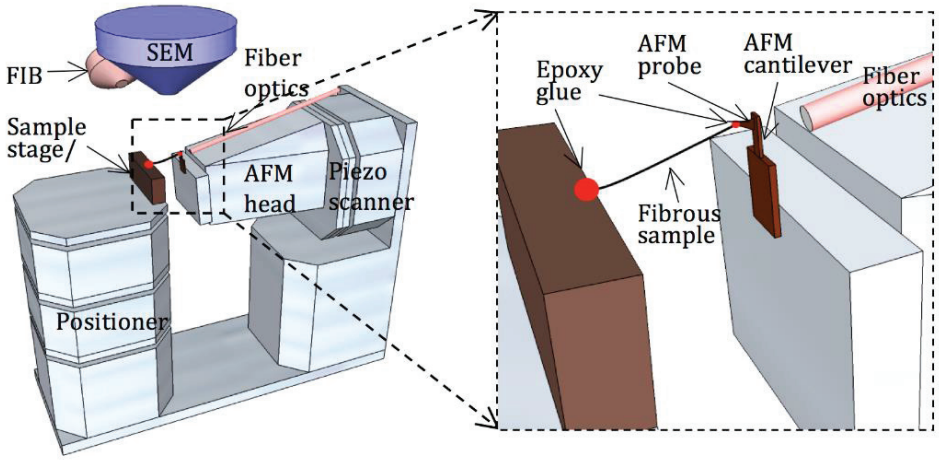

FIGURE 8 In-situ configuration of tensile tester using a nanofibre sample by the combined AFM and SEM mode. Reproduced from Ref. 58, with permission from IOP Publishing Ltd.

Commercial Nanotensile Testing System

Recently, commercialised universal micro/nano tensile testers such as the Nano Bionix® and Nano UTM® by Agilent® and microelectromechanical systems (MEMS)-based micro tensile testers have assisted in accurately measuring the load-displacement relationship for single nanofibres.

The Nano Bionix System can be used to conduct the tensile test of electrospun nanofibres with varied lengths from millimeters to several centimeters. The load test capability of the Nano Bionix system is in the nanonewton (nN) range with 50 nN load resolution, at an extension resolution of 35 nm and a frequency up to 50 Hz.[57] For sample preparation, a single fibre is collected on a cardboard frame and futher mounted on the tester. Subsequently, the frame edges of cardboard are cut prior to the test**.** Tan

et al.[60] used this system to characterise the tensile properties of single electrospun polycaprolactone (PCL) ultrafine fibres with an average diameter of 300 nm. Figure 9 shows a nanotensile tester with a single PCL nanofibre mounted on a frame.

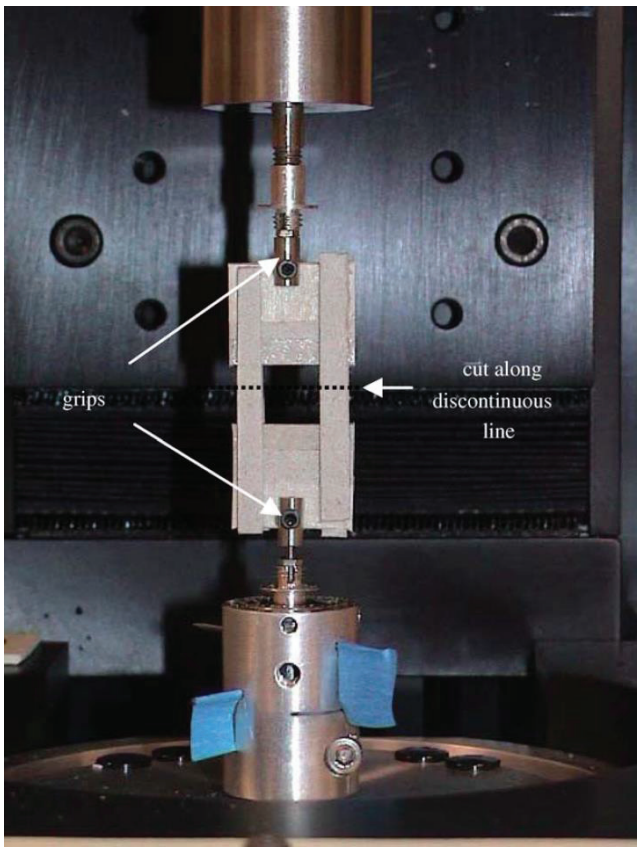

FIGURE 9 Nanotensile tester mounted with a single PCL nanofibre (NanoBionix, MTS, USA). Reproduced from Ref. 60, with permission from Elsevier.

Electrospun poly(L-Lactic acid) (PLLA), polycaprolacton (PCL), poly[(*R*)-3-hydroxybutyrate-*co*-(*R*)-3-hydroxyvalerate] (PHBV), poly(trimethyl hexamethylene terephthalamide) (PA 6(3)T) poly(caprolactone-co-ethylethylene phosphate) (PCLEEP), collagen–chitosan complex and polyacrylonitrile single nanofibres have been tested using such a nanotensile tester with far more accurate results owing to extremely small-load resolution and small-extension resolution as compared to the conventional tensile testing facility.[60,75-86]

Chen et al.[87] used a laboratory-made high-resolution micro tensile station, similar to the Nano UTM to characterise the tensile modulus and tensile strength of electrospun polyimide [poly(p -phenylene

biphenyltetra-carboximide), BPDA/PPA] (PI) nanofibres with a fibre diameter of typically 300 nm. The experimental results showed that PI nanofibres possessed an average ultimate tensile strength of 1.7 GPa, axial tensile modulus of 76 GPa and ultimate strain of ~3%.

In a similar manner, Bazbouz et al.[57] designed a laboratory set-up for tensile test using the configuration of two linear springs in series based on the vibration fundamental principle. The nanotester set-up consists of a movable head as an actuator that moves by attaching it to a digital syringe pump. Its velocity can be controlled by the pump software and ranging from several nanometers per second to several millimeters per second. A spring acts as a transducer for measuring the tensile load while a cardboard frame works with adhesive for holding the nanofibre vertically. Additionally, a fixed head clamp was used for holding the nanofibre frame, and a ruler was employed for reading the spring displacement and two grips for holding the frame-spring and movable head in series. Figure 10 show a schematic set-up of the lab designed tensile tester.

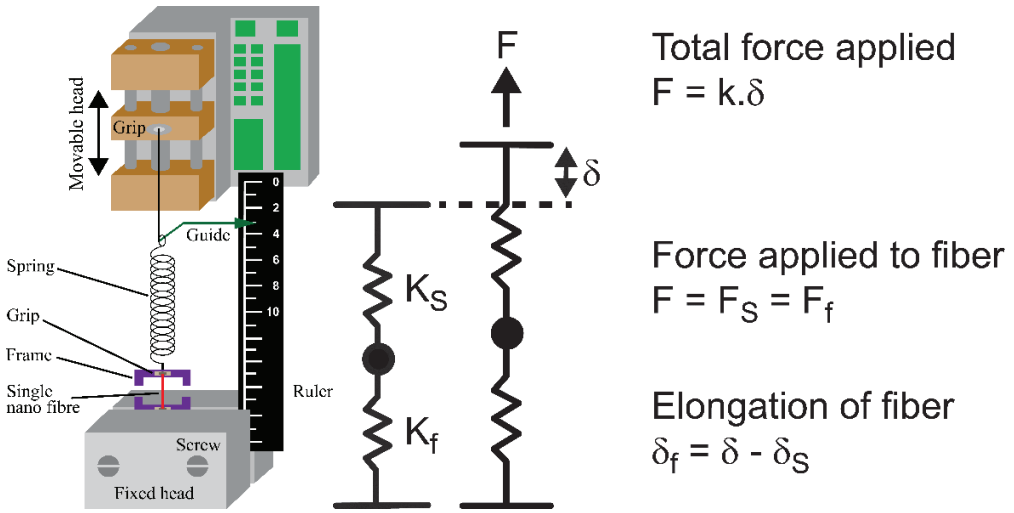

FIGURE 10 (a) schematic diagram of laboratory designed tensile tester and (b) spring fibre-transducer series configuration**.** Reproduced from Ref. 57, with permission from Wiley Periodicals, Inc.

Microelectromechanical Systems (MEMS)

Microelectromechanical system MEMS devices with an on-chip leaf-spring load cell and actuators with grips for sample mounting have been developed to measure the load-displacement relationship of single nanofibres.[58,88-91] To position the nanofibre between gripping elements, high manipulation accuracy is required under the observation by using an optical microscope[88,89] or SEM[91,92]. MEMS force sensor

appears to be accurate, but their use requires in-situ SEM[92] or the sensor needs to glued to the fibre after being mounted onto the MEMS testing platform.[88,90]

Naraghi et al.[89] used a MEMS based device with an on-chip leaf-spring load cell and grips for samples by a piezoelectric actuator at three nominal strain rates of 2.5 $\times 10^{-4}$, 2.5×10^{-3} and 2.5×10^{-2} s^{-1} under an optical microscope at ×500 magnification. The mechanical deformation was investigated for electrospun PAN nanofibres with diameters of 300–600 nm and a length of 12 µm. Nanofibres were mounted onto the grips by a micromanipulator and attached by epoxy adhesive (Figure11). The deflection of the load cell and displacement of fibre grips were measured synchronously from optical images.

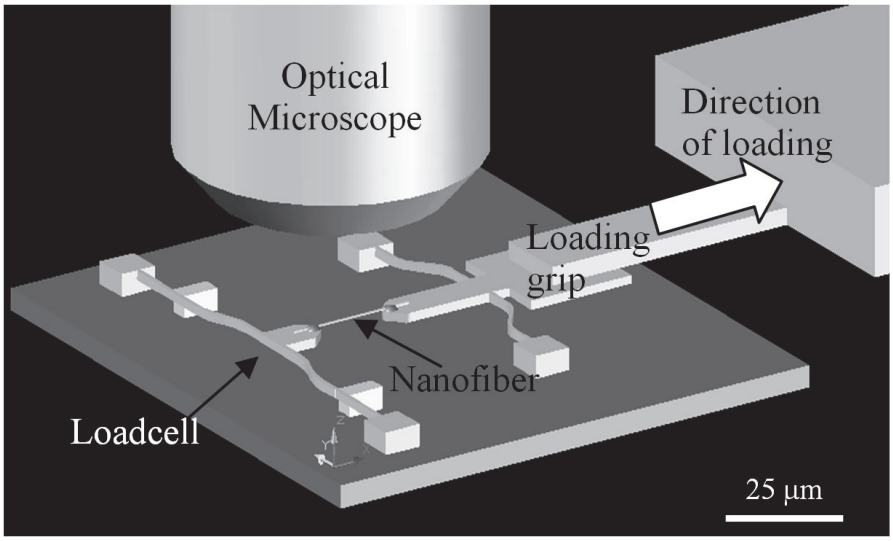

FIGURE 11 Microtensile testing platform for mechanical characterisation of single electrospun nanofibre. Reproduced from Ref. 89, with permission from AIP Publishing.

Samuel et al.[92] used this method with a piezomotor actuator to test the mechanical properties of pyrolysed poly-furfuryl alcohol (PFA) nanofibres with diameters from 150 to 300 nm. The Young's modulus was observed to be within the range of 1.3–2 GPa and the stress–strain curves for the nanofibres demonstrated a linear relationship with a strictly linear elastic range up to 4% strain. Moreover, the evidence of nano-necking and local yielding was found in the nanoscaled specimens, which have not been observed yet in their microscaled counterparts.

Naraghi et al.[88] investigated the mechanical behaviour of single electrospun PAN nanofibre using a MEMS platform with an on-chip load cell. The load cell was operated under an optical microscope with an external piezoelectric transducer. In order to increase the accuracy of force measurement, the stiffness of load cell was tuned using a focused ion beam (FIB). An elastic modulus of 7.6±1.5 GPa was

reported for electrospun PAN nanofibres with diameters in range of 300-600 nm at a strain rate of 0.025 s^{-1}. PAN nanofibres demonstrated perfect elastic-plastic behaviour with the ductility exceeding 220%. The elastic modulus and yield strength of single electrospun PAN nanofibre using a MEMS-based nanomechanical testing platform have been reported by other groups as well.[89,90,93-95]

The mechanical properties of electrospun PLLA nanofibres with diameters in range of 150 nm to 2 µm were determined based on a MEMS.[91] To obtain the stress–strain curves for nanofibres, video recording was used with experiments carried out in a SEM. The MEMS system consists of two movable components, namely pulling and bending cantilevers. The pulling cantilever comprises a pulling ring and a sample platform, which is guided by two rails attached to the silicon chip in order to achieve a linear motion. The bending cantilever has a sample platform and a silicon bar connected at both ends to the silicon chip that was used as a flat spring. The tested fibre is attached to two sample platforms such that pulling and bending cantilevers are joined by the fibre (Figure 12). When the pulling cantilever is moved, the flat spring applies a force on the fibre. With the assumption of linear elastic behaviour for the silicon bar, the force can be calculated from the displacement of the flat spring. The strain of the fibre was determined from the difference between the displacements of two sample platforms.

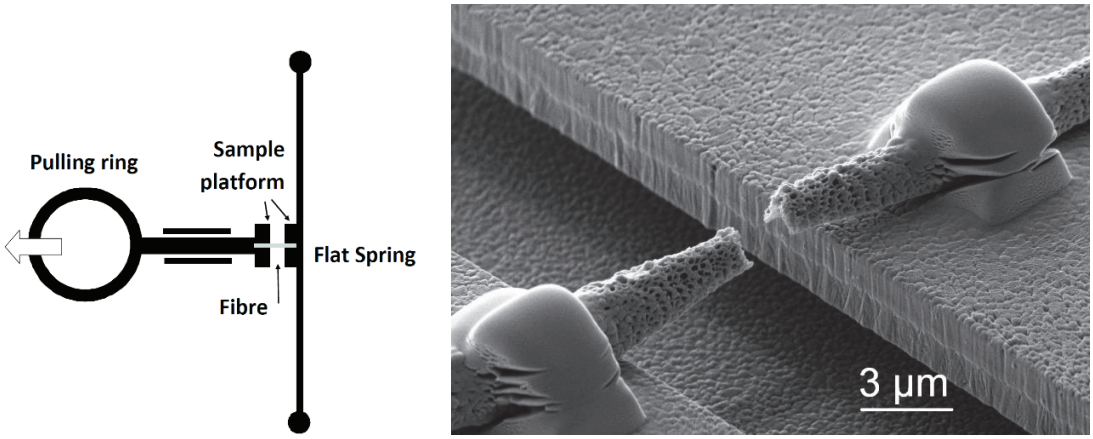

(a) (b)

FIGURE 12 (a) Set-up of MEMS based tensile tester and (b) SEM image of single nanofibre after tensile test. Reproduced from Ref. 91, with permission from Wiley Periodicals, Inc.

Fee et al.[96] fabricated a micro tensile testing platform using a precision screw-type linear actuator and a 1.1 N load cell that were both controlled by a customised LabView® program. They applied fluorescent strain marker on arrays of individual PCL nanofibres to record the fibre strain optically. The true strain

along the length of an electrospun nanofibre and the engineering stress at failure were measured with mean values of 17.89% and 50.14 MPa respectively.

Stretching Method

Guthold et al.[97] combined an AFM/fluorescence microscope to study the mechanical properties of individually electrospun fibrinogen fibres in an aqueous buffer. Fibres with an average diameter of 208 nm were suspended over 12 μm-wide grooves in a striated and transparent substrate. The AFM, situated above the sample, was used to laterally stretch the fibres. To measure the applied force, the fluorescence microscope, situated below the sample, was employed to visualise the stretching process (Figure 13). As for the evaluation of mechanical properties of individually electrospun fibrinogen fibres in dry and ambient conditions, the same method with optical microscope was performed.[98] The results demonstrate that electrospun fibrinogen fibres (diameter in range of 30–200 nm) can be stretched up to 74% elongation before rupturing at a stress of 2.1 GPa. They can also be stretched elastically up to 15% elongation. In a similar way, mechanical properties of single electrospun collagen type I nanofibre with a radius of 160 -783 nm were determined.[99] It has been reported that electrospun collagen undergoes severe strain softening, and the modulus and peak stress of individual electrospun collagen type I fibres are dependent of radius.

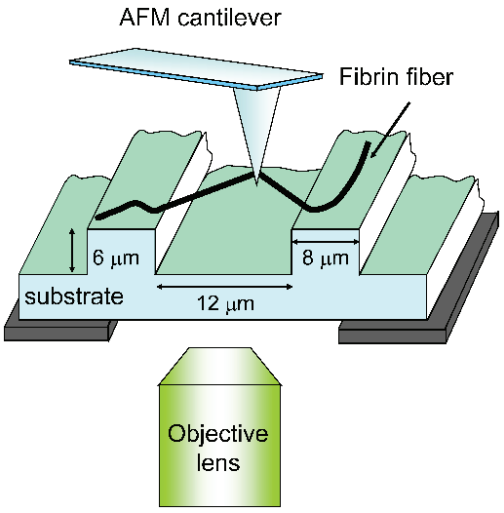

FIGURE 13 Schematic diagram of AFM/optical microscopic set-up. The AFM tip was used to stretch fibres that were suspended over the grooves of a striated substrate. Reproduced from Ref. 97, with permission from Elsevier.

Hwang et al.[29] also used a similar technique via a nanomanipulator and an AFM cantilever in a SEM to stretch a nylon 6 electrospun nanofibre suspended over a trench in the transverse direction. The midpoint of nanofibre was hooked by an AFM cantilever and elongated until the fibre fractured (Figure 14). The applied force was then calculated using the cantilever deflection while the fibre strain was measured by the motion of the cantilever observed by the SEM.

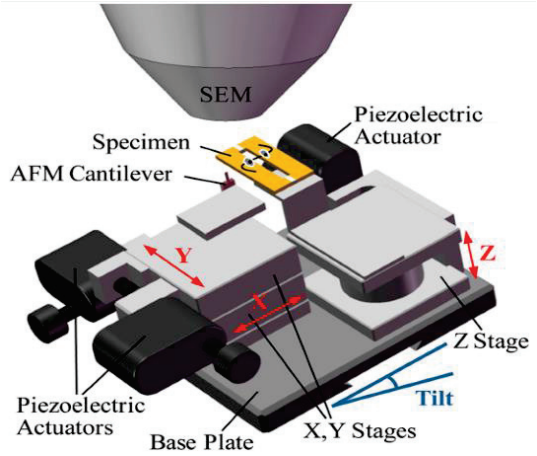

FIGURE 14 3D schematic diagram of the nanomanipulator with the AFM cantilever and nanofibre sample in a SEM. Reproduced from Ref. 29, with permission from Elsevier.

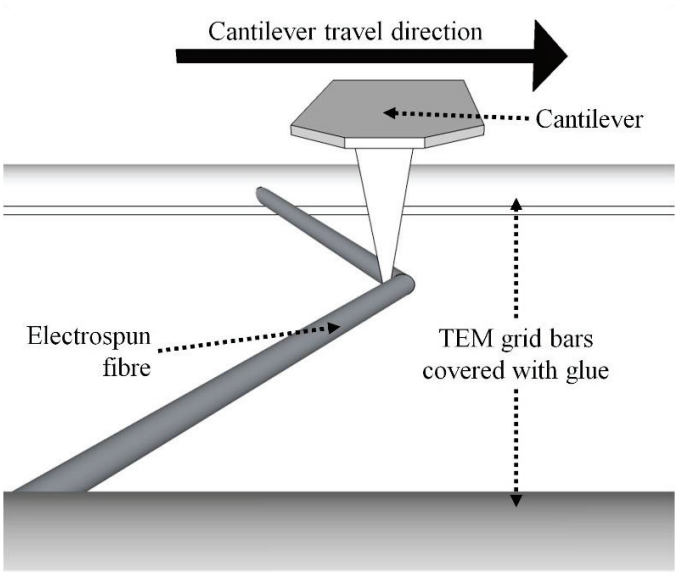

FIGURE 15 An AFM cantilever laterally scanning and dragging an electrospun fibre that is glued at both ends to the bars of a TEM grid. Reproduced from Ref. 100, with permission from Elsevier.

Gestos et al.[100] reported the mechanical characterisation of three different types of electrospun nanofibres, namely glassy, rubbery and gel polymeric nanofibres using a similar technique. The fibres were electrospun onto TEM grids with parallel bars that were previously glued. As a result, the nanofibre was fixed and suspended over the bars. Through the lateral movement of AFM cantilever tip, the suspended nanofibre was streched to high strains (Figure 15). The resulting data were captured using a real time data scanner within the control software.

Bending Test Method

The AFM system paves the way for the mechanical measurement of single electrospun nanofibres by its ability to apply forces in the range of nano and pico-Newton on the surface of nanofibres and measure the cantilever deflection in the Angstrom range.[56,57] Here both two-point and three-point bending tests are reviewed based on the AFM system.

Two-Point Bending Test

Gu et al.[59] performed a two-point bending test on single electrospun PAN nanofibre. Single electrospun nanofibre was attached to the end of an AFM cantilever using epoxy glue and the other end was freely loaded by a substrate edge (Figure. 16).

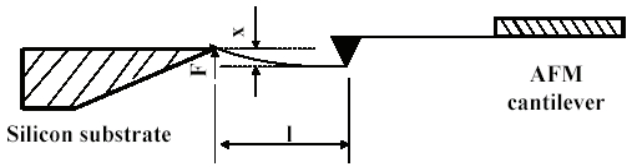

FIGURE 16 Schematic of two-point bending test for single electrospun nanofibre. Reproduced from Ref. 59, with permission from Wiley-VCH.

For recording the displacement of the fibre, an optical microscope was used. The force F can be calculated from the displacement and spring constant of the cantilever. The Young's modulus of the fibre E is calculated from the following:

$$E = \frac{4}{3\pi} \times \frac{F}{x} \times \frac{l^3}{r^4} \quad (1)$$

Where *l* is the fibre length and *r* is the radius of the fibre. *F/x* is equal to the product of the spring constant of cantilever and the slope of fitting line for the force-displacement curve.

Three-Point Bending Test

As for three-point bending test, firstly the single nanofibre is fabricated or deposited over an etched groove (usually in glass, polydimethylsiloxane or silicone)[76,101-103] (Figure 17(a)). The nanofibre segment is clamped at the two ends by the adhesive. A transverse force is then induced by the AFM tip at the center point of the suspended nanofibre length (Figure 17(b)).[38,56,66,101]

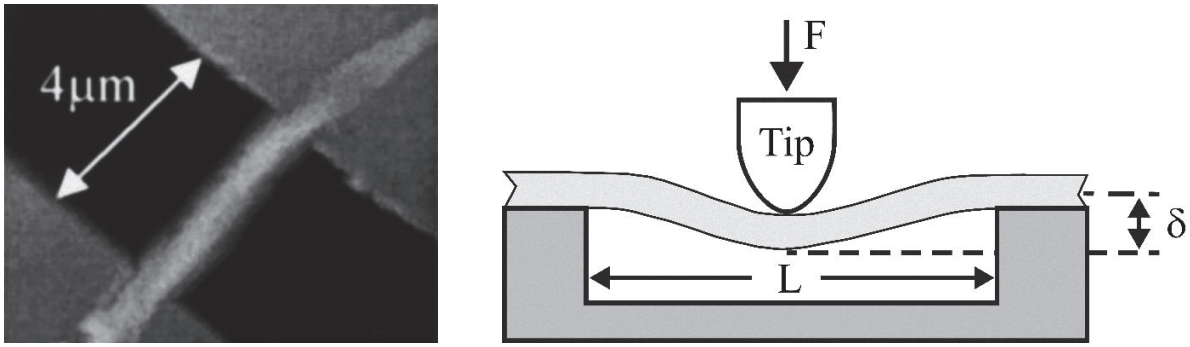

(a) (b)

FIGURE 17 (a) A single electrospun nanofibre suspended over etched grooves of silicon wafer and (b) schematic diagram of a nanofibre with mid-span deflected by an AFM tip. Reproduced from Ref. 101, with permission from AIP Publishing.

The elastic modulus was determined from a classic beam bending theory.[104] The nanofibre is assumed to be a prismatically elastic beam with both ends fixed, but subjected to pure bending (i.e. negligible shear deformation). The relevant equation is given by:

$$E = \frac{FL^3}{192\delta I} \quad (2)$$

Where *P* is the maximum force applied, *L* is the suspended length, *v* is the deflection of the beam at the midspan and *I* is the second moment of area of the beam (where $I = \pi D^4/64$ and D is the beam diameter). The method to obtain v can be found in other studies.[101]

The elastic moduli of electrospun TiO_2 (anatase) and TiO_2/PVP nanocomposite fibres with average diameters of 53 and 109 nm, respectively, were reported using this method.[105] The Young's moduli for TiO_2 and TiO2/PVP nanofibres were 0.9 and 75.6 GPa, respectively. For other electrospun nanofibres and nanocomposites, this technique has been used to investigate their elastic modulus.[66,76,106-119]

Guhados et al.[120] introduced a multi-point bending test based on the fundamental concept of three-point bending. In this bending method, a known force was applied by the cantilever at multiple points

along a suspended fibre while the fibre deflection was measured and recorded for each point (Figure 18 (a)).

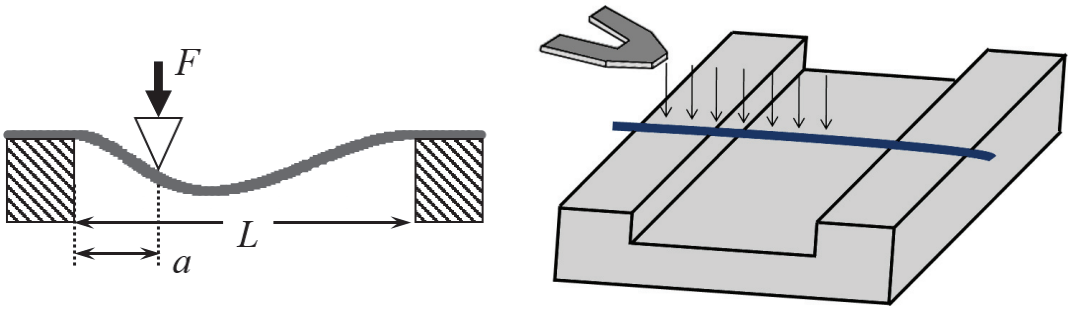

(a) (b)

FIGURE 18 (a) Model for the shape of a fibre clamped to supports a distance L apart under the deformation by a vertical force F applied at the distance *a* from one end of the fibre.[120] (b) Schematic diagram of three-point bending test of single electrospun nanofibre.[121] Reproduced from Refs. 120 and 121 with permission from American Chemical Society and Elsevier, respectively.

To avoid damage to the fibre surface and reduce the amount of indentation during the multi-point bending test, the tip of the AFM cantilever can be removed and the nanofibre was bent by the tipless cantilever.[103,121] Deflection versus piezodisplacement curves were recorded at different positions along the fibre suspended across the channel (Figure 18(b)). The main advantage if this multi-point bending test method is that it eliminates the requirement to detect the exact centre point of the fibre.[120]

Resonance Frequency Method

The mechanical resonance technique is a non-destructive method that applies an electrically or mechanically induced periodic force (approaching the nanofibre's resonance frequency) for the excitation of a nanofibre clamped to the cantilever tip inside a SEM. The resulting frequency responses of the nanofibre is then recorded and the resonance peaks are obtained in order to calculate Young's modulus.

Zussman et al.[71] used the natural resonance vibration method to investigate mechanical properties of single carbon nanofibre. The fibre was attached to the tip of an AFM cantilever using EBID while the cantilever was connected to a piezoelectric bimorph actuator. By applying an alternating electric potential to this piezoactuator, the fibre was driven into mechanical resonance (Figure 19). The modulus-frequency relationship is obtained from the classic linear elasticity.

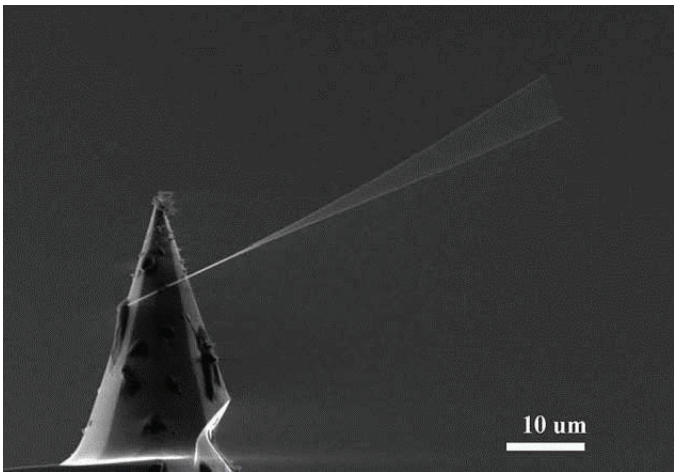

FIGURE 19 A typical example of a nanofibre driven at its fundamental resonance by the piezoelectric actuator. Reproduced from Ref. 71, with permission from Elsevier.

Xu et al.[68] deduced the Young's modulus of individual electrospun TiO_2 nanofibres (diameter of 101 nm) from the analysis of their *in-situ* resonance behaviour in response to an oscillating electric field. A digital function generator was used to supply an AC current to the nanoprobe with resonant vibrations for both the charge and force. When the applied frequency was the same as the natural frequency of the nanofibre, the resonance in the form of mechanical vibration was induced.

Turner et al.[122] extracted the elastic modulus of single electrospun PAN nanofibre dynamically through the natural frequencies of a pair of AFM microcantilevers linked by a nanofibre segment (Figure 20). The theory of this technique is based on the dynamic relationship between the fibre stiffness (spring constant) and the resonance frequencies of cantilever vibration mode.

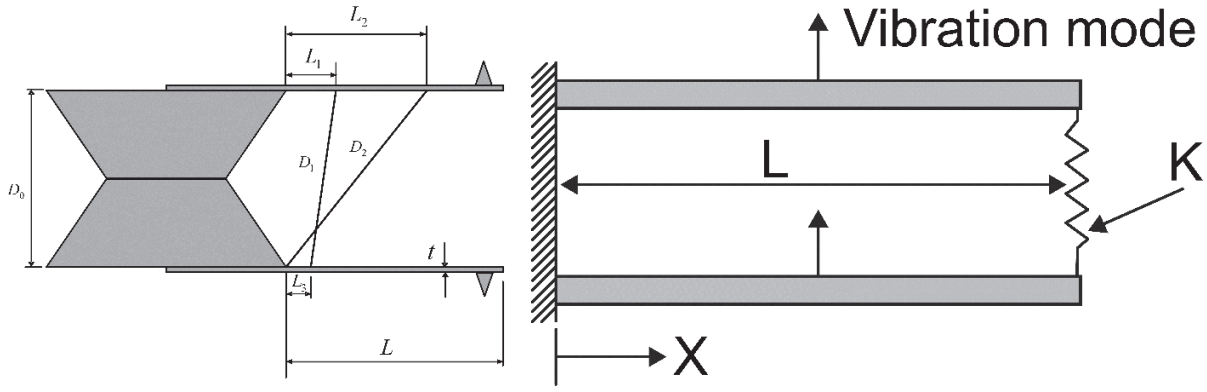

(a) (b)

FIGURE 20 (a) Schematic that shows how the nanofibres are attached and the distance is obtained from the fixed end of the cantilever.[122] (b) Schematic of the theory of conventional beam dynamics, showing

two prismatic beams cantilevered at one end and coupled with a nanofibre of stiffness k at the other end.[57] Reproduced from Refs. 57 and 122, with permission from Wiley Periodicals, Inc. and AIP Publishing.

Liu et al.[123] used an atomic force acoustic microscopy (AFAM) technique based on ultrasonic frequency oscillations to excite an AFM cantilever when the tip was in contact with a sample. Fibres were distributed randomly on a silicon substrate that was then mounted on the ultrasonic transducer. The AFM cantilever was brought into contact with the sample, and the resulting vibrational frequencies in the cantilever were measured with the laser-photodiode system (Figure 21).

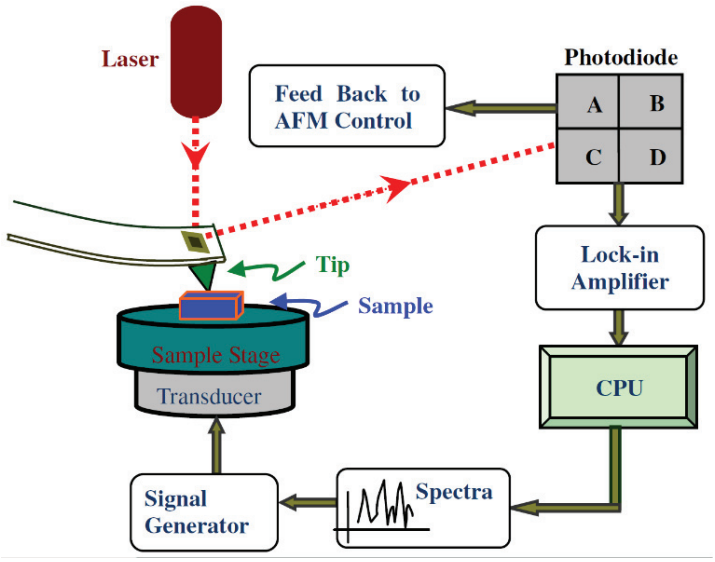

FIGURE 21 Schematic of AFAM setup. Reproduced from Ref. 124, with permission from Elsevier.

The tip-sample contact stiffness was modelled as a linear spring. Using a cantilever beam model, the equations of motion can be solved analytically provided that the amplitudes remain sufficiently small, yielding the contact stiffness as a function of vibrational frequency.

A different method based on a model of the resonant frequency dependent of the bob's free flight was used to measure the elastic modulus of as-spun nylon 6,6.[125] A ball was glued to a nanofibre and suspended from a cantilever beam that was attached to a piezoelectric-actuated base (Figure 22(a)). Such a system can be considered as a string pendulum (Figure 22(b)), experiencing regular oscillation under the elastic force (Figure 22(c)) along with free flight only subjected to gravity under easy track (Figure 22(d)). An optical microscope was employed to record the resonant frequency of such a string pendulum, resulting in the determination of Young's modulus.

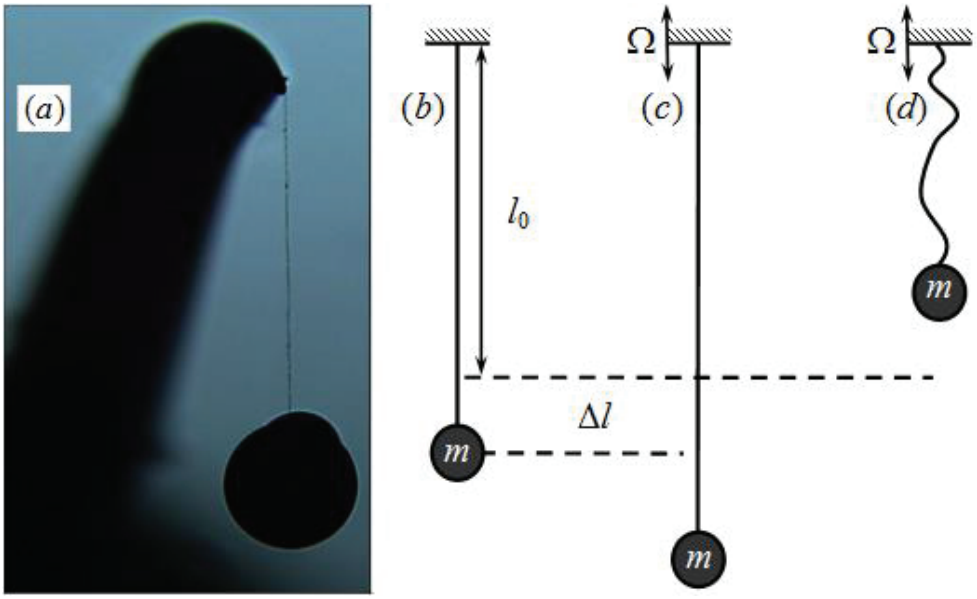

FIGURE 22 A string pendulum: (a) a sideview of a ball attached to a nanofibre and suspended from a cantilever beam, which is connected to the actuated base, (b) the equilibrium state, (c) the downward displacement of the bob flight and (d) the upward displacement of the bob flight. Reproduced from Ref.125, with permission from AIP Publishing.

Nanoindentation Method

Of all the nanomechanical characterisation techniques mentioned, nanoindentation may be the most convenient method to perform since the sample can be simply prepared by depositing a nanofibre on a flat and hard substrate with the sufficient adhesion to the substrate. By using an AFM tip, a normal force is applied to produce a small indentation on the fibre surface (Figure 23). The Young's modulus can then be obtained by probing the localised curvature created on the fibre surface after the indentation.[56]

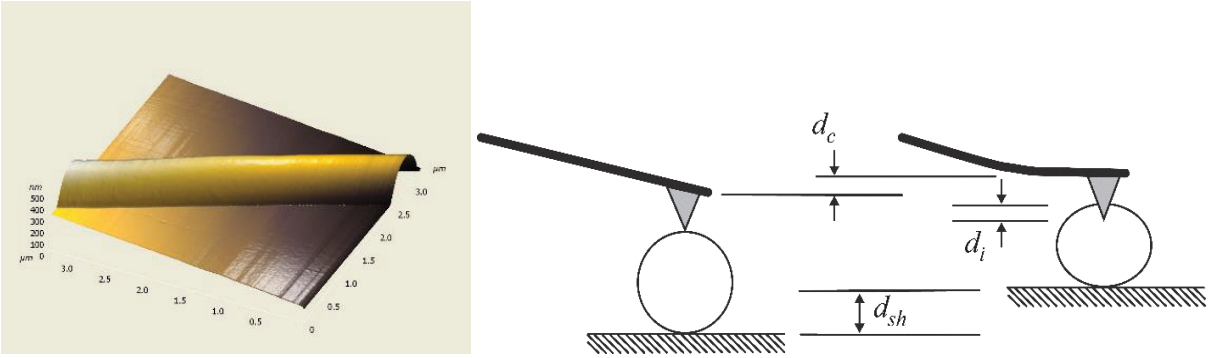

(a) (b)

FIGURE 23 (a) Individual nanofibres on a solid silicon substrate for indentation testing.[114] (b) Schematic diagram explaining the deformation process in the AFM measurement: before deformation (left) and after deformation (right).[67] Reproduced from Refs. 67 and 114 with permission from Elsevier and Wiley Periodicals, Inc., respectively.

Fitting the data with appropriate indentation models[126] leads to the determination of elastic modulus of the nanofibre. Mechanical properties of electrospun nanofibres have also been characterised by employing this technique.[67,114,127-136]

Nanoindentation is an indirect method and involves localised deformation that is used to predict the elastic modulus of the nanofibre based on the applied load and contact radius of the indenter tip.[137] When the sample thickness is very small, the nanoindenter's tip can "feel" the underlying substrate after compressing the sample. Consequently, an overestimated value of the Young's modulus is obtained. Although nanoindentation is one of the easiest nanomechanical characterisation experiments performed on a nanofibre, many factors should be considered for this method with some uncertainties.[56] Furthermore, such local measurements do not provide information concerning the dominant mode of deformation and failure of nanofibres in their expected application under the axial stretching.[88]

Shear Modulation Force Microscopy (SMFM) Method

In this technique, a fibre bundle is suspended across the gap of a grating where the AFM tip induces an additional small oscillation parallel to the sample axis resulting in the deformation. (Figure 24).

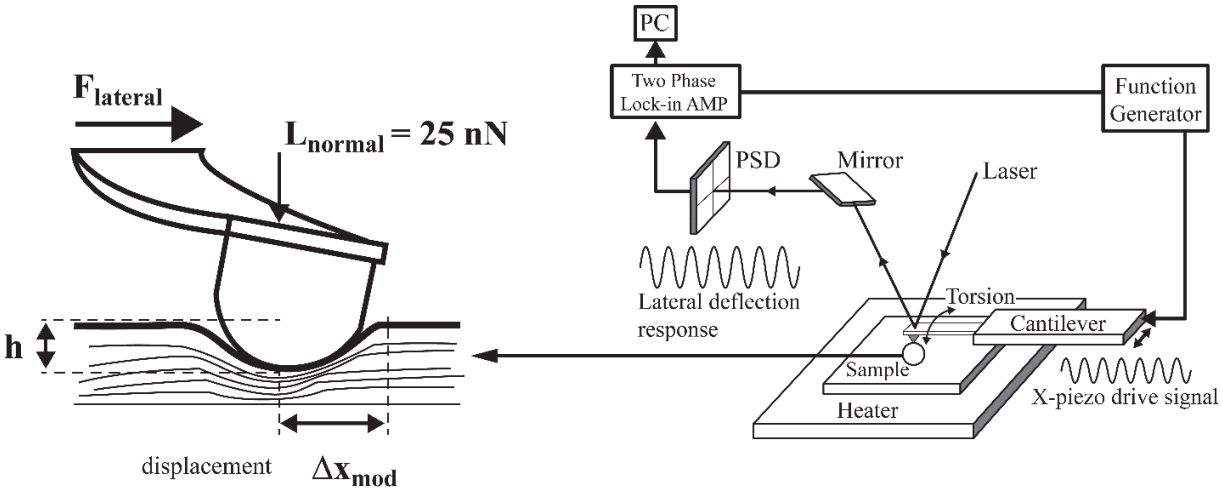

FIGURE 24 Schematic of shear modulation force microscopy. Reproduced from Ref. 31, with permission from the American Chemical Society.

Based on the Hertz model and amplitude of the lateral deflection, the fibre modulus can be calculated from the force-distance curve of the AFM probe using the expression below:[31,138]

$$E = 2(1 + \nu) G \quad (3)$$

Where ν is the Poisson's ratio. E and G are Young's modulus and shear modulus, respectively.[31] This method only provides an estimation of mechanical properties of individual nanofibres with more sensitivity to fibre surface properties.

Other Mechanical Characterisation Techniques

Lin et al.[139] suggested a different method to measure the mechanical properties of nanofibres through their interaction with air streams. The nanofibre was captured directly during electrospinning between two steel rods that functioned as the grips of the tensile testing apparatus. Tension was applied by stretching the nanofibre at a controlled rate (or in steps), moving the upper grip laterally away from the fixed one. The nanofibre was deflected by a laminar air flow along a direction perpendicular to the fibre axis at a measured velocity (Figure 25(a)).

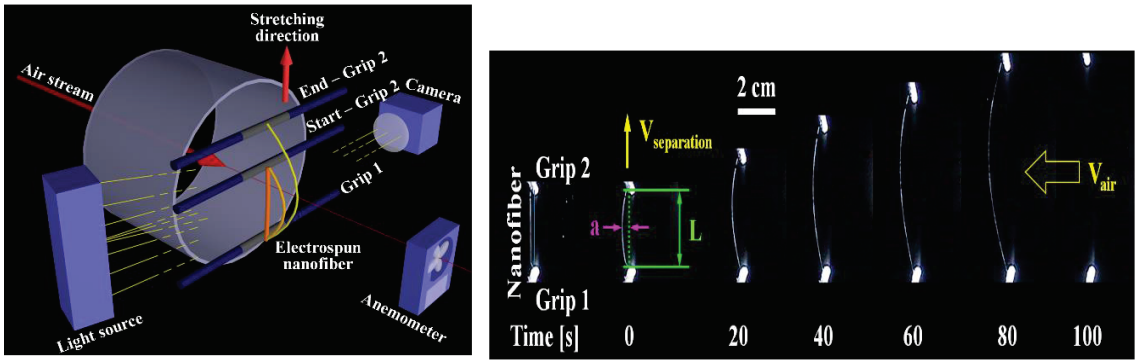

(a) (b)

FIGURE 25 (a) Schematic drawing of the experimental set-up used to perform mechanical tests of air-stream assisted single fibre. (b) Seven successive images of a tensile test on a PEO nanofibre. The grips were separated at a rate of 0.055 cm/s. The air velocity v_{air} = 0.86 m/s, was chosen to produce a small fibre deflection. Reproduced from Ref. 139, with permission from Elsevier.

Images of optically illuminated fibres observed against a dark background were gathered by using a camcorder to view the deflected position and nanofibre shape. The diameter was measured by SEM with the mechanical properties being calculated from the image analysis of captured catenary shapes (Figure 25(b)).

Table 1 shows a summary of mechanical characterisation methods for various types of electrospun nanofibres.

TABLE 1 Mechanical charctarisation of electrospun nanofibre

Test method	Instruments and Techniques	Materials	References
Tensile test	AFM based method	PAN-derived carbon nanofibre	[71]
		Polyethylene oxide (PEO) nanofibre	[69]
		Polyvinyl alcohol (PVA) nanofibre	[58]
		Nylon-6 nanofibre	[58]
		nylon-6,6 nanofibre	[70]
	Commercial nanotensile tester	Poly(L-lactide) acid (PLLA) nanofibre	[75-77]
		Nylon 6 nanofibre	[57]
		Polycaprolactone (PCL)nanofibre	[60,78,80,81,84]
		Polylactic acid (PLA) nanofibre	[79]
		Poly[(R)-3-hydroxybutyrate-co-(R)-3-hydroxyvalerate] (PHBV)	[82]

		nanofibre	
		Poly(caprolactone-co-ethyl ethylene phosphate) (PCLEEP)	[84]
		Polyimide nanofibre	[87]
		Collagen-chitosan nanofibre	[85]
		Polyacrylonitrile nanofibre (PAN)	[86]
		Poly(trimethylhexamethylene terephthalamide) (PA 6(3)T) nanofibre	[83]
	Microelectromechanical systems (MEMS)	Pyrolysed poly-furfuryl alcohol (PFA) nanofibre	[92]
		Polyacrylonitrile (PAN) nanofibre	[88-90,93]
		Poly(L-lactic acid) (PLLA) nanofibre	[91]
		Carbon nanofibre	[94, 95]
		Polycaprolactone (PCL) nanofibre	[96]
Stretching method		Fibrinogen fibres	[97,98]
		Collagen nanofibre	[99]
		Nylon 6 nanofibre	[29]
		Poly(acrylic acid) (PAA) nanofibre	[100]
		Poly(styrene-b-isobutylene-b-styrene) (SIBS) nanofibre	[100]
		Polystyrene (PS) nanofibre	[100]
Bending Method	Two-point bending test	polyacrylonitrile (PAN) nanofibre	[59]
	Three-point bending test	Poly(L-lactic acid) (PLLA) nanofibre	[76,101]
		Polyvinyl-alcohol (PVA) nanofibre	[66,110,112,114,118]
		TiO2 nanofibre	[105]
		Polyethylene oxide (PEO) nanofibre	[107,112]
		Nylon-6 nanofibre	[107]
		Nylon-6/SiO2 nanofibre	[109]
		ZnO nanofibre	[111]
		Bisphenol A Polycarbonate (BPAPC) nanofibre	[116]
		Polystyrene/MWNT nanofibre	[117]
		PVA/TiO2 nanofibre	[118]
		Polylactic acid (PLA) nanofibre	[119]
		Polyacrylonitrile (PAN) nanofibre	[88,115]
	Multi-point bending test	Collagen nanofibre	[103]
		Poly(e-caprolactone) (PCL) nanofibre	[121]
		Cellulose nanofibre	[120]
Resonance Frequency Method		carbon nanofibre	[71]
		TiO2 nanofibre	[68]

	Polyacrylonitrile (PAN) nanofibres	[122]
	Poly-(ethylene-co-vinyl acetate) (PEVA) nanofibre	[123]
	Nylon-66 nanofibre	[125]
	Low-density polyethylene (LDPE) nanofibre	[123]
Nanoindentation method	PAN nanofibre	[127,128]
	PAN-SWNTs nanofibre	[127]
	PAN/GNP (graphite nanoplatelets) nanofibre	[128]
	polyethylene oxide nanofibre	[129]
	polyvinyl-alcohol (PVA) nanofibre	[114]
	Vanadium-ZnO piezoelectric nanofibre	[130]
	Polyvinylidene fluoride (PVDF)/ (MWCNT) nanofibre	[131]
	Poly(butylene terephthalate)/CNT nanofibre	[67]
	Silk/ Polyethylene oxide (PEO) nanofibre	[133]
	Polycaprolactone (PCL) nanofibre	[124]
	Chitosan-poly(ethylene oxide) nanofibre	[135]
	poly(L-lactic acid) (PLLA) nanofibre	[136]
Shear modulation force microscopy method	PS/clay nanocomposite fibre	[31]
	Low-density polyethylene (LDPE) nanofibre	[123]
	Polystyrene/MWNT nanofibre	[117]

MECHANICAL PROPERTIES OF ELECTROSPUN NANOFIBRE

With the improvement in mechanical characterisation of single electrospun nanofibre, it is feasible to study the mechanical behaviour of electrospun nanofibre and correlate the releavant mechanical properties with their geometrical, material, and processing parameters. Understanding and controlling the mechanical behaviour of electrospun nanofibres becomes increasingly relevant, aiming to ultimately optimise their mechanical properties in order to fulfill structural and functional applications.

Effect of Diameter on Mechanical Properties

One of the unique mechanical characteristics of electrospun nanofibre was found experimentally, which is essentially different from their large-diameter and bulk counterparts. The axial modulus and ultimate

tensile strength of electrospun polymeric nanofibres increases abruptly when the fibre diameter is below a certain value (Figure 26).

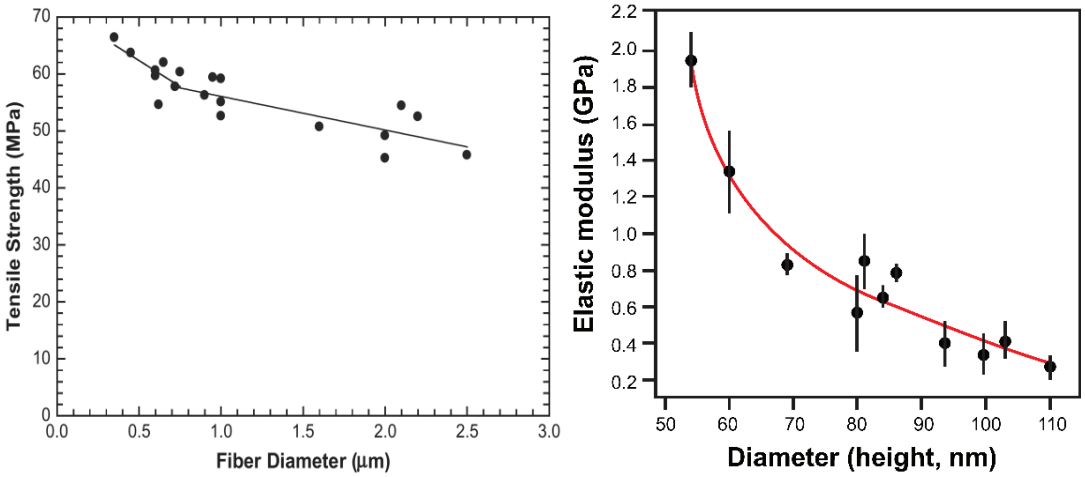

(a) (b)

FIGURE 26 (a) Tensile strength and tensile modulus versus diameter.[80] (b) Variation of measured elastic modulus as a function of diameter for PAMPS nanofibre.[106] Reproduced from Refs. 80 and 106 with permission from Elsevier and AIP Publishing, respectively.

Several groups have studied the dependence of mechanical properties of electrospun nanofibre with their diameter.[78,125,140] Tan and Lim[101] found that the mechanical properties varied with the fibre diameter of PLLA nanofibres produced by phase separation. This elastic modulus was found to be 1.0 ± 0.2 GPa for fibre diameters less than 350 nm, but it then decreased with increasing fibre diameters in excess of 350 nm. Later, this dependency was observed for electrospun PCL nanofibres.[60] Both tensile strength and yield stress decreased but ductility increased with increasing the fibre diameter. The ultimate strength was nearly doubled when the fibre diameter decreased from 1.7 to 1.03 μm. It was noted that the narrowing of the jet during its travel to the collector was analogous to a drawing process in gravity for melt spun fibres. The smaller fibres exhibited higher strength and lower ductility, indicating that a higher 'draw ratio' was applied. The same trend was found for TiO_2 nanofibres, which is attributed to higher influence of shear deformations at lower aspect ratios.[105] It was also reported that the Young's modulus of poly (2-acrylamido-2-methyl-1-propanesulfonic acid) (PAMPS) electrospun nanofibre increased exponentially from 0.3 to 2.1 GPa when fibre diameters decreased from 110 to 55 nm.[106] Ji et al.[31] measured the elastic modulus of PS and PS/clay nanofibres with the diameter ranging from 4 μm to 150 nm. The same behaviour was observed though the modulus values became much higher with the additional nanoclays. A substantial increase of elastic modulus was demonstrated for

diameters less than ~ 500 nm, which is explained by the alignment of shear-induced molecular chains during electrospinning. This trend was reported for other electrospun nanofibres elsewhere.[29,78,80,81,83,84,86,90,95,99,115,116,121,123,125,140,141]

Several factors may contribute to the size-effect of nanofibres like surface tension[142-144], chain alignment and formation of crystalline and semi-crystalline structures[29,80,81,106]. However, the sole contribution of surface energy is insufficient to understand such behaviour in the modulus and tensile strength of polymeric nanofibres.[145] Moreover, it was demonstrated that only minor increases were observed in the crystallinity and orientation of nanofibres with increasing their diameters (Figure 27). This moderate increase cannot be the reason for the dramatic change in the Young's modulus of nanofibres.[66,140]

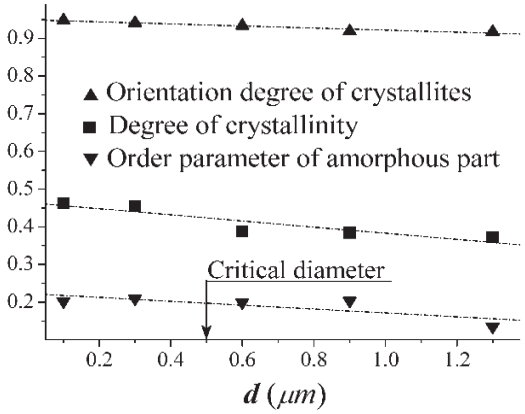

FIGURE 27 Orientation degree of crystallites along the fibre axis, degree of crystallinity, and order parameter of macromolecular orientation in the amorphous phase of the fibre versus fibre diameter *d* of electrospun nylon 6.6 nanofibres. Reproduced from Ref. 140, with permission from Nature Publishing Group.

In contrast, Papkov et al.[86] reported that with decreasing average fibre diameters of electrospun PAN nanofibres, the crystallinity was reduced significantly despite the higher chain orientation. Some studies attribute this effect to the core-shell nanofibre morphology.[66,146,147] Arinsten et al.[140,148] suggested a model based on the concept of a supramolecular structure of the amorphous phase, consisting of oriented fragments of polymer chains. Comprehensive studies of the above-mentioned models and efficient factors regarding size dependency behaviour of nanofibres can be found elsewhere.[16,64]

Effect of Collector Type and Take-up Velocity on Mechanical Properties

The type of collector used for collecting electrospun fibres could have a noticeable effect on the tensile properties of fibres. In general, a randomly oriented web of fibres is collected on static targets; whereas aligned fibres are collected on a rotating disc collector.[33] The latter results in anisotropic properties.[127,144] The tensile strength and modulus of aligned nanofibres have been proven to be higher than those of randomly oriented fibres. This is because molecular chains in the fibres are aligned along the fibre axis, which is in the loading direction. As a result, the samples exhibited enhanced tensile properties.[16,150]

It was reported that the tensile modulus and strength increased with the take-up velocity (TUV) while the elongation at break decreased (Figure 28 (a, b)), which is mainly ascribed to the increase in molecular orientation and crystallinity (Figure 28(c)).[70,75,77,90,149,151-154]

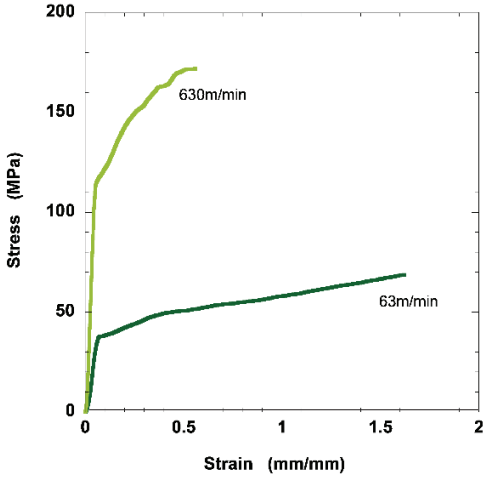

(a)

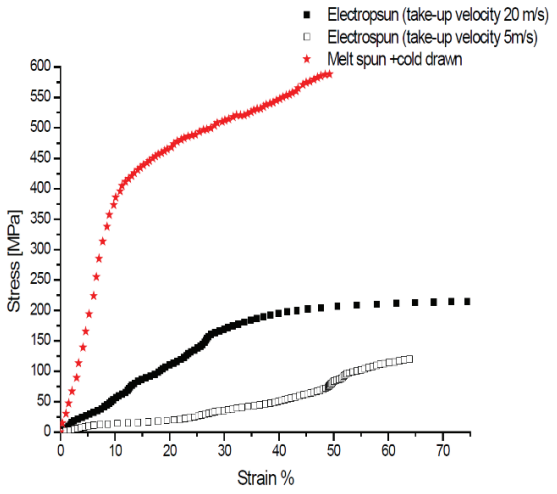

(b)

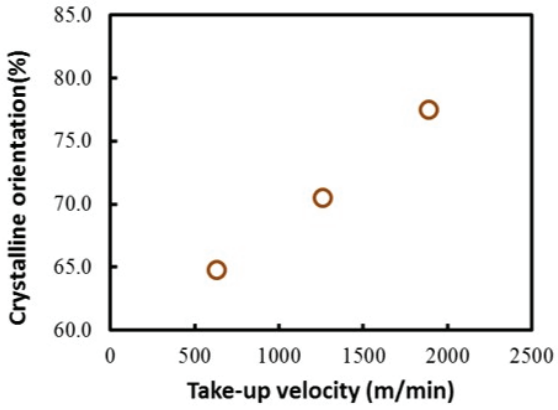

(c)

FIGURE 28 (a) Tensile stress-strain curves for PLLA nanofibres at different take-up velocities of 63 and 630 m /min.[75] (b) stress-strain curves of individual PA66 nanofibres collected at take-up velocities of 5 and 20 m/s, and a commercial PA66 microfibre that was prepared by melt extrusion and further followed by cold drawing.[70] (c) Crystallinity orientation for take-up velocities of 630, 1260 and 1890 m/min.[79] Reproduced from Refs. 70, 75 and 79, with permission from Wiley Periodicals, Inc., IOP Publishing Ltd and Elsevier, respectively.

Furthermore, increasing the take-up velocity leads to a decrease of average fibre diameter, indicating that an increase of pulling force causes fibre stretching and alignment (Figure 29).[151]

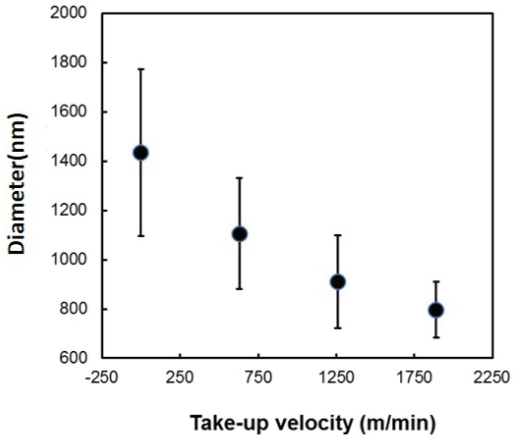

FIGURE 29 Diameter of porous PLLA nanofibres as a function of take-up velocity. Reproduced from Ref. 79, with permission from Elsevier.

Iani et al.[75] investigated the effect of take-up velocity on mechanical properties of electrospun nanofibres. Aligned PLLA nanofibres were electrospun at different disc rotation speeds of 100 and 1000 rpm, corresponding to take-up velocities of 63 and 630 m/min, respectively. The tensile strengths for 63 and 630 m/min were 89 and 183 MPa, respectively. XRD analysis demonstrated that the increased take-up velocity induced a highly ordered molecular structure. Similarly, Zussman et al.[70] showed that by increasing the take-up velocity from 5 to 20 m/s using a rotary target, the Young's modulus of nylon 6,6 fibres increased from 453 MP to 950 MPa, which can be interpreted by a higher orientation uniformity of electrospun nanofibres at a higher take-up velocity. It was clearly shown that a higher collecting speed induces a higher degree of orientation in these nanofibres (Figure 30).[155]

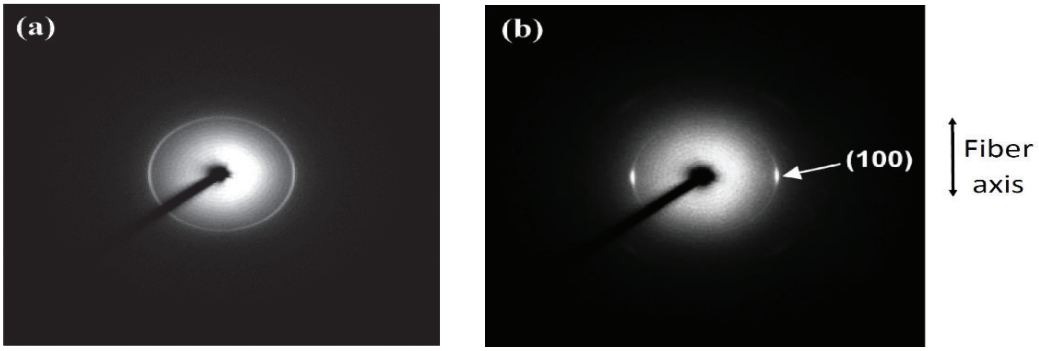

FIGURE 30 Two-dimensional WAXD patterns for the 100 reflection of aligned polyoxymethylene nanofibres at different take-up velocities: (a) 630 m/min and (b) 1890 m/min. Reproduced from Ref. 155, with permission from American Chemical Society.

ELECTROSPUN NANOFIBRE AS A REINFORCEMENT FOR POLYMER BASED COMPOSITES

In fibre-reinforced composites (FRCs), fibres are embedded or bonded to matrices with distinct interfaces between them. The matrices hold the fibres to form the desired shape while the reinforcing fibres improve the overall mechanical properties of matrices. In such composites, fibres are the main source of strength and principal load-carrying members while the matrices act as a load transfer medium and protect the reinforcements from environmental damages.[1]

The classification of FRCs can be defined based on fibre reinforcements and matrices. In the case of structural applications, the fibres in the composite structure can be divided into two classes, namely laminar composites (or composite laminates) and bulk composites.[1,156] The former structure contains short or continuous fibres embedded into matrices while the latter is made by stacking a number of thin layers of fibres and matrices, and consolidating them into the desired thickness. Fibre orientation in each layer as well as the stacking sequence of various layers in a composite laminate can be controlled easily, which helps to generate a wide range of physical and mechanical properties for composite laminates.[1]

The rationale at the basis of nanocomposite concept is that a decrease in the size of fillers gives rise to a large increase of interfacial area. This in turn greatly changes the macroscopic properties of the material.[157] From the viewpoint of composite mechanics, one-dimensional fillers are preferred to particles since they can provide larger load transfer according to some well-known toughening mechanisms, such as fibre bridging and fibre pull-out.[158] Consequently, composite fabrication, when incorporated with reinforcing electrospun nanofibres, has attracted increasing interest.

Bulk Reinforcement of Polymer Matrices

The mechanical properties of polymer/fibre composites are primarily dominated by the contribution of fibres to composites. The four main factors that govern the fibre contribution are (1) the basic mechanical properties of fibres; (2) the surface interaction of fibres and polymer matrices (i.e. the interface); (3) homogeneous fibre dispersion into matrices and (4) fibre orientation in composites.[1]

Electrospun nanofibres can satisfy the above-mentioned factors due to the following reasons: Firstly the continuously long electrospun fibres have high aspect ratios (i.e. length to diameter, *L/d*), and fibres do not present fibre edges (ends) that can act as obvious stress concentration zones. Secondly, high stretching rate (estimated at $10^5\ s^{-1}$) and the high elongation (draw ratio up to 10^4) of the solidified jet cause polymer molecular chains to align along the fibre direction, leading to the production of mechanically strong fibres. In addition, due to the small diameter of nanofibres (< 500 nm), they exhibit a high specific surface area, about 100 times larger than that of conventional fibres. Hence a substantial improvement of interfacial bonding strength between reinforcements and matrices can be achieved. This leads to better reinforcement of electrospun nanofibres than that of conventional fibres, and further facilitates the load transfer under external stress. [55,159-165] In addition to this, electrospinning process presents an opportunity to control the orientation of polymer functional groups within the liquid jet and upon solvent evaporation. The surface behaviour of electrospun polymer fibres was shown to change when compared to equivalent bulk polymer owing to a proposed organisation of polymer chains in the electrical field. This characteristic can benefit the improvement of interfacial adhesion between polymer matrices and nanofibres, which is critical to achieve excellent mechanical performance of composites.[166-169] Finally, electrospun nanofibres can offer a potential homogeneous fibre dispersion throughout matrices by forming a fibre network via electrospinning.[170] Consequently, electrospun nanofibres can be regarded as a promising material candidate for composite reinforcement.

The reinforcing ability of electrospun nanofibres was firstly explored by Kim and Reneker[171] in 1999, as well as proposed by Bergshoef et al.[172] in the same year. Kim and Reneker[171] investigated the use of electrospun polybenzimidazole (PBI) nanofibre fabrics as reinforcements in epoxy and styrene–butadiene rubber matrices. To fabricate epoxy composites, 8 to 32 plies of fabric sheets were cut and folded to fit the compression mould. Subsequently, the nanofibre sheets were impregnated with resin prior to curing. The composites prepared by two different configurations including one with the tensile axis of the specimen along the winding direction of nanofibre sheets, and the other with the tensile axis perpendicular to the winding direction. Epoxy was observed to be toughened by the nanofibres, and

this reinforcement effect was higher than that of PBI fibroids (whisker-like particles). It was also reported that the fracture toughness and fracture energy of composites was dependent on the direction of fabrics and cracks. The fabric-reinforced composites in which the crack was transverse to the winding direction displayed higher fracture toughness and fracture energy compared to those samples in which the crack was along the winding direction. For rubber matrices, the mixture of chopped nanofibre sheets and rubber matrices were compression moulded into composite samples. The reinforcement effect of PBI nanofibres was proven as evidenced by substantial increases in elastic modulus and tear strength. (i.e. Young's modulus was 10 times higher and the tear strength was twice as large as those of unfilled rubber).

Bergshoef and Vancso[172] prepared ultrathin nylon-4, 6 fibres mats with diameters at 50-200 nm by electrospinning polymeric solutions in formic acid. The impregnation of resulting mats with epoxy improved the tensile strength and modulus of composite films while the composites still remained transparent. After these pioneering studies, researchers have been intrigued to evaluate the effect of different factors such as fibre content, diameter, alignment, structure, surface treatment, etc on the reinforcement ability of electrospun nanofibres.

Fibre Content

Fong[173] impregnated a small amount of nylon 6 nanofibre sheets (2.5-7.5 wt%, fibre diameter: 100–600 nm), layer-by-layer with a dental resin. The addition of 5 wt% nanofibres increased the flexural strength, elastic modulus, and work of fracture of dental resin by 36, 26 and 42%, respectively. By increasing the mass fraction from 5 to 7.5 wt%, no further improvement in mechanical properties was observed.

Chen et al.[174] embedded cellulose nanofibrous mats (CNM) (200–800 nm in fibre diameter) in soybean protein matrices at different contents of 5–25 wt %. The mechanical strength and modulus increased with increasing CNM while the strain at break decreased. For composite films with CNM contents of 7.5 and 20 wt%, mechanical strengths were 4 and 13 times relative to that of neat SPI films, respectively. With more reinforcing nanofibres impregnated into SPI resin, a higher volume of nanofibres per unit cross sectional area of composites contributes to the enhancement of strength and modulus. When 7.5 wt% CNM was embedded, the failure strain of composite films decreased significantly from 275 to 25%.

Similarly, CNM with different contents of 0-60 wt % was employed to reinforce PVA film.[175] By increasing the CNM content up to 40 wt%, both mechanical strength and Young's modulus of composites were improved by 50% and 600%, respectively compare to those of neat PVA. The further increase of CNM

contents up to 50 and 60 wt% did not lead to further enhancement of mechanical properties of composites (Figure 31). Strong hydrogen bonding with PVA matrices resulted in good adhesion at the fibre/PVA interfaces, which was also confirmed by the absence of fibre pull-out along the cross section, elevated stress transfer from PVA to cellulose nanofibres and increase in mechanical properties of composites. Cellulose nanofibres also demonstrated a reinforcing effect on poly(butylene succinate) matrices.[176] This indicates that cellolose nanofibres have the potential as fibre reinforcements for biocomposites.

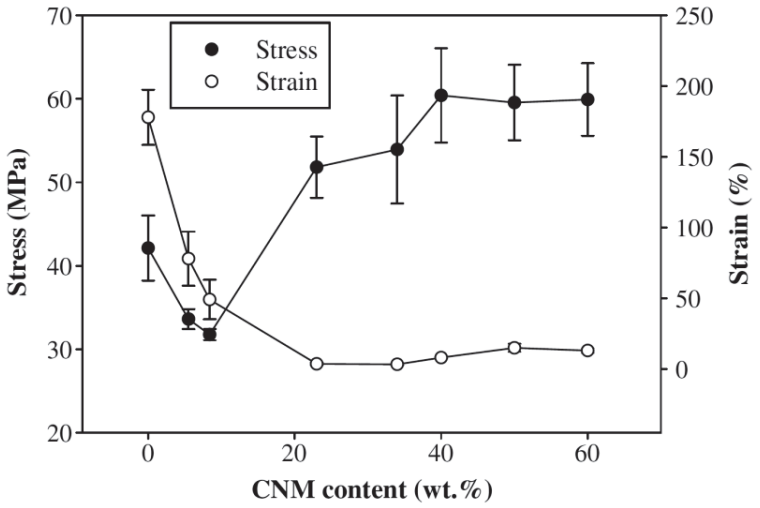

FIGURE 31 Stress and strain curves of PVA/CNM composites as a function of CNM content. Reproduced from Ref. 175, with permission from Elsevier.

Sun et al.[177] demonstrated that there is a critical nanofibre content in the reinforcement effect. Since nanofibres provide a high specific area, by increasing the surface area of nanofibres, more defects would be formed between fibres and matrices. This issue is due to the inferior impregnation arising from the air entrapment. Beyond the threshold of a certain nanofibre content, a further improvement in flexural properties of composites by increasing the nanofibre content would be difficult. Instead the mechanical properties tended to decrease with increasing number of defects. The critical nanofibre content for dental composites reinforced with 100% elongated polyacrylonitrile (PAN)- poly(methyl methacrylate) (PMMA) nanofibres was found to be between 1.2 and 1.6 wt%.

Neppalli et al.[178] fabricated PCL composites reinforced with electrospun nylon 6 fibres by inserting electrospun fibrous mats between PCL films, followed by the compression moulding at 90 ˚C. The composites containing a very low fibre content of 3 wt% exhibited not only improved stiffness and strength, but also increased ductility. This finding is opposite to the mechanical properties of generally

prepared PCL nanocomposites in which the increase of elastic modulus occur at the expense of eleongation at break. Analyses based on small-angle X-ray scattering (SAXS) and wide-angle X-ray diffraction (WAXD) have clearly demonstrated the dependence of modulus on the lamellar thickness and crystallinity (Figure 32(a)). The role of lamellar morphology was confirmed to contribute to the tailored mechanical performance of material samples. Figure 32(b) indicates that thicker lamellae are detrimental to material ductility in this case.

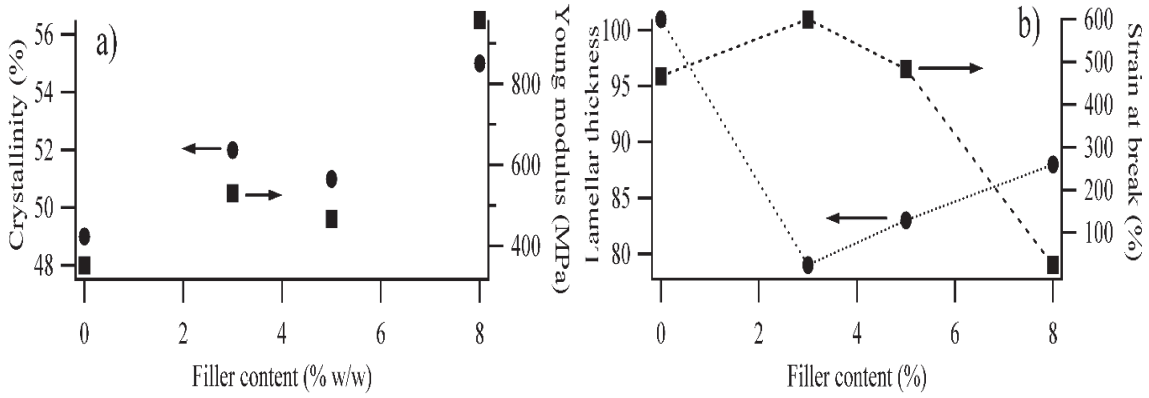

FIGURE 32 (a) Degree of crystallinity measured by WAXD and Young's modulus and (b) ultimate strain and lamella thickness as a function of filler content. Reproduced from Ref. 178, with permission from Elsevier.

In the other work[157], the microstructure of PLA composites with different contents of nylon 6 fibre mats (1.5 and 2.5 wt%) was evaluated. Such composites were prepared by keeping one and two nylon 6 fibre mats, respectively, between two compression moulded PLA sheets subjected to pressure and heat in a press. The tensile modulus increased three folds and 50% compare to PLA matrices for fibre contents of 1.5 and 2.5 wt%, respectively. In good agreement with previous work[178], it was shown that lamellar thickness was the prevalent factor to influence the modulus. The thickness of lamellae slightly decreased for composites with 2.5 wt% fibre mats, with respect to those with 1.5 wt% counterparts. Accordingly, despite the same degree of crystallinity for the fibre contents of 1.5 and 2.5 wt%, tensile moduli of PLA composites appear to be quite different, which were found to be 6.6 and 3.6 GPa respectively. Data presented in the above-mentioned study cannot single out the sole role of lamellar morphology in relation to better tensile behaviour of polymer composites, which is known to be influenced by many factors. Nonetheless, its effect is strongly evident. The additional electrospun nanofibres were found to decrease the material degradation rate and improve its dimensional stability in the degradation process.

Lu et al.[179] prepared high density polyethylene (HDPE) based composites reinforced with electrospun nylon-66 nanofibres by a hot-compaction method. Interestingly, increases in tensile strength and toughness coupled with ductility took place, but at higher nanofibre contents, the improvement was insignificant. Notwithstanding that the modulus exhibited a slight improvement at the low nanofibre content, a continuously increasing trend was manifested with increasing the nanofibre content (Figure 33(a)). SAXS results revealed that by increasing the fibre content, the degree of crystallinity monotonically increased from 62.5 to 71.2% with the nanofibre content up to 0.65 wt% while lamellae thickness remained unaffected. Such an improvement in mechanical properties was ascribed to the increase in the crystallinity and interlocked morphology of matrices and nanofibres due to the impregnation of HDPE melt in the inter-fibre voids during hot-compaction. Therefore, it caused nanofibres to be firmly embedded into matrices as a skeletal framework (Figure 33(b)). Moreover, the increase in toughness was mainly attributed to the increase in amorphous thickness since toughness generally dependeds on the chain mobility in the amorphous phase.

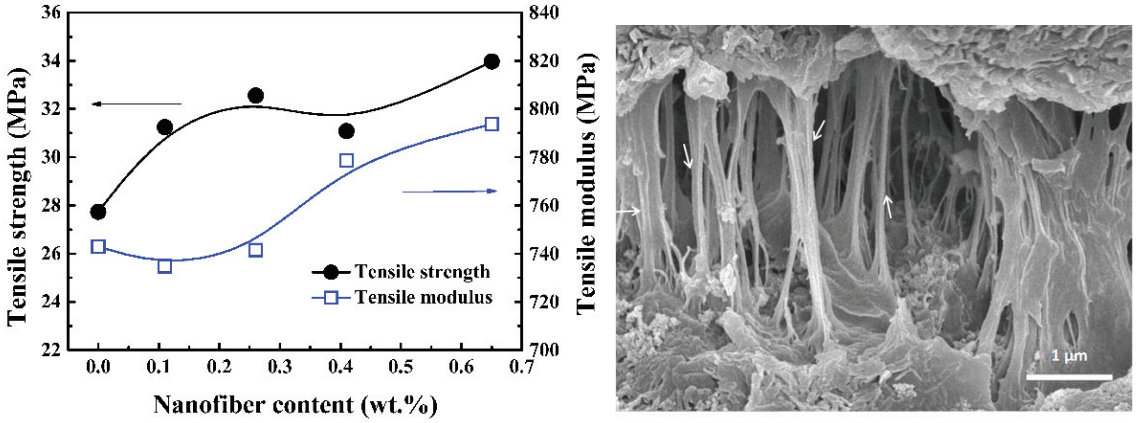

(a) (b)

FIGURE 33 (a) Tensile strength, modulus versus nanofibre content. (b) SEM micrograph of the cryofractured surface of composites reinforced with 0.26 wt% nanofibres. Reproduced from Ref. 179, with permission from Elsevier.

Wu et al.[180] reported that increasing polyacrylonitrile (PAN) nanofibre content from 0 to 16 wt% into PMMA steadily increased the tensile strength and modulus. In a case of uniform strain, the combination of fibres and matrices give the overall composite modulus (E_c):

$$E_c = E_f \times V + E_m \times (1-V) \quad (4)$$

Where V is the fibre volume fraction in the composites. E_f and E_m are elastic moduli of fibres and matrices, respectively. When V increases, the stiffer phase (e.g. fibres) dominates mechanical properties of composites. Measurements from Dynamic Mechanical Analysis (DMA) showed that embedded PAN nanofibres did not affect the T_g of PMMA matrices, but it significantly increased the stiffness of matrices in the glassy and glass-rubber transitional states. The value of storage modulus E' for neat PMMA film was 0.36 GPa and for composites with aligned fibre contents of 9 and 16 wt% at 65˚C (glass-rubber transition state) they were 1.25 and 2.3 GPa respectively. The E' increased with increasing the nanofibre content, which was probably because the presence of PAN nanofibres imparts the mechanical limitation to matrices and reduces its mobility and deformation, thereby enhancing the E' above T_g.

In the other work[181], DMA analysis proved that the presence of nanofibres enhanced the storage modulus in the glassy state. For composite film with randomly distributed CNM contents of 18 and 22 wt%, the E' values were 92.3 and 205 MPa above T_g, respectively, resulting in 57 and 127-fold increases over those of epoxy resin.

Lin et al.[182] found that increasing PAN and PMMA nanofibre content in 2,2'-bis-[4-(methacryloxypropoxy)-phenyl]-propane/tri-(ethylene glycol) dimethacrylate (Bis-GMA/TEGDMA) dental resin (50/50 wt %) shifted the damping peak of composites to a higher temperature, which might be attributed to the effect of nano-reinforcement to impede the segmental motion of polymer matrices. For PVA film reinforced with cellulose nanofibres using a solution impregnation method, it was observed that increasing the cellulose nanofibre content improved its storage modulus, especially in the melting zone (T_m=160˚C). This phenomenon is associated with intimate nanofibre/epoxy interfacial interactions, causing the limitated chain mobility within epoxy matrices as imposed by nanofibres (Figure 34(a)).[183] Jiang et al.[164] investigated the effect of fibre content on thermal stability of melamine–formaldehyde (MF) reinforced with nylon 6 nanofibres. TGA analysis demonstrated that with increasing the fibre content, the decomposition temperature increased from 386˚C for neat MF to 418˚C for composites at a nanofibre content of 62 wt% (Figure 34(b)).

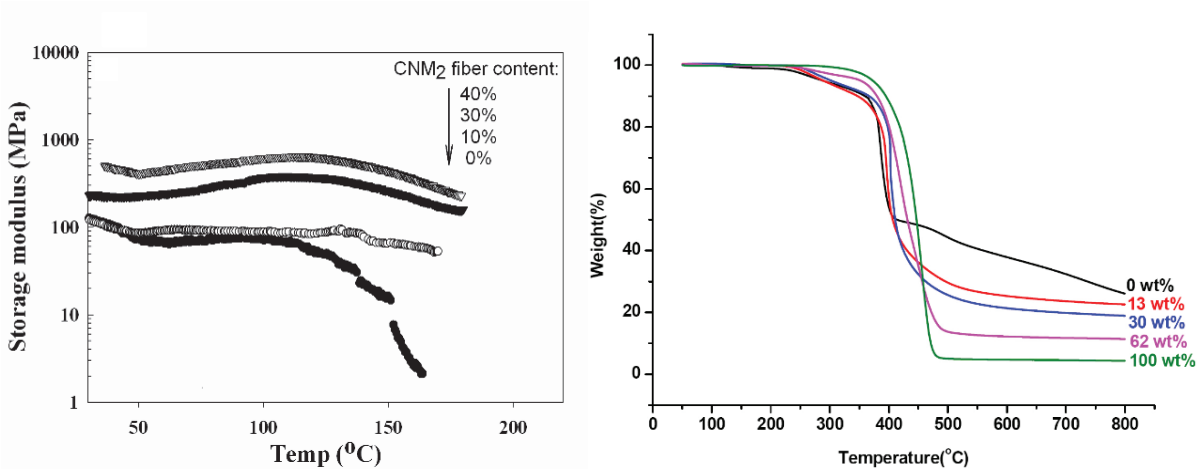

(a) (b)

FIGURE 34 (a) Storage modulus of PVA composite films as a function of temperature with various fibre contents.[183] (b) Thermal stability of pure MF resin, nylon-6 nanofibre sheets, and MF/nylon-6 nanocomposites with different amounts of nylon-6 nanofibres.[164] Reproduced from Refs. 164 and 183 with permission from American Chemical Society and Elsevier, respectively.

Recently, Dong et al.[165] used a stack lamination method to prepare epoxy/electrospun PLA nanofibre composites. Mechanical properties of composites were evaluated with different nanofibre contents of 1, 3 and 5 wt%. The optimum nanofibre content was determined to be 5 wt% with flexural modulus and strength increases of 50.8 and 31.6% as opposed to those of neat epoxy. Furthermore, DSC results indicated that by adding PLA nanofibres, the glass transition temperature (T_g) of composites increased compared to that of neat epoxy, which was attributed to fibrous networks to further restrict the intermolecular mobility of matrices.

The effect of nanofibre content on mechanical properties of composites was assessed by others as well.[162-164,182-193] In general, the increase in the fibre content leads to improved mechanical properties though an optimum content level of nanofibres is confirmed. Owing to a high specific area for nanofibres, a high possibility of resulting defects or voids between fibres and matrices occurs with higher surface areas. Hence, the further improvement in mechanical properties of composites becomes limited when increasing the fibre content, which is most likely due to more interfacial defects.[182]

Fibre Diameter

To investigate the effect of fibre diameter, Tang et al.[183] embedded electrospun cellulose nanofibre mats with different fibre diameters (520 and 250 nm) into poly(vinyl alcohol) (PVA) using a solution impregnation method. A significant difference was observed in the cross-sectional morphology of

composites with various diameters. The smaller diameter increased the surface area by almost 2 times compare to the larger counterpart, leading to a strong interfacial adhesion. In this case, the hydrogen bonding could be improved between nanofibres and PVA (Figure 35). The addition of 4 wt% nanofibres with diameter of 520 and 250 nm increased the Young's moduli of composites by 11 and 14 times, and improved the stiffness at the melting zone of 160˚C by 136 and 170 times when compared to those of neat PVA, respectively.

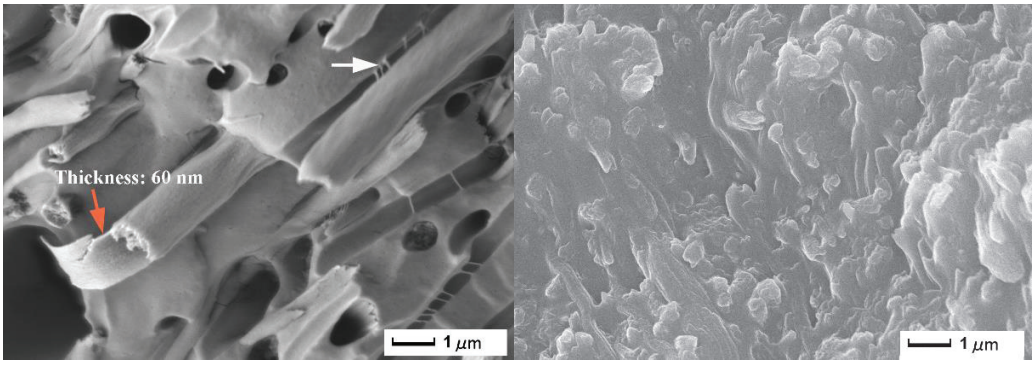

(a) (b)

FIGURE 35 Cross-section SEM images of PVA composite films reinforced with electrospun nanofibre mats at the fibre content of 20 wt% with different fibre diameters: (a) 520 nm and (b) 250 nm. Reproduced from Ref.183, with permission from Elsevier.

Neppali et al.[178] also demonstrated that the finest fibres were those that best adhered to matrices. Although this work focused on reinforcing PCL with nylon 6 nanofibres, they observed the presence of fibres with very small diameters, as the typical products of electrospinning, favoured a good interfacial adhesion between matrices and fibres. To simultaneously improve the physical mechanical properties and tune the biodegradation of polycaprolactone (PCL)-based composites, the same authors used nylon 6 (fibre diameter: 800 nm) as the reinforcement and polyvinylpirrolidone (PVP) (fibre diameter: 300 nm) to calibrate the biodegradation rate.[194] The critical effect of fibre diameter on the interfacial adhesion was manifested, and thinner fibres appeared to adhere more firmly to matrices as compared to their thicker counterparts.

Measurements taken from AFM showed that the surface roughness increased with increasing the fibre diameter.[161] From the observation of fracture surfaces of composites, it was found that larger fibres resulted in a poor interfacial adhesion to matrices with more pull-out fibres detected. However, thinner fibres adhered more firmly to the matrices. A comparison between electrospun and conventional glass nanofibres with fibre diameters of 400 nm and 10 μm as reinforcements confirmed that electrospun

glass fibres were superior to their conventional counterparts in term of reinforcement and toughening effects.[185] This was attributed to the high specific surface area of electrospun nanofibres that could result in more fibre-epoxy interfacial interactions and facilitate efficient stress transfer.

Fibre Length

The direct mixing of long electrospun nonwoven nanofibre mats with polymer matrices is limited by the strong entanglement of nanofibres. Accordingly, Jiang et al.[193] manufactured self-reinforced polyimide (PI) with short electrospun PI nanofibres based on a fundamental concept of better dispersion of short electrospun fibres in liquid media. Short nanofibres can be processed by liquid processing technique, and become independent from the limitation imposed by the electrospining process itself. In comparison to the neat PI film, the tensile strength and modulus were improved by 53% and 87%, respectively when 2 wt% short fibres with a fibre length of 50-500 µm were used. In comparison, long and continuous PI nanofibres with a much higher content of 38 wt% were required to achieve a similar mechanical strength. Low content and better dispersability of short fibres appear to achieve superior mechanical performance to long and continuous counterparts (Figure 36).

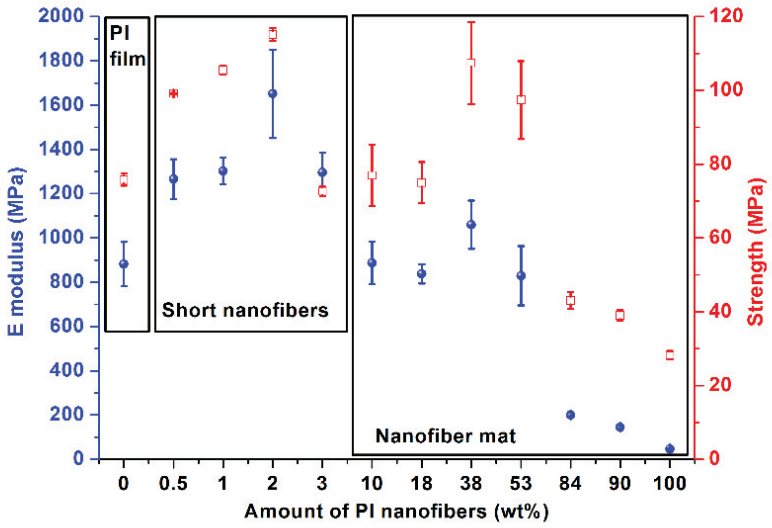

FIGURE 36 Comparison of elastic modulus E (●) and strength (□) of PI/PI nanofibre composite films and PI self-reinforced nanofibre composites with as-electrospun PI nanofibres and pure PI film. Reproduced from Ref.193, with permission from Elsevier.

The effect of short nylon-6 nanofibres in reinforcing mechanical properties of thermoplastic polyurethane (TPU) and PMMA was also evaluated by the same group.[162] The incorporation of 3.5 wt%

short and long nylon fibres into TPU increased the Young's moduli by 185% and 82%, respectively. In addition, the reinforcement effect of nanofibres was dependent upon polymer matrices. The increase in mechanical properties of TPU matrices was more significant than that for PMMA counterparts due to their hydrogen-bonding interactions with nylon-6 fibres. In the case of thermoplastic polyurethane, a reinforcement effect was achieved without losing its transparency.

A comprehensive summary to highlight the effect of physical features of different electrospun nanofibres on reinforcement effect of polymer matrices is listed in Table 2, which is based on the nanofibre content, diameter and length.

TABLE 2 Effect of physical features of different electrospun nanofibres on bulk reinforcement of polymer matrices

Fibre Property	Nanofibre	Polymer Matrices	Comment	Reference
Fibre Content	Nylon 6	• Bis-GMA/TEGDMA	• Increases in flexural strength, elastic modulus and work of fracture by 36%, 26%, and 42% over those of the neat resin with an optimal content of 5 wt% • Crack deflection in the presence of nanofibres	173
		• PCL	• Simultaneous improvement in stiffness, strength and ductility with the addition of 3% fillers • Indicative effect of lamellar thickness on ductility	178
		• PLA	• A three-fold increase in tensile modulus with a fibre content of 1.5 wt% with respect to neat PLA • The role of lamellar morphology on strength	157
		• Melamine-formaldehyde	• The effect of wetting procedure on reinforcing properties • Increase in decomposition temperature by increasing the fibre content up to 8% compared to neat melamine-formaldehyde resin	164

	Cellulose	• Soybean Protein	• Increases in mechanical strength and Young's modulus by 13 and 6 times more than those of neat soybean protein film with 75% light transparency, respectively	174
		• PVA	• Improved tensile strength and Young's modulus by 50% and 600%, respectively with an optimal fibre content of 40 wt%	175
			• Increase in storage modulus, especially in melting zone (170 times greater than that of neat PVA)	183
Fibre Content		• Poly(butylene succinate)	• The reinforcing effect of cellulose fibres in poly (butylene succinate)/ cellulose biocomposite.	176
		• Epoxy Resin	• Increase in storage modulus in the glassy state by increasing randomly oriented mat content up to 127 folds over that of epoxy resin	181
	Nylon-66	• HDPE	• A continuous increase on tensile modulus by increasing the nanofibre content • Improvement in toughness mainly due to the increase in amorphous thickness with increasing the fibre content	179
	PAN	• PMMA	• Steadily increase in reinforcing efficiency of PAN nanofibres with increasing the fibre loading • Increase in storage modulus in glassy and glass-rubber transitional states	180
	PLA	• Epoxy	• Increase in flexural modulus and strength by 50.8 and 31.6%, respectively with an optimum content of 5 wt%	165
	Cellulose	• PVA	• Increase of Young's modulus	

Fibre Diameter			• with the incorporation of smaller fibres (1.2 times more than larger fibres) • Improvement of storage modulus for smaller fibre diameter at the melting zone as opposed to larger counterpart	183
Fibre Diameter	Ethylene vinyl alcohol copolymer	• PLA	• Increase in roughness by increasing the fibre diameter • Thinner fibres adhered more firmly to polymer matrices	161
Fibre Length	PI	• PI	• Superior mechanical performance of short fibres compared to those of long fibres • Long fibre require more fibre content (38 wt%) to achieve a similar mechanical strength of its short counterparts (2 wt%)	193
	Nylon 6	• TPU and PMMA	• Improvement in Young's modulus by 82% and 185% for long and short fibres reinforced composites, respectively	162

Fibre Structure

The innovation of electrospinning technology could act as a good stimulus to design and fabricate new nanofibre-reinforced composites with improved mechanical performances, especially using the chemical and physical modifications of electrospun nanofibres to improve fibre–matrix adhesion.

Tian et al.[189] employed electrospun nylon 6/fibrillar silicate nanocomposite fibres to reinforce Bis-GMA/TEGDMA dental composites. For homogenous dispersion of nanofibres into matrices, electrospun mats were firstly impregnated with the dental resin, then cured composites were milled into fine particles, and further mixed with fresh dental resin prior to final curing. The hypothesis was that the uniform distribution of nano-scaled and highly aligned single crystals of fibrillar silicates into electrospun nylon 6 nanofibres would improve mechanical properties of resulting nanocomposite nanofibres, thus leading to the

effective reinforcement of dental composites. Three-point flexural results further supported this. The flexural strengths, elastic modulus and work of fracture, by incorporating an optimum filler content of 2 wt% nylon 6 nanofibres, was 106 MPa, 2.4 GPa and 6.7 kJ/m^2, respectively. In comparison, for nylon 6/fibrillar silicate nanocomposite fibres, these same properties were found to be 117 MPa, 2.5 GPa and 8.5 kJ/m^2, accordingly.

Zhang et al.[195] reinforced triglycidyl amino phenol (TGAP) epoxy resin with electrospun polyetherketone cardo (PEK-C) nanofibres containing vapour-grown carbon nanofibres (VGCNFs). The addition of electrospun PEK-C/VGCNF nanofibres to epoxy resin led to the distribution of VGCNFs primarily within the phase-separated PEK-C-rich domains. Such a unique phase and carbon nanofibre dispersion structure resulted in synergistic increases in flexural strength, toughness and hardness with almost an negligible drop in elastic modulus at the optimum content of 5 wt% for PEK-C/VGCNF nanofibre inclusions.

Chen et al.[196] attempted to fabricate self-reinforced polyimide (PI) films by using highly aligned electrospun nanofibres and nanocomposite fibres with carbon nanotubes (CNTs). Compared with neat PI film, PI composite films reinforced with aligned PI nanofibres possessed increases of tensile strength and elongation at break by approximately 97 and 46%, respectively. In the case of 2 wt% CNTs/PI nanofibres, the corresponding properties were increased by 138 and 104%. Such significant increases can be ascribed to good compatibility between electrospun nanofibres and matrices as well as high nanofibre orientation in matrices. Increasing the CNT content from 3.5 to 5 wt% decreased the tensile properties of composites owing to the CNT agglomeration (Figure 37).

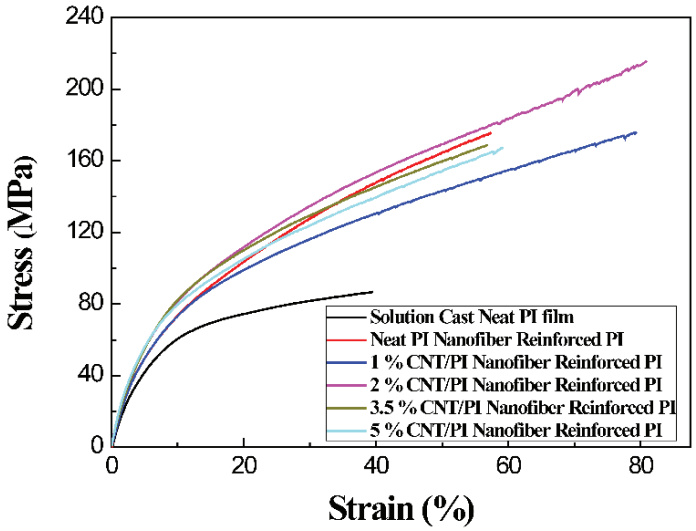

FIGURE 37 Stress–strain curves of solution cast PI films, PI films reinforced with neat PI nanofibre membrane, and PI films reinforced with CNT/PI composite nanofibres. Reproduced from Ref.196, with permission from Elsevier.

Chang[192] fabricated functionalised carbon nanotubes (FCCNs) composite nanofibres based on high-melting-point polyurethane (PU_H) as matrices via electrospinning. Later they were stacked alternately with low-melting-point polyurethane (PU_L) films into composite nanofibre reinforced composites under a hot press. The tensile strength of composites with 30 wt% FCCNs reached 54.3 MPa, 187% higher than that of PU_L film. Besides, the elongation at break increased with increasing the filler content, indicating a high compatibility of FCCNs / PU_H and PU_L matrices.

To assess the effect of different nanoparticles and dispersion method on mechanical properties of polymer nanocomposites reinforced with aligned electrospun PMMA fibres, either neat PMMA fibres or those embedded with multiwall carbon nanotubes (MWCNTs) or with graphene nanoplatelets (GNPs) with a mean diameter of 1–2 μm were used as reinforcements for PCL using a matrix film stacking technique.[197] Initially, MWCNTs and GNPs were accurately disentangled and dispersed into N, N-Dimethylformamide (DMF) by means of sonication. In some cases, sonicated GNPs were further dispersed with the aid of the centrifugation. The addition of carbonaceous nanofillers within the fibres resulted in both cases to a further increase of yield stress despite the very low nominal content (0.07 wt% in the final PCL/nanofiller loaded PMMA composites). This finding could be attributed to the small nanofiller amount and their uniform distribution within PMMA fibres. Moreover, the increase of yield strength for composites was believed to be related to the corresponding strength increase in electrospun fibres. The best results were obtained for samples prepared from the centrifuged dispersion of GNPs (yield stress = 14.0 ± 0.5 MPa). DSC analysis demonstrated slight lower crystallinity for PCL composites when compare to that of neat PCL. This can be explained by the hindrance effect of fillers on the formation of crystalline regions during the cooling stage in composite manufacturing. However, it was also indicated that unidirectional reinforcement has more pronounced effect on mechanical properties of composites as compared to the decrease of crystallinity level of matrices**.**

Papila et al.[198] incorporated MWCNTs into surface-modified, reactive poly(styrene-co-glycidyl methacrylate) P(St-co-GMA) nanofibres by electrospinning to strengthen epoxy matrices. The addition of a very low weight fraction of composite fibres at 0.2 wt% increased the flexural modulus of epoxy composites by over 20%. Such an increase was attributed to the combined effect of two factors: the strength of well dispersed MWCNTs in the structure and the modified surface chemistry of electrospun fibres leading to bonding across the cross-linked polymer matrix−nanofibre interface. The absence of

perceptible variation in tensile strength with increasing the MWCNT content revealed that the increase in strength was mainly due to the cross-linked nanofibres and interface reinforcement.

Electrospun polystyrene (PS)/TiO_2 composite fibres were used by Neppalli et al.[199] as the reinforcement for biodegradable poly(butylene succinate-co-adipate) (PBSA) matrices by means of a compression moulding technique. Compared to neat PBSA with a Young's modulus of 378 MPa, the incorporation of PS/TiO_2 composite fibres (0.08% w/w of TiO_2) into PBSA composites improved the modulus up to 542 MPa. Conversely, increasing the TiO_2 content decreased the modulus in good accordance with the relevant microstructures of composites detected by SAXS (Figure 38). In addition, by varying the TiO_2 content, the hydrolytic degradation rate of composites was also tunable.

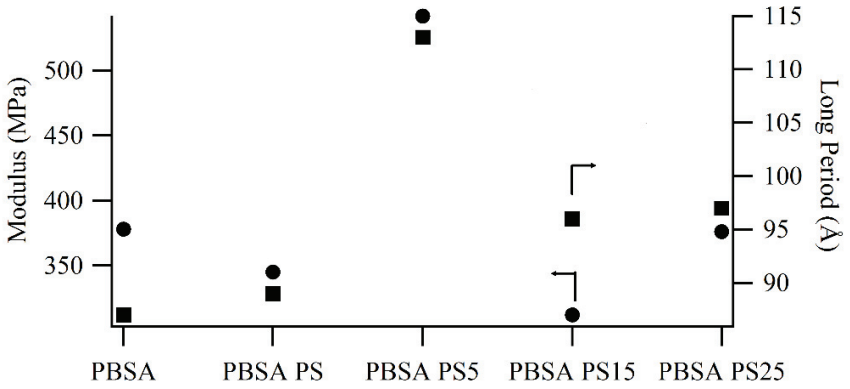

FIGURE 38 Modulus (left scale) and long period (right scale) of selected material samples. Reproduced from Ref. 199, with permission from Elsevier.

Liu et al.[159] manufactured epoxy composites by the impregnation of epoxy resin with thermoplastic polyurethane (TPU)/MWNTs nonwoven mats. With only 3 wt% MWNTs embedded in mats, the increasing mechanical response was observed with increases of 29, 4 and 19% in tensile strength, elastic modulus and tensile strain, respectively, in contrast with those of neat epoxy (Figure 39). Such relative increases were due to the MWNT effect on the enhancement of in-situ properties of nanofibres to sustain higher loads, increase in inherent strength of nanowebs, as well as the restraining effect of nanofibres on crack propagation and good interfacial bonding and infiltration between nanofibres and epoxy resin.

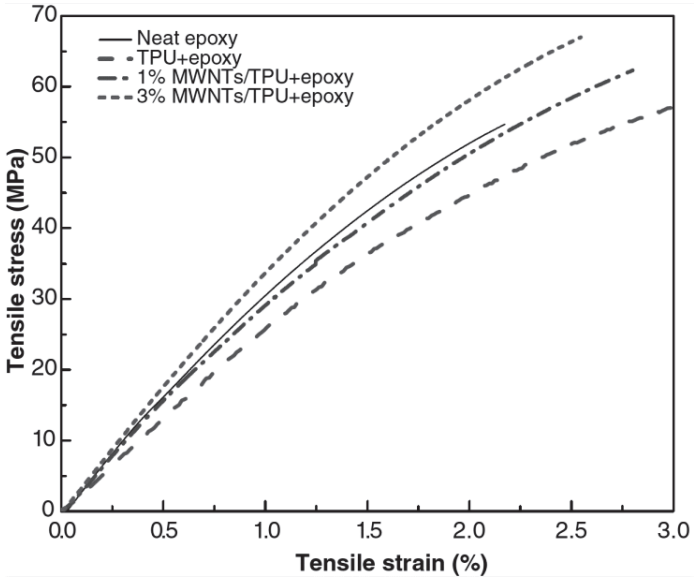

FIGURE 39 Stress–strain curves of neat epoxy and nanophased epoxy composites. Reproduced from Ref. 159, with permission from SAGE.

Lin et al.[182] prepared PAN core-PMMA shell nanofibres by co-electrospining of polymer blends (diameter range of 200–500 nm) to reinforce Bis-GMA/TEGDMA resin. With a filler content of 7.5 wt%, flexural strength, flexural modulus and work of fracture were improved by 18.7, 14.1 and 64.8%, respectively, as opposed to those of pristine resin. The improvement effect could be caused by the formation of semi-interpenetrating polymer network (IPN) structure between nanofibres and matrices, which resulted in an 'in-situ nano-interface' that could provide good interfacial adhesion. For further improvement in mechanical properties, a post-drawing treatment was performed by stretching nanofibres along the fibre direction at 120˚C.[187] The effectiveness of post treatment was confirmed since the incorporation of 1.2 wt% post drawn nanofibres were detected to enhance flexural strength, modulus and work of fracture by 51.6, 64.3 and 152%, respectively.

Recently, Cheng et al.[158] developed a Bis-GMA/TEGDMA dental resin by loading an antibacterial component sodiumfluoride (NaF) into PAN core-PMMA shell nanofibres as reinforcements to obtain the benefit from strengthening effects of core–shell nanofibres and their ability as drug delivery carriers. The strengthening effect of PAN-PMMA nanofibres was reported though increasing the thickness of PMMA caused a slight decrease in flexural strength and modulus. Moreover, core–shell nanofibres were proven to be a good carrier to perform sustained fluoride-ion release with a minor initial burst release.

Chen et al.[188] proposed a different method for manufacturing nanocomposites based on a core-shell nanofibre structure via coaxial electrospinning. Nylon 6 and PMMA were chosen as cores and shells,

respectively. Ten layers of composite nanofibre membranes were stacked in a mould and underwent a hot press treatment. As a result, PMMA shell material was melted while the nylon 6 core material maintained its original fibrous structure, thereby resulting in nanofibre reinforced composites. The optimum content of nylon 6 for the mechanical improvement was 2.5 wt% though a slight decrease in transparency was reported.

Wang et al.[200] employed the same method by hot pressing multilayers of PMMA/PA-6 core-shell nanofibres (fibre diameter: 270-2800 nm) to fabricate transparent PMMA composites reinforced with PA-6 nanofibres. In comparison, the same composites were also prepared by interlacing PA-6 with PMMA nanofibrous (fibre diameter: 100-390 nm) membranes. It was found that the composite based on core-shell structure possessed not only a better mechanical performance (20% increase in tensile strength and modulus) but also a better transparency with only 10% loss compared to composites prepared from laminated PA-6 with PMMA nanofibrous mats. Although the core-shell based composites contained fibres with larger diameters, better interface between fibres and matrices, lower voids content and more uniform distribution of nanofibres led to better mechanical properties. Oh et al.[201] also reinforced epoxy adhesive with meta-aramid/epoxy nanofibres in core-shell structures by coaxial electrospinning. An increase in lap shear strength of reinforced adhesive was mainifested. Gue et al.[202] aminated the surface of electrospun core-shell structured styrene-butadiene-styrene (SBS) block copolymer as a rubbery core and PAN as a hard sheath to improve the interaction between the electrospun fibres and epoxy resin. The Charpy impact energy of composites was increased by 150% when embedded with 4 wt% laminated core-shell fibres. Besides, the reinforcing effect of core-shell fibres was more than that of PAN nanofibres and PAN powders owing to the presence of rubbery SBS cores. DMA analysis showed embedding core-shell nanofibres in epoxy would not decrease the heat resistance of epoxy.

Hybrid fibres were produced by electrospinning poly(methyl methacrylate)-graft-poly(dimethyl siloxane) copolymers (PMMA-g-PDMS) with various PDMS contents to assess the possibility of reinforcing silicone rubber matrices with fibres having silicon components.[203] It was found that both stiffness and extensibility increased in the presence of hybrid fibres, which is due to fibre compatibility with matrices as well as the yield of silicone-rich fibres detected after tensile tests.

PCL-based green composites were prepared by direct electrospinning of PLA or PLA/PCL blend nanofibres on a PCL sheets prior to drying by vacuum.[187] The coated sheets were alternatively stacked before compression moulding. Compared to neat PLA nanofibres, using minor PCL component in

electrospun blend fibres increased the affinity between fibres and PCL matrices, thus enhancing the interfacial adhesion for a better mechanical performance. It was stated that the mechanical response was dependent on PLA/PCL ratio since further increasing the PCL ratio decreased the strength and modulus of composites without any further contribution to the affinity improvement. The optimum ratio of PLA/PCL blend fibres for best reinforcement effect was 90/10.

To improve the fibre–matrix adhesion in engineered composite materials, Meng et al.[190] designed a new 3D architecture with growing thorns on an electrospun nanofibre surface. The thorn-like fibres, composed of polyarylene ether nitriles (PEN) ''stems'' and iron phthalocyanine (FePc) ''thorns'', were prepared by combining electrospinning and controlled temperature-induced self-assembly. The nanofibre structure and the length of thorn could be controlled through processing time and temperature. By embedding thorn-like fibres into epoxy resin, the thorns could tie molecules and interlock with the surrounding epoxy, leading to the formation of a stronger fibre-matrix interface (Figures 40 (a)-(d)). Better flexural properties were achieved with the incorporation of thorn-like fibres as opposed to their untreated counterparts. In other work, Meng et al.[163] investigated the effect of thorn-like nanofibres on the storage modulus of composites. The incorporation of thorns-like fibres increased E' of composites while the damping ratio decreased compare to untreated nanofibres. The incorporation of 6 wt% thorn-like fibres treated at 200˚C enhanced the flexural strength and modulus by 36 and 38%, respectively.

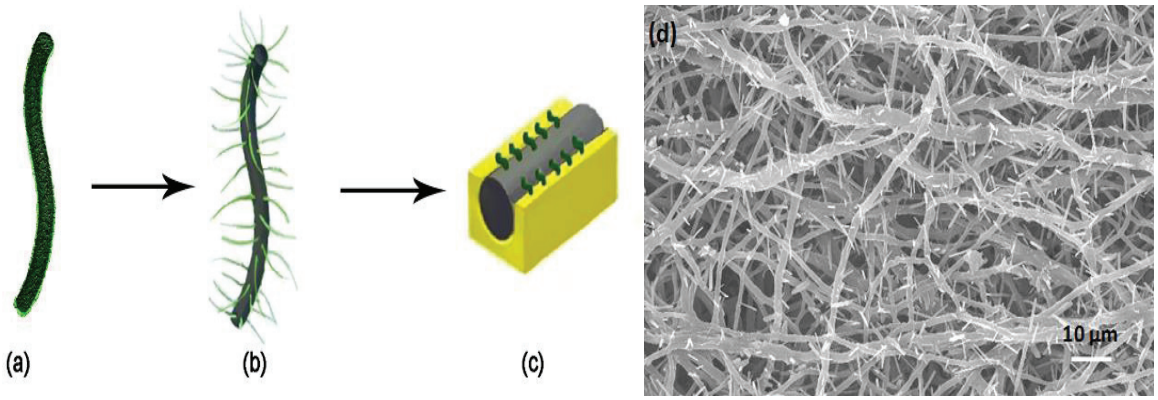

FIGURE 40 Schematic representation of strengthening the fibre–matrix adhesion: (a) PEN/FePc micro/nanofibres without treatment, (b) thorn-like micro/nanofibres and (c) the ''thorns'' interlocking the surrounding epoxy resin. (d) SEM images of PEN/FePc thorn-like fibres after heat treatment. Reproduced from Ref. 190, with permission from The Royal Society of Chemistry.

Fibre Alignment

Very few reports have evaluated the effect of nanofibre alignment on the mechanical performance of resulting polymer nanocomposites. Liao et al.[181] fabricated aligned and randomly distributed cellulose nanofibres using a rotational cylinder and stationary collector, respectively. Epoxy composites were prepared by embedding nanofibres into matrices using a solution impregnation method. In the case of aligned nanofibres, the tensile strength of composites in the longitudinal direction was dramatically increased to 35 MPa, which was 7 times as much as that of their randomly distributed counterpart; whereas in the transverse direction the strength value dropped to 2.5 MPa (Figure 41). Tensile strengths of epoxy composites reinforced with 24 wt% aligned and randomly oriented mats were 33 and 17.2 MPa, respectively, indicating higher efficiency of aligned nanofibres in terms of mechanical performance. The light transmittance of both composites was quite similar, which suggested that the alignment of reinforcing fibres had a minor impact on the light transmittance of composite films, as compared to two other key factors, namely fibre diameter and interfacial adhesion.

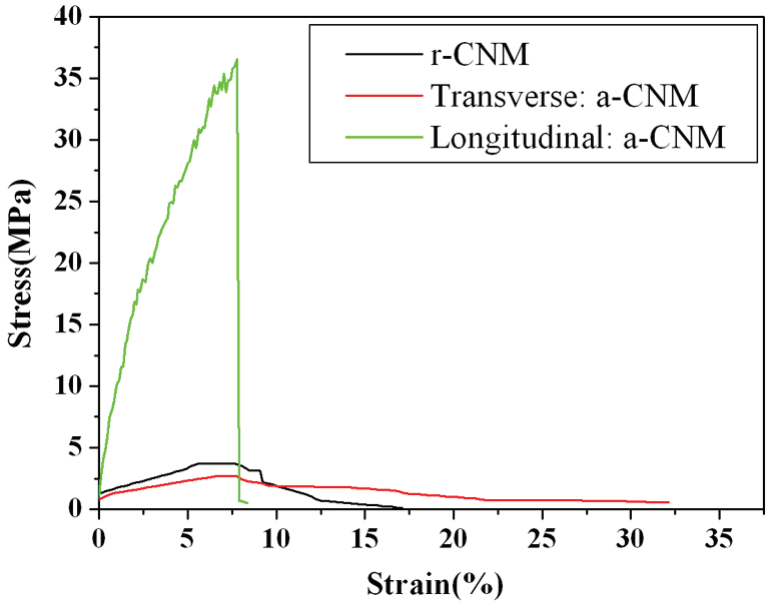

FIGURE 41 Typical stress–strain curves of CNM mats. Reproduced from Ref. 181, with permission from Springer.

Chen et al.[204] also investigated the effect of alignment on polyamide 6 composites reinforced with electrospun aligned and randomly overlaid polyimide (PI) fibrous mats. PI/PA6 composites with 50 wt% of aligned PI nanofibres possessed tensile strength and modulus of 447 MPa and 3.0 GPa in the longitudinal direction, respectively, which represented increases of 700 and 500% when compared to

those of neat PA6. It is noteworthy that tensile strengths in the longitudinal and transverse directions were almost similar, which was ascribed to a small amount of randomly overlaid PI nanofibres presented in aligned fibrous mats since the roller could only introduced a certain degree of fibre alignment.

Similarly, Wu et al.[180] embedded randomly organised and uniaxially aligned PAN nanofibres into PMMA using the solution impregnation technique. It was confirmed that fibre orientation had a positive effect on the mechanical properties of corresponding composites. The tensile strength and Young's modulus of composite films reinforced with 16 wt% aligned fibres achieved 40 and 30% increases as opposed to those of randomly organised fibres. Moreover, the aligned orientation enhanced the stiffness of composites in their glassy and glass-rubber transition states relative to randomly oriented counterparts.

Non-woven and aligned electrospun nanofibre mats from copolymers of polyacrylonitrile-graft-poly(dimethyl siloxane) (PAN-g-PDMS) were used as fillers for silicone elastomer composites.[191] The graft copolymer of PAN was synthesised to enhance the compatibility between fibres and silicone matrices. Interestingly, non-woven composites demonstrated superior characteristics of extensibility as well as toughness owing to their failure mechanism. Fibre bridging hindered the crack propagation after the failure of stressed fibres at the crack tips, and other unstressed fibres replaced them and countered the strain. This 'fracture and replacement' of continuous fibres due to the random fibre arrangement in the non-woven mat led to the increase in fracture elongation. On the other hand, aligned fibre composites showed a much higher stiffness level due to the predominantly unidirectional fibre arrangement in silicone elastomer matrices.

Overall, these studies highlight the potential of different electrospun nanofibre structures and alignemt for reinforcing polymer matrices and the asscoaited results are summarised in Table 3.

TABLE 3 Effect of different nanofibre structures and alignemt on the bulk reinforcement of polymer matrices

Fibre Structure	Nanofibre	Polymer Matrices	Comment	Reference
	Nylon 6/Fibrillar Silicates	• Bis-GMA/TEGDMA	• 98% improvement in work of fracture by addition of 2 wt% nylon 6/fibrillar silicate nanocomposite • Better mechanical performance incorporated with nylon 6/fibrillar silicates when compared to nylon 6 nanofibres.	189

Electrospun Nanocomposites	PEK-C/VGCNFs	• TGAP Epoxy Resin	• Synergic increases in strength, toughness and hardness with an insignificant drop in elastic modulus due to the formation of particulate phase structure	195
	PI/CNTs	• PI	• Increases in tensile strength and elongation at break by 138% and 104%, respectively with the addition of 2 wt% PI/CNTs relative to those of neat PI film • Decreases in tensile properties at higher CNT content above 3.5% due to the CNT agglomeration	196
	PU_H/FCCNs	• PU_L	• Increase in elongation at break by increasing the filler content indicating the high compatibility between matrices and PU_H/FCCNs • Increases of tensile modulus and elongation at break by 187% and 939% when embedded with 30 wt% composite nanofibres	192
	P(St-co-GMA) /MWCNTs	• Epoxy	• Considerable improvement in flexural modulus up to over 20% by embedding a very low content of composite fibres at 0.2 wt%	198
	TPU/MWCNTs	• Epoxy	• Improvement up to 29% in tensile strength, 4% in elastic modulus and 19% in tensile strain for composites compared with those of neat epoxy with inclusions of 3 wt% MWCNTs	159
	PS/TiO_2	• PBSA	• No significant differences observed in stress at yield and failure upon the addition of PS/TiO2 nanofibres, • Potential benefits of composites reinforced with electrospun fibres as fillers and/or reinforcing networks for the preparation of tunable polymer-based composites. • Adjustable hydrolytic degradation by varying the TiO2 content	199

Core-Shell Structure	PAN/PMMA	• Bis-GMA/TEGDMA	• Improvement in mechanical properties due to the formation of semi-IPN structure between fibres and matrices • Improvement of work of fracture by 64.8% with 7.5 wt% core-shell nanofibres compared with that of neat resin • Ability of core-shell nanofibres as a drug delivery carrier by a sustained release of NaF • A slight decrease in flexural strength and modulus by increasing the PMMA thickness	182 158
Core-Shell Structure	Nylon 6/PMMA	____	• Proposed different method for fabricating nanocomposites by stacking and hot pressing core-shell nanofibres • Increases in tensile strength and modulus by 20% and 32% for nanocomposites, respectively, compared with those of pure PMMA plate	188
	PA-6/PMMA	____	• Fabricating nanocomposite by hot pressing multilayers of core-shell nanofibres • Increases of tensile properties of composites using core-shell nanofibres to nearly 20% with a minor loss less than 10% in transparency	200
	SBS/PAN	• Epoxy Resin	• Improvement on Charpy impact energy by 150% with 4 wt % aminated core-sheath fibres	202
Thorn-like Structure	PEN stems/FePc thorns	• Epoxy Resin	• Strong fibre-matrices interface formation due to the thorn-like structure that could tie molecules and interlock with surrounding epoxy leading to improved flexural properties of composites • Increase in storage modulus and decrease in damping ratio • For 6 wt% thorns-like fibres embedded composites, increases in flexural strength and modulus by 36% and 38%, respectively, compared with those of neat resin.	190 163

Fibre Alignment	Cellulose	• Epoxy	• With same amount of fibre content, increases in mechanical strength and Young's modulus by 71 and 61%, respectively for composites reinforced with aligned fibres compared to those of randomly oriented counterpart. • No effect of fibre alignment on composite transparency • A significant increase in tensile strength in the longitudinal direction for aligned fibre reinforced composites (7 times of randomly oriented counterparts)	181
	PI	• PA6	• Similar tensile strengths in the longitudinal and transverse direction	204
	PAN	• PMMA	• 40% and 30% improvements in tensile strength and Young's modulus for aligned nanofibre reinforced composites In comparison with randomly oriented nanofibre reinforced counterparts • More improvement in stiffness of composites in glassy and glass-rubber transition states by employing aligned fibres compared to randomly oriented counterparts	180
	PAN-g-PDMS	• Silicone Elastomer	• Better extensibility and toughness for nonwoven orientation due to "fracture and replacement" mechanism • Higher stiffness for aligned fibre composites due to the unidirectional fibres arrangement	191

Fibre Modification

Tang et al.[183] demonstrated the effect of affinity between nanofibre and matrices on resulting composite performance by comparing the reinforcement capability of hydrophobic cellulose acetate (CA) and hydrophilic cellulose nanofibrous mats on PVA composites fabricated again by a solution impregnation method. The fracture surface of CA based composites revealed the presence of interfacial debonding

due to poor wettability of CA with PVA; whereas strong interfacial adhesion due to hydrogen bonding interaction was observed for cellulose nanofibrous composites. As a result, the addition of 40 wt% CA and cellulose nanofibres to PVA matrices showed higher Young's moduli by 4.8 and 11 times than that of neat PVA film, which signified the effect of interfacial adhesion on mechanical performance. Liao et al.[184] also illustrated the influence of surface chemistry and roughness of electrospun fibres on epoxy matrices. By means of a solution impregnation technique, epoxy composites were fabricated with three different electrospun mats, namely CA, polyurethane (PU) and PU/CA composites. The cross sectional morphology of composites reinforced with PU demonstrated interfacial debonding and pull-out of nanofibres due to their smooth surfaces. CA led to a strong interfacial adhesion because of the hydrogen bond between fibres and matrices and its rough surface. This interfacial adhesion was directly reflected on the mechanical performance of composites. The maximum strength was observed for epoxy/CA nanofibre composites with the fibre content of 23 wt%, which was improved by 3.4 times compared to that of pure epoxy. These difference in interfacial interactions also influenced the visible light transmittance of composite films. The best and worst optical properties were observed for epoxy/CA and epoxy/PU films, respectively.

Consequently, for the purpose of improving the fibre-matrix interfacial interaction, the application of surface-modified nanofibres has been considered. Chen et al.[185] silanised electrospun glass nanofibres with two different functional groups of amine and epoxy. The modified nanofibres were used to strengthen epoxy resin. Generally, silane treated nanofibres demonstrated a better mechanical performance when compared to their untreated counterparts, due to the stronger interface between modified nanofibres and matrices. The addition of 1 wt% untreated glass fibres, treated glass fibres with epoxy and amine groups improved the elastic moduli by 33, 40 and 201%, as well as work of fracture by 52, 67 and 22%, respectively. Epoxy treated fibres showed a better toughening effect while amine treated fibres revealed a higher degree of reinforcement on account of the difference in interfacial strength resulting from different processing methods. During the preparation of composite resins, the epoxy functional groups on electrospun glass nanofibres with epoxy end groups (G-EGNFs) did not react with epoxy molecules in matrices until the curing process; whereas the amine functional groups on A-EGNFs reacted with epoxy molecules and form chemical bonds prior to curing process, resulting in a stronger fibre-matrix interfacial bonding strength than that of G-EGNFs.

Electrospun cellulose diacetate nanofibres were alkali treated, and then integrated into cellulose diacetate matrices by film casting in order to fabricate cellulose based composites.[205] Alkali treatment of

cellulose diacetate nanofibres removed acetyl groups and induced crystallinity. The inclusion of 15 wt% nanofibre treated for 7 hours in cellulose diacetate matrices increased tensile strength and elastic modulus by 1.7 and 2.2 times, respectively. Such a finding could result from the dual effect of increases in nanofibre crystallinity induced by alkali treatment as well as the good compability with cellulose diacetate matrices due to the presence of residual acetyl groups.

Ozden et al.[170] studied the reinforcement capability of three different electrospun polymer fibres embedded into epoxy, including polystyrene (PSt), poly(styrene-co-glycidyl methacrylate) P(St-*co*-GMA) and P(St-*co*-GMA)/ ethylenediammine (EDA). The latter was sprayed with EDA as a supplementary cross-linking agent before embedded into epoxy resin. DMA analysis revealed that the storage modulus of P(S-co-GMA)/EDA fibre-reinforced epoxy composites was 10 and 2.5 times higher than that of neat and P(S-co-GMA) fibre-reinforced counterparts, respectively. Besides, the addition of 0.2 wt% P(S-co-GMA)/EDA fibres within epoxy matrices increased flexural modulus of composites by 30% with respect to that of epoxy. Substantial increase in mechanical response could benefit from cross-linking fibre surface and surface modification of electrospun fibres leading to improved fibre-matrix interfacial bonding.

Fabrication Method

Apart from fibre characteristics and structure, wetting and fabrication methods also play a significant role on composite properties. Altered wetting procedure could result in a drastic change in the morphology of wet fibres, in turn influencing resulting composite properties.

Jiang et al.[164] applied two different wetting methods to fabricate melamine-formaldehyde (MF) composites reinforced with electrospun nylon-6 nanofibre mats. One method was dip-coating of nanofibre mats into a melamine−formaldehyde−water solution. The other was to pass a MF solution through the nylon-6, which is similar to the liquid filtration method. After wetting of nanofibres, two impregnated sheets were dried and then hot pressed. Compared to the immersion method, passing through the MF solution resulted in the formation of a core-shell morphology and significant improvement in properties. The incorporation of fibre mats with almost the same fibre content from the filtration method led to tougher composites (17.6 J/g) relative to those using the dip-coated wetting method (7.8 J/g). This result was ascribed to an irregular and incomplete wetting procedure in the dip coating method. Later a novel layer-by-layer (LBL) composite fabrication method was proposed based on solution casting, electrospinning and film stacking to prepare highly transparent TPU composite films reinforced with nylon-6 nanofibres with small amounts of reinforcing fibres.[186] First, a PU solution was

cast on a glass slide, and then nanofibres were directly spun on thermoplastic solutions for different time intervals to control their amounts prior to drying. Nanocomposites were prepared by repeating this procedure. A very small amount of nylon fibres (0.4 wt%) could enhance mechanical properties significantly without sacrificing optical properties like the transparency of TPU. The coaxial electrospinning of core-shell composites followed by hot-press treatment is another way to fabricate composites with the provision of a better distribution of reinforcing element and less voids at the interfaces.[188]

Transparent Composites

The fabrication of optical transparent or translucent fibre-reinforced composites is useful for some applications. Compared with traditional reinforcing fibres, the ultrathin size of electrospun fibres with fibre diameters smaller or close to the wavelength of a visible light (400-700 nm) as reinforcements can be a significant advantage in the development of transparent composites.[174,188] The effect of nanofibre content on transparency was investigated, which confirmed that the light transmittance decreased with increasing the fibre content in composite films because of increasing interfacial areas.[164,174,175,181,186] The differences in refractive index between the fibres and polymer matrices as well as the nanofibre dispersion in matrices should also be considered.[162,174] Fibre diameter is another factor that has a significant effect on the light transmittance of electrospun nanofibre reinforced composites. Larger fibre diameter could lead to a reduced transparency.[183,188] Moreover, the stronger interfacial adhesion improves the transparency of resulting composites.[162,183,184,200] It was indicated that fibre alignment did not affect the light transmittance of composite films, as compared to the aforementioned parameters.[180,181]

Interface Reinforcement of Composite Laminates

Due to the ply-by-ply nature of composite laminates, delamination is often the dominating failure mode in composite laminates subjected to impact and fatigue loading. It is a crack that is formed between adjacent plies. The appearance of delamination damage greatly reduces the stiffness and strength of a structure with the possibility of serious failure during service.[206-209]

In order to enhance delamination resistance, one must increase the interlaminar strength and fracture toughness at the delamination front.[210] Various methods have been applied to mitigate the delamination such as matrix-toughening[211,212], the addition of small particles[213,214], optimisation of stacking sequence[215-217], laminate stitching[218,219], braiding technique[220,221], edge cap reinforcement[222] and

critical ply termination[223]. Employing these methods improves the delamination but leads to the geometric alteration and significant cost or weight penalties. Dzenis and Reneker[224] patented the idea of a novel method to improve delamination resistance by the incoporation of small-diameter fibres at ply interfaces. A nano-interlayer in the form of polymeric nanofibrous non-woven mats was fabricated via electrospinning process into ply-to-ply interfaces of composite laminates. Unidirectional graphite/epoxy prepreg T2G190/F263 were interleaved by non-woven electrospun PBI fabrics with fibre diameters ranging from 300-500 nm. It was found that with a minimal increase of laminate weight, laminates with nano-reinforcements at the interface exhibited substantial increase in interlaminar fracture resistance compared to their unmodified counterparts. For Mode I and Mode II fracture, the critical energy release rates were increased by 130 and 15%, respectively. It was shown that the incorporation of an entangled nanofibrous layer within laminated composites might contribute to improved interlaminar fracture resistance, much like the ‘‘hooks and loops’’ in Velcro. [225]

Using nanofibrous layers can be a feasible way to reduce the stress concentration (due to the mismatch of ply properties) and to bond adjacent plies. By this means, it would not reduce in-plane properties or else increase composite weight or laminate thickness.[206,226] Depending on loading conditions, delamination growth can be categorised as an opening mode (mode I), a sliding mode (mode II) or a tearing mode (mode III). To characterise these modes, a strain-energy release rate was defined with their critical values known as G_{IC}, G_{IIC} and $G_{IIIC,}$ respectively, representing interlaminar fracture toughness.[227]

Nanofibre mats can be deposited between laminate layers manually[209,228] or can be placed by directly spinning on to the surface of the reinforcement[229-231]. The latter method is preferable in this case since nanofibre mats are not damaged during transport or processing. Moreover, direct deposition results in a slightly better mechanical response of nanoreinforced laminates compared to the insertion of nanointerlayers, which is possibly due to the direct contact that facilitated the load transfer.[232]

The double cantilever beam (DCB) and end-notch flexure (ENF) are the most used testing methods to evaluate interfacial mechanical properties (i.e. interlaminar fracture toughness and fracture energy).[233] In particular, the DCB testing procedure is used to evaluate the critical normal energy release rate G_{Ic}, while by using the ENF test the critical shear energy release rate G_{IIc} can be obtained.[233]

Nanofibre interleaved composites (AS4/3501-6) were compared with those of commercial thermoplastic particles interleaved composites (T800H/3900-2).[234] Notwithstanding comparable improvement in

fracture toughness resistance and impact damage resistance, nanofibre interlayered composites were accompanied with no weight penalty or loss of in-plane properties. Nano-fabric interleaving marginally increased the laminate thickness while it increased the threshold impact force by about 60%, reduced the rate of impact damage growth to one-half with impact height, and also decreased the impact damage growth rate from 0.115 to 0.105 mm^2/N as a function of impact force.[235] Later Sihn et al.[210] found that the number of microcracks generated from delamination stresses during uniaxial tension loading decreased by about 22% after the incorporation of electrospun polycarbonate nanofibres (average diameter of 200 nm) in the inter-ply regions of carbon fibre reinforced composites.

Based on a report[236] demonstrating the toughening effect of polysulfone (PSF) film through the mechanism of reaction-induced phase separation, Li et al.[231,237] investigated its toughening effect in form of electrospun fibrous mats by interleaving carbon fibre/epoxy prepreg plies with electrospun PSF nanofibres, and then followed by hot pressing. Complete phase separation occurred during the curing at high temperatures and spherical PSF particles were formed. Due to the high porosity and high specific surface area of nanofibrous mats, they could be well-impregnated and evenly distributed. It was found that PSF spheres at diameters of 2–6 μm, with uneven distribution can be attributed to the high scattering of nanofibre diameters. In contrast, PSF films were formed locally with a uniform distribution of PSF spheres. The mode I fracture toughness of nanofibres reinforced composites was 140 and 280% higher than those of PSF films toughened and untoughened composites respectively, due to the homegeneous dispersion of PSF spheres. Their research was expanded by directly electrospinning epoxy-based functional MWNT (MWNTs-EP) /PSF hybrid nanofibres onto carbon fibre/epoxy prepeg to toughen and reinforce CFRP composites concurrently.[238] By increasing MWNTs-EP loading in hybrid fibres up to 20 wt%, the flexural strength and modulus of laminate composites were enhanced by 13.3 and 22.8%, respectively. This finding may benefit from the improvement in interfacial interactions between matrix-fibre and the reinforcement effect of aligned MWNTs-EP. When MWNTs-EP content was less than 5 wt%, a negligible increase in mode II interlaminar fracture toughness was noted. Furthermore, it reached its peak with 48.4% improvement at the MWNTs-EP loading of 10 wt%, compared to that of PSF nanofibre reinforced CFRP composites.

The efficiency of P(St-co-GMA) copolymer and P(St-co-GMA)/MWCNT based nanofibres as interlayers on conventionally unidirectional carbon fibre reinforced epoxy composite laminates was assessed.[239] The resistance against delamination was measured in mode II by end notched flexure (ENF) tests; whereas transverse matrix cracking resistance was characterised by transverse Charpy impact tests and

transversal tension test. Improvements up to 70 and 20% in mode II strain energy release rate (G_{IIc}) and impact energy absorbance were recorded for the laminates with nanocomposite interlayers. The integration of P(St-co-GMA) and P(St-co-GMA)/MWCNTs interlayers increased transverse tensile strength up to 17 and 27%, corresponding to non-interlayered specimens, respectively. This improvement was due to the compatibility of interlayers with the surrounding matrices, resulting in the improved resistance against matrix cracking. It also confirmed the ability of P(St-co-GMA) nanofibres as an effective interlayer. In their subsequent work,[240] it was reported that the longitudinal tensile strengths of uni-directional and 0/90 twill woven carbon fibre/epoxy prepreg interlayered by P(St-co-GMA) nanofibre were increased by 12 and 18%, respectively. Moreover, the concept of localised interlayer toughening laminates was assessed by adding interlayers just in the vicinity of highly stressed region of the 0/90 twill weaved laminates. Open-hole tension test exhibited 9% increase in maximum failure strength, suggesting that the localisation procedure provided efficiency in both use of time and material compared to the interlayer application on the entire ply surfaces.

Magniez et al.[241] electrospun poly(hydroxyether of bisphenol A) (phenoxy) nanofibres directly onto a pre-impregnated carbon fibre material (Toray G83C) at various concentrations of 0.5 - 2 wt %. The fracture toughness in mode I and mode II was improved by up to 150 and 30%, respectively. These improvements were ascribed to the formation of inverse phase domain morphology through complex micromechanisms of failure. During curing, phenoxy diffuses through epoxy resin to form a semi interpenetrating network with an inverse phase type of morphology where epoxy became the co-continuous phase with a nodular morphology. Moreover, interlaminar shear stress was quite similar for pristine and reinforced composite laminates, indicating interleaving did not affect in-plane stiffness of composites.

Zhang et al.[242] stressed the critical effect of polymerisation-induced phase separation for toughening interlayers by thermoplastic nanofibres. Three different electrospun nanofibres of PCL, poly(vinylidene fluoride) (PVDF) and PAN were utilised between carbon/epoxy composites layers, and their effect was compared with the consideration of relevant toughening mechanism. The results showed that only PCL could toughen epoxy due to the polymerisation-induced phase separation with epoxy. PAN and PVDF only demonstrated an indiscernible toughening effect. On the other hand, Magniez et al.[243] observed a 57% increase in mode II interlaminar fracture toughness accompanied by slightly decreases in mode I fracture toughness (20%) for carbon-fibre reinforced composites toughened with PVDF nanofibres. The

decrease in mode I toughness was attributed to the complexity in the micromechanisms of failure during mode I testing.

Saghafi et al.[244] ascribed the different toughening behaviour of PVDF in previous work[242,243] to the curing processes. Specimens were cured at two designated temperatures,[242,243] namely 150 and 175 ˚C. In the former, the nanofibre did not melt but in the latter the nanofibres were fully melted. Saghafi et al.[234] claimed by employing an appropriate curing process and thickness of nanofibrous mats, the addition of PVDF nanofibres could increase the fracture toughness in mode I. With the use of a 4-step cycle curing process, the fracture toughness was improved by 43 and 36% in the initiation and propagation stages of fracture, mainly because of plastic deformation of matrices and melted PVDF.

As for GFRP, it was stated that PVDF nanofibres are not a very good choice for toughening epoxy and improving the impact damage resistance of resulting laminates.[245] Maximum absorption energy of interleaved composites for nanofibre mats with thickness of 39 and 64 μm was increased by only 9.5 and 13.4%, respectively, as a result of bridging mechanism during failure. With the incorporation of PCL nanofibres, the total impact energy was not changed but the damage area was decreased by almost 27% owing to the phase separation mechanism of PCL during curing process.[246] Clerck et al.[247] highlighted the influence of nanofibre configuration on the interlaminar toughening of epoxy/glass fibre composite laminates reinforced by PCL nanofibre nonwovens using resin transfer moulding. Three different configurations were applied, namely a single layer of nanofibres that was directly electrospun on one side of glass fibre mats (SLD), one layer of nanofibres electrospun on each side of glass fibre mats (DLD) and one layer of nanofibre nonwovens placed in between the glass fibre mats (IL). Embedding PCL nanofibres improved the fracture toughness of laminates due to a good adhesion of deposited nanofibres onto glass fibre mats, as well as inherently tough and ductile properties of PCL nanofibres. This resulted in the bridging of glass fibres and crack path deflection effect during the initiation of delamination. In the case of DLD, the delamination crack propagated partially through the nanofibre toughened interlayers while in the SLD configuration, the crack path stayed preferentially above nanofibrous layers. Hence, the DLD arrangement casued superior effect on the interlaminar toughness of composites to other configurations. By incoporating 20 g/m^2 of PCL nanofibres, a 100% improvement in fracture toughness was reported for the DLD configuration.

The toughening effect of electrospun tetra ethyl orthosilicate (TEOS) nanofibres on mode I fracture toughness of glass fibre/epoxy composite laminates was investigated by Kelkar et al.[248] No improvement was observed, which may be ascribed to the insufficient amount of electrospun nanofibre layers. Hence

no significant difference could be found in the mode I fracture toughness since only one layer was inserted between 10 layers of glass fabrics. In their recent attempt[249], a different procedure was employed by modifying resin using different contents of chopped electrospun TEOS nanofibres. The unmodified resin and nanofibres modified resin were then used to fabricate glass fibre reinforced polymer composites (GFRP) using the heated vacuum-assisted resin transfer moulding (H-VARTM) method. 0.6 wt% of TEOS nanofibres in epoxy resin offered the enhancement in intelaminar shear strength of 15% with respect to their unmodified counterpart.

Hamer et al.[250] fabricated epoxy/carbon interleaved composite laminates with electrospun nylon 6,6 nanofibril mats (fibre diameter: 500 nm) and commercial spun-bonded nonwoven mats (CEREX®, fibre diameter: 20 μm). In comparison with CEREX®, nylon 66 nanofibril mats demonstrated weaker fibre-epoxy adhesion. Nevertheless, mode I interlaminar fracture toughness was improved by 337-425% and 255-322%, respectively, compared to that of pristine laminates. The combination of bridging fibres and creation of a plastic zone mechanism was attributed to this improvement, for which, in the case of electrospun nanofibres, due to the weak fibre-epoxy adhesion, the latter mechanism was responsible. Pallazetti et al.[206] showed when the laminates were subjected to interlaminar crack propagation, the presence of nylon 66 nanofibrous mats placed at the mid-plane of epoxy /carbon fibre composite laminates increased the absorbable amount of mechanical energy under mode I and mode II loading conditions by 23 and 8%, respectively, as opposed to virgin laminates. Reinforcing nylon 66 nanofibril mats with MWCNTs resulted in higher improvements of fracture energy in both modes I and II relative to neat nylon 6,6 nanofibres.[251] The addition of MWCNTs increased the stiffness of nanofibril mats and also facilitated the formation of a plastic zone near the crack tip in both loading modes, thereby causing a further increase in fracture toughness.

It is possible to benefit from the efficiency of individual nanofibres in mode I and mode II by combining appropriate nanofibres. For this purpose, electrospun nylon 6,6, PCL and nylon 6,6/PCL mixed nanofibres were placed at the mid-plane of epoxy/unidirectional glass composite laminates, which were further subjected to DCB and ENF fracture tests.[252] The effect of PCL nanofibres on energy release rate for both modes was quite similar, with 25 and 24% increases in G_I and G_{II}, respectively. On the other hand, nylon 66 was only useful for mode II loading with a 68% improvement in G_{II} as compared to a modest increase of 4.5% for mode I. The combination of these nanofibres gave rise to the exploitation from each nanofibres in modes I and II. Nylon 6,6/ PCL mixed nanofibres possessed 21 and 56% increases in G_I and G_{II}, which were between the values of individual nanofibres. The fracture surface

proved that the melting behaviour of PCL nanofibres acting as a secondary phase while nylon 6,6 presented a rubbery behaviour. The incorporation of nylon 6,6 in laminates decreased the release rate of strain energy by 3% at the propagation stage. Microscopic analysis indicated that the shortage of nylon 6,6 at the propagation stage was derived from the crack deviation to non-modified layers.[253]

A hybrid multi-scaled composite made of conventional carbon fibre fabrics with the interlaminar region containing electrospun nanofibre mats can be fabricated by two different methods. One is to prepare carbon nanofibres in advance with thermal treatments of electrospun PAN copolymer nanofibres.[228] The other is to directly electrospin PAN copolymer nanofibres onto carbon fibre fabrics with different collection time, and then use the thermal treatment by carbonisation in argon environment[230]. In general, the presence of nanofibres deflect the microcrack and increase the resistance to crack propagation. Moreover, the interfacial bonding was improved due to the high specific surface areas of carbon nanfibres, and thus increased the flexural strength of composites. Interestingly, the higher mechanical performance was obtained from direct electrospinning compared to other methods to prepare carbon fibres in advance. This behaviour was related to the difference in the thickness of nanointerlayers that in the former method was 20 μm and for the latter was 40 μm. The thickness of nanoreinforcement between two laminas has a significant effect on mechanical properties of composites and the maximal penetration to each laminar/ply by nano-reinforcements was 10 μm.[254] Hence, the optimal thickness of nano-reinforcements should be 20 μm or less. The optimal time period for nanofibre collection on carbon fibre fabrics was 10 min. As a result, composites demonstrated improvements in flexural strength, elastic modulus and shear strength of 23.5, 105 and 221%, respectively, compared to typical epoxy/carbon fabric composites. Increasing the collection time led to a decrease in mechanical performance of composites, which might result from increasing nanofibre defects and easy separation of copolymer nanofibres from carbon fabrics (Figure 42).

Using a different method, multi-scaled hybrid composites with woven fabrics of conventional carbon fibres were manufactured using electrospun carbon nanofibres, vapour growth carbon nanofibres (VGCNFs) and graphite carbon nanofibres (GCNFs) for the preparation of nano-epoxy resins. Prepared resins were further investigated for the fabrication of composites via VARTM technique.[255] The incorporation of electrospun carbon nanofibres outperformed GCNFs and VGCNFs. In case of electrospun carbon nanofibres, the impact absorption energy, interlaminar shear strength and flexural strength of composites were improved by 79.1, 42.2 and 13.6% respectively. Such an improvement arose from better matrix-fibre interfacial bonding. By increasing the nanofibre content over 0.3 wt%, the

mechanical performance of composites deteriorated due to the nanofibre agglomeration or filter-out of nanofibres by carbon fabrics. Due to the formation of aggregation during the treatment process in case of GCNFs nanofibres, they demonstrated a slightly lower reinforcing effect compared to electrospun carbon nanofibres and VGCNFs nanofibres. Similarly, multi-scaled hybrid composites were fabricated from nano-epoxy resins containing electrospun glass nanofibres and conventional glass microfibres.[256] Superior mechanical performance was obtained from electrospun nanofibres relative to microfibres. It was believed to be induced by higher mechanical strength and larger surface areas of nanofibres. The optimum fibre content was determined to be 0.25 wt% to improve flexural strength, tensile strength and work of fracture by 86.2, 69.4 and 90% for glass nanofibres, as well as by 58.7, 36.2 and 50%, respectively, for glass microfibres when compared to epoxy/carbon fabric composites.

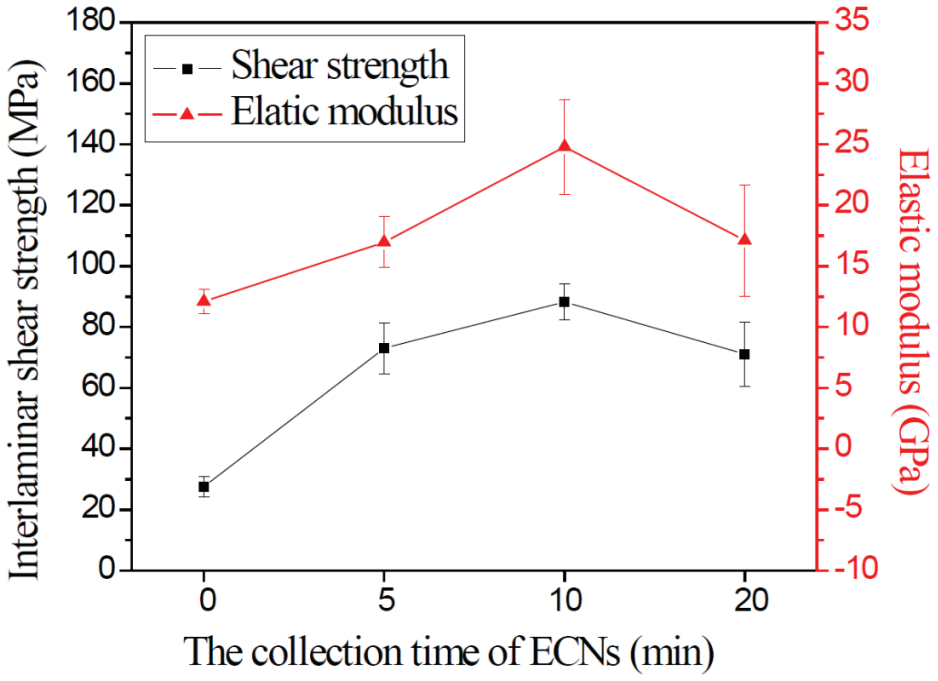

FIGURE 42 Interlaminar shear strength and elastic modulus of epoxy composites reinforced with conventional carbon fibre fabrics (CF) or electrospun carbon nanofibre-carbon fibre fabrics/mats (ECN-CF); the time periods for collection of electrospun PAN copolymer (precursor) nanofibres on CF fabrics were set at 0 (i.e., CF fabrics without ECNs), 5, 10 and 20 min, respectively. Reproduced from Ref. 230, with permission from Elsevier.

The toughening effect of PCL[242] and polyetherketone cardo (PEK-C)[229] nanofibres with different diameters on epoxy/carbon composites was investigated. Both nanofibres improved the fracture toughness due to the phase separation of nanofibres with epoxy matrices during curing. The increases of strain energy release rate for crack initiation ($G_{IC\text{-}INI}$) for PEK-C nanofibres with diameters of 450, 750

and 950 nm were 65, 51 and 60%, respectively. In comparison, PCL nanofibre modified composites achieved 55, 92 and 87% increases in $G_{IC\text{-}INI}$, when nanofibres with diameters of 103, 125 and 210 nm were used. However, the enhancement in strain energy release rate for crack propagation ($G_{IC\text{-}PROP}$) was less significant for PCL nanofibre modified composites than PEK-C nanofibre modified composites. Moreover flexural properties of PEK-C interleaved composite laminates were remarkably decreased when thick fibres (fibre diameter: 950 nm) were used. Nanofibres with larger fibre diameter caused higher local concentration of PCL or PEK-C in epoxy resin, resulting in larger PCL-rich or PEK-C-rich particulate phases. During the delamination process, with the same fibre loading, fibres with smaller diameters caused better improvements in interlaminar properties by stabilising crack propagation due to the reduced distance between the PEK-C or PCL phases without sacrificing composite in-plane performance (Figure 43(a)). The effect of interlayer thickness was investigated for PEK-C reinforced composite laminates as well. It was found that by increasing the thickness, the fracture toughness was improved at the expense of flexural performance. The critical energy required for the propagation of crack initiation was increased by almost 60 and 80%, respectively, in the case of mat thickness of 70 and 105 µm (Figure 43(b)).

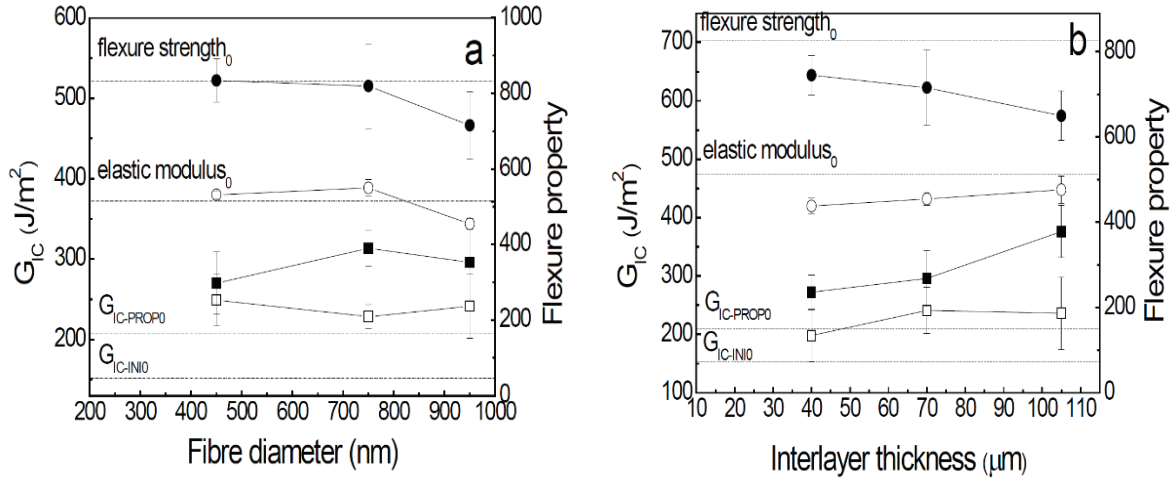

FIGURE 43 Mode I delamination fracture toughness and flexural properties of nanofibre modified composites as a function of (a) nanofibre diameter and (b) interlayer thickness. Reproduced from Ref. 229, with permission from Elsevier.

Pallazetti et al.[257] noted that material characteristics were dependent upon the loading conditions of electrospun fibres with different diameters. In the mode I condition, the smaller diameter resulted in better laminate response. According to mode II test results, small nanofibres were preferable if the nanoreinfocements were used to increase the energy absorption capability of composite laminates. It

appeared that a larger diameter was more suitable to increase the maximum load that specimens could carry. When the effect of nanolayer thickness of nylon 6,6 nanofibres on epoxy/woven carbon fibre composites was assessed, DCB tests revealed that a poorer mechanical response of interfaces occurred by increasing the nanoreinforcement thickness from 25 to 50 μm. Consequently, thinner nanolayers were more effective to reinforce the interface subjected to mode I loading. However, Alessi et al.[258] reported a 50% improvement for initial fracture toughness under mode I loading for nylon 6,6 interleaved CFRP laminates with little difference for interlayers at the thickness of 210 and 100 nm. Palazzetti[259] investigated the influence of number of nylon 6,6 interlayers (10, 16 and 18 layers) in glass fibre reinforced composites under mode II fracture. The effectiveness of interleaving was observed in composite laminates made of 10 and 16 layers, while for thicker specimens the effect of reinforcement was almost negligible. Moreover, the influence of fibre materials on reinforcement performance was evaluated by comparing the ENF test result of unidirectional prepegs including epoxy/glass fibre and epoxy/carbon fibre composite laminates interleaved with nylon 6,6 nanofibres. It was stated the fibre materials had an important role in the nanofibre reinforcement mechanism. Carbon specimens exhibited a significant higher ratio of "$\sigma_{max}/\sigma_{max\ Virgin}$" compared to their glass fibre counterparts where σ_{max} and $\sigma_{max\ Virgin}$ represent maximum stresses for composites and virgin material, respectively.

Liu et al.[260] assessed the effect of both the type of electrospun polymeric nanofibres and mat thickness used as ply-to-ply interleaving material in epoxy/ glass microfibre composite laminates. Three types of electrospun nanofibres with different mechanical behaviour including nylon 6 (fibre diameter 150-500 nm), epoxy 609 (fibre diameter 350-1200 nm) and TPU (fibre diameter 300-600 nm) with mat thickness in range of 20–150 μm were prepared. A critical thickness for each of three types of nanofibrous membranes was observed, below which no effect or even increasing role on the flexural and shear strengths as well as flexural modulus of laminated composites took place. SEM analysis demonstrated that better impregnation led to higher mechanical properties which would be hard to achieve by increasing the mat thickness. The different values of critical thickness measured for tested polymers were ascribed to the different ability of matrices to impregnate materials. Moreover, by choosing a suitable nanofibre material, the mechanical performance of composites could be well tailored. Subsequently, the influence of thickness and their stacking position of ultrathin nanofibrous sheets on mode I (G_{IC})[209] and mode II (G_{IIC})[261] fracture toughness was also evaluated. In good accordance with the work from Liu et al.[260], the existence of threshold thickness values was reported in both modes of load conditions. As far as the stacking position of nanofibrous mats is concerned, it did not have significant variations in G_{IC} in spite of a significant influence on G_{IIC}.

The toughening effect of PAN nanofibres on both unidirectional and woven carbon fabric-reinforced epoxy composites was investigated.[226] The incorporation of about 50 wt% nanofibres improved the interlaminar shear strength and flexural modulus of composites by 11 and 54% for unidirectional fabrics and by 7 and 13% for woven fabrics, respectively, when compared to those of pristine laminates. The difference in improvement was caused by the fabric structure. The waviness and complex geometry of interacting surfaces for woven fibres resulted in a moderate improvement in interlaminar shear strength. However, surprisingly a significant increase in impact energy was found in Charpy impact test as composites hit parallel to the plane of reinforcing layers and the toughening interleaves with the initiation energy increasing three-fold.

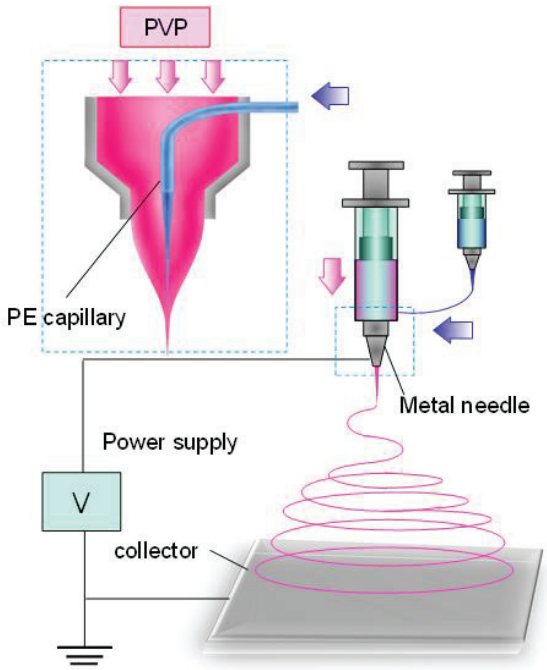

Figure 44 Coaxial electrospinneret and fibre spinning process. Reproduced from Ref. 262, with permission from Wiley Periodicals, Inc.

An alternative, rather new and promising approach was proposed by Park and Braun[262] in which coaxial electrospinning was adopted to create a network of core-shell fibre morphology with beads on strings to release healing substances in an epoxy matrix. A dimethylsiloxane healing agent was coaxially electrospun into poly(vinyl pyrrolidone) fibres, resulting in beads of healing agents on a polymer string (Figure. 44). Fibres containing the healing agents were electospun onto substrates and then coated with

an optical adhesive polymer to form a thin film. It was demonstrated that the healing substances were homogeneously distributed throughout the matrices by using electrospun fibres, and effectively imparted a healing capability to the coating even upon repeated crack induction.

Sinha-Ray et al[263] encapsulated two types of healing agents inside polymer nanofibres using three different techniques including coelectrospinning, emulsion electrospinning and emulsion solution blowing. The presence of healing agents in the core was confirmed. Further to validate the deliverability of self-healing agent at composite interfaces, epoxy/carbon fibre composites reinforced with ultrathin nanofibrous interlayers of self-healing core–shell nanofibres were fabricated. The SEM-based fractographical analysis showed a failed core–shell structure with an empty core region due to the release of healing agents. Moreover pull-out, debonding, breakage, plastic necking, matrix cracking and related stress shielding and crack kinking in failure modes of matrix interlayers were observed, which suggested a significant strain-energy dissipation compared to pure resin failure.

In another work,[264] flexural stiffness recovery was investigated for composites reinforced with carbon fibres using electrospun core-shell nanofibres to deliver the healing agents. Ultrathin core–shell nanofibre mats loaded with healing agents, with a diameter of several hundred nanometers to several micrometers, were coelectrospun. Using the wet lay-up that is followed by the vacuum-assisted resin transfer molding process, these nanofibres were incorporated at 4 laminate interfaces of an epoxy composite with unidirectionally preimpregnated and cross-woven carbon fibre plies, containing 0.5 wt% Grubbs catalyst in epoxy matrices. To evaluate the damage-healing efficiency of composite laminates after pre-damage, three-point bending tests were performed. Samples were bent until interlaminar cracking occurred, and then they were allowed to self-heal for 2 hours at room temperature. It was shown after the three-point pre-damage test, the flexural stiffness was decreased substantially from the 144.8–163.9 kN/m to 46.3– 61.2 kN/m. After 2-hour damage healing under free-loading conditions, the as-healed stiffness was increased up to 99.0–159.0 kN/m, yielding a flexural stiffness recovery of 70 to 100%.

CONCLUSIONS

Electrospun nanofibres have been demonstrated to be a good alternative reinforcement candidate for composites. In spite of possessing many ideal features required for good nanofillers (e.g. good mechanical performance, tunable chemical and physical properties, low cost and low density), relatively little work has been done in using electrospun nanofibres as potential reinforcements. The main reason for this is that electrospun polymers possess the mechanical properties that are lower than those of

their conventional counterparts. Hence there is a need to enhance mechanical properties of nanofibres by post treatment or through fabrication of electrospun nanofibre reinforced composites. Another limiting factor for the use of nanofibres as reinforcements is due to the restriction in the type of nanofibrous architecture that can be fabricated with. Typical architecture of electrospun nanofibres is nonwoven mesh. If further developments in electrospinning technology can be made to fabricate three-dimensional structures and nanofibrous yarns, the reinforcing potential of nanofibres can be more accurately assessed. Finally, a better understanding of reinforcement mechanism of electrospun nanofibres is anticipated through combined sophisticated experimental studies and theoretical modelling in the future.

REFERENCES AND NOTES

1. Q. T. H. Shubhra, In Natural Rubber Materials, Composites and Nanocomposites; S. Thomas, H. J. Maria, J. Joy, C. H. Chan, L. A. Pothen, Eds.; the Royal Society of Chemistry, **2014**; Vol. 2, Chapter 9, pp 247-289.
2. D. H. Reneker, J. Doshi, *Nanotechnology* **1996**, *7*, 216-223.
3. Y. Dzenis, *Science* **2004**, *304*, 1917-1919.
4. D. H. Reneker, A. L. Yarin, E. Zussman, H. Xu, *Adv. Appl. Mech.* **2007**, *41*, 345-346.
5. D. H. Reneker, A. L. Yarin, *Polymer* **2008**, *49*, 2387-2425.
6. W. J. Morton, US patent, 705691, **1902**.
7. J. F. Cooley, US patent, 692631, **1902**.
8. A. Formhals, US patent, 1975504, **1934**.
9. L. Larrondo, R. St. John Manley, *J. Polym. Sci. Polym., Phys. Ed.* **1981**, *19*, 909-920.
10. D. Li, Y. Xia, *Adv. Mater*. **2004**, *16*, 1151-1170.
11. Z. M. Huang, Y. Z. Zhang, M. Kotaki, S. Ramakrishna, *Compos. Sci. Technol*. **2003**, *63*, 2223-2253.
12. W. E. Teo, S. Ramakrishna, *Compos. Sci. Technol*. **2009**, *69*, 1804–1817.
13. A. Kulkarni, V. A. Bambole, P. A. Mahanwar*, Polym. Plast. Technol. Eng.* **2010**, *49*, 427-441.
14. N. Bhardwaj, S. C. Kundu, *Biotechnol. Adv*. **2010**, *28*, 325-347.
15. X. Hu, S. Liu, G. Zhou, Y. Huang, Z. Xie, X. Jing, *J. Control Release*. **2014**, *185*, 12-21.
16. A. Baji, Y-W. Mai, S-C. Wong, M. Abtahi, P. Chen, *Compos. Sci. Technol*. **2010**, *70*, 703-718.
17. A. L. Yarin, S. Koombhongse, D. H. Reneker , *J. Appl. Phys*. **2001**, *89*, 3018–3026.
18. F. Li, Y. Zhao, Y. Song, In Nanofibers; A. Kumar, Ed.; Intech: Croatia, **2010**; Chapter 22, pp. 419–438.
19. Z. Yanga, B. Xu*, J. Mater. Chem.* **2007**, *17*, 2385–2393.
20. P. X. Ma, R. Zhang, *J. Biomed. Mater. Res.***1999**, *46*, 60—72.
21. C. J. Ellison, A. Phatak, D. W. Giles, C. W. Macosko, F. S. Bates, *Polymer* **2007**, *48*, 3306-3316.
22. H. Li, Y. Ke, Y. Hu, *J. Appl. Polym. Sci.* **2006**, *99*, 1018–1023.
23. R. Sahay, P. Suresh Kumar, R. Sridhar, J. Sundaramurthy, J. Venugopal, S. G. Mhaisalkar, S. Ramakrishna, *J. Mater. Chem.* **2012**, *22*, 12953-12971.
24. A. Rogina, *Appl. Surf. Sci.* **2014**, *296*, 221-230.

25.D. Li, J. T. McCann, Y. Xia, *J. Am. Ceram. Soc*. **2006**, *89*, 1861–1869.
26.I. S. Chronakis, *J. Mater. Process. Technol*. **2005**, *167*, 283-293.
27.K. Molnar, L. M. Vas, In Synthetic Polymer-Polymer Composites; D. Bhattacharyya, S. Fakirov, Eds.; Hanser Pub Inc, **2012**; Chapter 10, pp 301-349.
28.K. M. Sawicka, P. Gouma, *J. Nanopart. Res*. **2006**, *8*, 769-781.
29.K. Y. Hwang, S-D. Kim, Y-W. Kim, W-R. Yu, *Polym. Test*. **2010**, *29*, 375-380.
30.D. H. Reneker, L. A. Yarin, H. Fong, S. Koombhongse, *J. Appl. Phys*. **2000**, *87*, 4531–4547.
31.Y. Ji, B. Li, S. Ge, J. C. Sokolov, M. H. Rafailovich, *Langmuir* **2006**, *22*, 1321-1328.
32.V. Pillay, C. Dott, Y. E. Choonara, C. Tyagi, L. Tomar, P. Kumar, L. C. du Toit, V. M. K. Ndesendo, *J. Nano Mat*. **2013**, *2013*
33.N. E. Zander, *Polymer* **2013**, *5*, 19-44.
34.C. Feng, K. C. Khulbe, T. Matsuura, *J. Appl. Polym. Sci*. **2010**, *115*, 756-776.
35.J. Yao, C. W. M. Bastiaansen, T. Peijs, *Fibers* **2014**, *2*, 158-187.
36.S. A. Theron, A. L. Yarin, E. Zussman, E. Kroll, *Polymer* **2005**, *46*, 2889-2899.
37.D. H. Reneker, A. L. Yarin, E. Zussman, and H. Xu, *Adv. Appl. Mech*. **2007**, *41*, 43-195.
38.X. F. Wu, Z. Zhou, A. Rahman, A. Bedarkar, In Nanostructures: Properties, Production Methods and Applications; Y. Dong, Ed; Nova Science Publishers Inc: New York, **2013**; Chapter 8, pp 247-286.
39.O. Jirsak, F. Sanetrnik, D. Lukas, V. Kotek, L. Martinova, J. Chaloupek, International Patent WO /2005/024101, **2005**.
40.H. Niu, X. Wang, T. Lin, *J. Textile Inst*. **2012**, *103*, 787–794.
41.B. Lu, Y. Wang, Y. Liu, H. Duan, J. Zhou, Z. Zhang, Y. Wang, X. Li, W. Wang, W. Lan, E. Xie, *Small* **2010**, *6*, 1612-1616.
42.H. Niu, X. Wang, T. Lin, In Nanofibers - production, properties and functional applications; T. lin, Ed.; InTech, **2011**; Chapter 2, pp 17-36.
43.M. R. Badrossamay, H. A. McIlwee, J. A. Goss, K. K. Parker, *Nano Lett.* **2010**, *10*, 2257–2261.
44.G. Taylor, Proc. R. Soc. London, Ser. A, *Math. Phys. Sci.* **1964**, *280*, 383–397.
45.D. H. Reneker, A. L. Yarin, H. Fong, S. Koombhongse, *J. Appl. Phys*. **2000**, *87*, 4531–4547.
46. T. A. Kowalewski, S. Blonski, S. Barral, *Bull. Pol. Acad. Sci., Tech Sci*. **2005**, *53*, 385–394.
47.M. M. Hohman, M. Shin, G. Rutledge, M. P. Brenner, *Phys. Fluids*. **2001**, *13*, 2201–2220.
48.A. L. Yarin, S. Koombhongse, D. H. Reneker, *J. Appl. Phys.* **2001**, *89*, 3018–3026.
49.J. J. Feng, *Phys. Fluids*, **2002**, *14*, 3912–3926.
50.J. J. Feng, J. Nonnewton. *Fluid. Mech*. **2003**, *116*, 55-70.
51.X. F. Wu, Y. Salkovskiy, Y. A. Dzenis, *Appl. Phys. Lett*. *2011*, **98**, 223108.
52.F. Jian, N. HaiTao, L. Tong, W. XunGai, *Chin. Sci. Bull*. **2008**, *53*, 2265-2286.
53.V. Shabafroozi, M. Mozafaril, D. Vashaee, L. Tayebil, *J. Nanosci. Nanotechnol*. **2014**, *14*, 522-534.
54.J. Fang, X. Wang, T. Lin, In Nanofibers - Production, Properties and Functional Applications; T. Lin, Ed; InTech, **2011**; Chapter 14, pp 287-326.
55.P. Lu, B. Ding, *Recent. Pat. Nanotechnol*. **2008**, *2*, 169-182.
56.E. P. S. Tan, C. T. Lim, *Compos. Sci. Technol*. **2006**, *66*, 1102-1111.
57.M. B. Bazbouz, G. K. Stylios, *J. Polym. Sci.* **2010**, *48*, 1719-1731.
58.F. Hang, D. Lu, R. J. Bailey, I. Jimenez-Palomar, U. Stachewicz, B. Cortes-Ballesteros, M. Davies, M. Zech, C. Bodefeld, A. H. Barber, *Nanotechnology* **2011**, *22*, 365708.
59.S-Y. Gu, Q-L. Wu, J. Ren, G. J. Vancso, *Macromol. Rapid Commun.* **2005**, *26*, 716-720.

60.E. P. S. Tan, S. Y. Ng, C. T. Lim, *Biomaterials* **2005**, *26*, 1453–1456.
61.K. H. Lee, H. Y. Kim, M. S. Khil, Y. M. Ra, D. R. Lee, *Polymer* **2003**, *44*, 1287-1294.
62.L. M. Hansen, D. J. Smith, D. H. Reneker, W. Kataphinan*, J. Appl. Polym. Sci*. **2005**, *95*, 427– 434.
63.X. Wei, Z. Xia, S-C. Wong, A. Baji, *Int. J. Exp. Comput. Biomech*. **2009**, 1, 45–57.
64.M. Richard-Lacroix, C. Pellerin, *Macromolecules* **2013**, *46*, 9473-9493.
65.S. Makaremi, Master Dissertation, University of Western Ontario, Canada, **2012,** Electronic Thesis and Dissertation Repository. Paper 1027.
66.U. Stachewicz, R. J. Bailey, W. Wang, A. H. Barber, *Polymer* **2012**, *53*, 5132-5137.
67.G. Mathewa , J. P. Hong, J. M. Rhee, H. S. Lee, C. Nah, Polym. Test. 2005, 24, 712–717.
68.S. Xu, A. Li, G. Poirier, N. Yao, *Scanning* **2012**, *34*, 341–346.
69.E. P. S. Tan, C. N. Goh, C. H. Sow, C. T. Lim , *Appl. Phys. Lett.* **2005**, *86*, 073115.
70.E. Zussman, M. Burman, A. L. Yarin, R. Khalfin, Y. Cohen, *J. Polym. Sci., Part B: Polym. Phys*. **2006**, *44*, 1482-1489.
71.E. Zussman, X. Chen, W. Ding, L. Calabri, D. A. Dikin, J. P. Quintana, R. S. Ruoff, *Carbon* **2005**, *43*, 2175-2185.
72.M. F. Yu, M. J. Dyer, G. D. Skidmore, H. W. Rohrs, X. Lu, K. D. Ausman, J. R. Von Her, R. S. Ruoff, *Nanotechnology* **1999**, *10*, 244-252.
73.M-F. Yu, O. Lourie, M. J. Dyer, K. Moloni, T. F. Kelly, R. S. Ruoff, *Science* **2000**, *287*, 637–640.
74.E. P. S. Tan, C. T. Lim*, Rev. Sci. Instrum*. **2004**, *75*, 2581-2585.
75.R. Inai, M. Kotaki, S. Ramakrishna, *Nanotechnology* **2005**, *16*, 208-213.
76.E. P. S. Tan, C .T. Lim, *Nanotechnology* **2006**, *17*, 2649–2654.
77.X. Zhang, R. Nakagawa, K. H. K. Chan, M. Kotaki, *Macromolecules* **2012**, *45*, 5494−5500.
78.B. Yuan, J. Wang, R. P. S. Han, *J. Mech. Behav. Biomed. Mater.* **2015**, *42*, 26-31.
79.Y. Li, C. T. Lim, M. Kotaki, *Polymer* **2015**, *56*, 572-580.
80.S-C. Wong, A. Baji, S. Leng, *Polymer* **2008**, *49*, 4713-4722.
81.C. T. Lim, E. P. S. Tan, S. Y. Ng, *Appl. Phys. Lett*. **2008**, *92*, 141908.
82.K. H. K. Chan, S. Y. Wong, X. Li, Y. Z. Zhang, P. C. Lim, C. T. Lim, M. Kotaki, C. B. He*, J. Phys. Chem. B,* **2009**, *113*, 13179-13185.
83.C-L. Pai, M. C. Boyce, G. C. Rutledge, *Polymer* **2011**, *52*, 2295-2301.
84.S. Y. Chew, T. C. Hufnagel, C. T. Lim, K. Leong, *Nanotechnology* **2006**, *17*, 3880-3891.
85.Z. Chen, B. Wei, X. Mo, C. T. Lim, S. Ramakrishna, F. Cui, *Mater. Sci. Eng., C.* **2009**, *29*, 2428–2435.
86.D. Papkov, Y. Zou, M. N. Andalib, A. Goponenko, S. Z. D. Cheng, Y. A. Dzenis, *Acs Nano* **2013**, *7*, 3324-3331.
87.F. Chen, X. Peng, T. Li, S. Chen, X-F. Wu, D. H. Reneker, H. Hou, *J. Phys. D: Appl. Phys.* **2008**, *41*, 025308.
88.M. Naraghi, I. Chasiotis, H. Kahn, Y. Wen, Y. Dzenis, *Rev. Sci. Instrum.* **2007**, *78*, 085108.
89.M. Naraghi, I. Chasiotis, H. Kahn, Y. Wen, Y. Dzenis *, Appl. Phys. Lett*. **2007**, *91*, 151901.
90.M. Naraghi, S. N. Arshad, I. Chasiotis, *Polymer* **2011**, *52*, 1612-1618.
91.D. Jaeger, J. Schischka, J. Bagdahn, R. Jaeger, *J. Appl. Polym. Sci*. **2009**, *114*, 3774–3779.
92.B. A. Samuel, M. A. Haque, B. Yi, R. Rajagopalan, H. C. Foley, *Nanotechnology* **2007**, *18*, 115704.
93.M. Naraghi, T. Ozkan, I. Chasiotis, S. S. Hazra, M. P. de Boer, *J. Micromech. Microeng*. **2010**, *20*, 125022.
94.S. N. Arshad, M. Naraghi, I. Chasiotis. *Carbon* **2011**, *49*, 1710-1719.
95.A. M. Beese, D. Papkov, S. Li, Y. Dzenis, H. D. Espinosa, *Carbon* **2013**, *60*, 246 –253.
96.T. J. Fee, D. R. Dean, A. W. Eberhardt, J. L. Berry, *J. Biomech. Eng*. **2012**, *134*, 104503.
97.C. R. Carlisle, C. Coulais, M. Namboothiry, D. L. Carroll, R. R. Hantgan, M. Guthold, *Biomaterials* **2009**, *30*, 1205–1213.

98.S. Baker , J. Sigley , C. C. Helms , J. Stitzel , J. Berry, K. Bonin, M. Guthold, *Mater. Sci. Eng., C*. **2012**, *32*, 215–221.
99.C. R. Carlisle, C. Coulais, M. Guthold, *Acta. Biomater*. **2010**, *6*, 2997–3003.
100.A. Gestos, P. G. Whitten, G. M. Spinks, G. G. Wallace, *Polym. Test*. **2013**, *32*, 655-664.
101.E. P. S. Tan, C. T. Lim, *Appl. Phys. Lett*. **2004**, *84*, 1603-1605.
102.L. Yang, K. O. van der Werf, B. F. J. M. Koopman, V. Subramaniam, M. L. Bennink, P. J. Dijkstra, J. Feijen, *J. Biomed. Mater. Res. A.* **2007**, *82*, 160–168.
103.L. Yang, C. F. C. Fitie´, K. O. van der Werf, M. L. Bennink, P. J. Dijkstra, J. Feijen, *Biomaterials* **2008**, *29*, 955–962.
104. O. A. Bauchau, J. I. Craig, In Structural Analysis: With Applications to Aerospace Structures; Springer, **2009**; Part II, pp 173-221.
105.S-H. Lee, C. Tekmen, W. M. Sigmund, *Mater. Sci. Eng. A-Struct*. **2005**, *398*, 77-81
106.M. K. Shin, S. I. Kim, S. J. Kim, S-K. Kim, H. Lee, G. M. Spinks, *Appl. Phys. Lett.* **2006**, *89*, 231929.
107.L. M. Bellan, J. Kameoka, H. G. Craighead, *Nanotechnology* **2005**, *16*, 1095–1099.
108.L. Li, L. M. Bellan, H. G. Craighead, M. W. Frey, *Polymer* **2006**, *47*, 6208-6217.
109.Y. Ding, P. Zhan, Y. Jiang, F. Xu, J. Yin, Y. Zuo, *Mater. Lett.* **2009**, *63*, 34–36.
110.Q. Fu, Y. Jin, X. Song, J. Gao, X. Han, X. Jiang, Q. Zhao, D. Yu, *Nanotechnology* **2010**, *21*, 95703.
111.H. Ren, Y. Ding, Y. Jiang, F. Xu, Z. Long, P. Zhang, *J. Sol-Gel Sci. Technol*. **2009**, *52*, 287–290.
112.B. Jankovic, J. Pelipenko, M. Skarabot, I. Musevi, J. Kristl, *Int. J. Pharm*. **2013**, *455*, 338–347.
113. K. A. Khalil, S. W. Kim, K. W. Kim, N. Dharmaraj, H. Y. Kim, *Int. J. Appl. Ceram. Technol*. **2011**, *8*, 523–531.
114.W. Wang, A. H.Barber*, J. Polym. Sci., Part B: Polym. Phys*. **2012**, *50*, 546-551.
115.C-C. Liao, C-C. Wang, C-Y. Chen, W-J. Lai, *Polymer* **2011**, *52*, 2263-2275.
116.C-C. Liao, C-C. Wang, K-C. Shih, C-Y. Chen, *Eur. Polym. J.* **2011**, *47*, 911–924.
117.Y. Ji, C. Li, G. Wang, J. Koo, S. Ge, B. Li, J. Jiang, B. Herzberg, T. Klein, S. Chen, J. C. Sokolov, M. H. Rafailovich, *Europhys. Lett*. **2008**, *84*, 56002.
118.N. Wu, L. Chen, Q. Wei, Q. Liu, J. Li*, J. Text. I.* **2012**, *103*, 154–158.
119.C-C. Liao, C-C. Wang, C-Y. Chen, *Polymer* **2011**, *52*, 4303-4318.
120.G. Guhados, W. Wan, J. L. Hutter, *Langmuir* **2005**, *21*, 6642-6646.
121.F. Croisier, A.-S. Duwez , C. Jérôme, A. F. Léonard , K. O. van der Werf , P. J. Dijkstra, M. L. Bennink, *Acta. Biomater*. **2012**, *8*, 218-224.
122.P. A. Yuya, Y. Wen, J. A. Turner, Y. A. Dzenis, Z. Li, *Appl. Phys. Lett.* **2007**, *90*, 111909.
123.Y. Liu, S. Chen, E. Zussman, C. S. Korach, W. Zhao, M. Rafailovich, *Macromolecules* **2011**, *44*, 4439–4444.
124.W. Zhao, R. P. Singh, C. S. Korach, *Compos. Part A-Appl. S.* **2009**, *40*, 675–678.
125.M. Burman, A. Arinstein, E. Zussman, *Appl. Phys. Lett.* **2008**, *93*, 193118.
126.A-Y. Jee, M. Lee, *Polym. Test*. **2010**, *29*, 95-99.
127.F. Ko, Y. Gogotsi, A. Ali, N. Naguib, H. Ye, G. Yang, C. Li, P. Willis, *Adv. Mater*. **2003**, *15*, 1161–1165.
128.J. J. Mack, L. M. Viculis, A. Ali, R. Luoh, G. Yang, H. T. Hahn, F. K. Ko , R. B. Kaner, *Adv. Mater*. **2005**, *17*, 77-80.
129.W. Wang, T. Peijs, A. H. Barber, *Nanotechnology* **2010**, *21*, 035705.
130.Y. Q. Chen, X. J. Zheng, S. X. Mao, W. Li, *J. Appl. Phys*. **2010**, *107*, 094302.
131.Z. H. Liua, C. T. Pana, L. W. Lind, H. W. Lai, Sensor. *Actuat. A-Phys*. **2013**, *193*, 13–24.
132.B. W. Ahn, M. H. Hahn, T. J. Kang, ICCM 18 - 18th International Conference on Composite Materials, **2011**, South Korea
133.M. Wang, H-J. Jin, D. L. Kaplan, G. C. Rutledge, Macromolecules **2004**, *37*, 6856-6864.

134.V. Thomas, M. V. Jose, S. Chowdhury, J. F. Sullivan, D. R. Dean, Y. K. Vohra, *J. Biomater. Sci., Polym. Ed*. **2006**, *17*, 969-984.
135. J. L. Vondran, W. Sun, C. L. Schauer, *J. Appl. Polym. Sci*. **2008**, *109*, 968–975.
136.E. P. S. Tan, C. T. Lim, *Appl. Phys. Lett*. **2005**, *87*, 123106.
137.J. Y. Kim, B. W. Lee, D. T. Read, D. Kwon*, Scripta Mater*. *2005*, *52*, 353-358.
138.S. Ge, Y. Pu, W. Zhang, M. Rafailovich, J. Sokolov, *Phys. Rev. Lett*. **2000**, *85*, 2340-2343.
139.Y. Lin, D. M. Clark, X. Yu , Z. Zhong , K. Liu, D. H. Reneker, *Polymer* **2012**, *53*, 782-790.
140.A. Arinstein, M. Burman, O. Gendelman, E. Zussman, *Nat. Nanotechnol*. **2007**, *2*, 59-62.
141.A. Baji, Y-W. Mai, S-C. Wong, *Polym. Eng. Sci*. **2014**
142.X-F. Wu, Y. A. Dzenis*, J. Appl. Phys*. **2007**, *102*, 044306.
143.R. Dingreville, J. Qu, M. Cherkaoui*, J. Mech. Phys. Solids*. **2005**, *53*, 1827-1854.
144.S. Cuenot, C. Fretigny, S. Demoustier-Champagne, B. Nysten, *Phys. Rev. B*. **2004**, *69*, 165410.
145.X-F. Wu, Y. Y. Kostogorova-Beller, A. V. Goponenko, H. Hou, Y. A. Dzenis, *Phys. Rev. E*. **2008**, *78*, 061804.
146.S. Prilutsky, E. Zussman, Y. Cohen, *Nanotechnology* **2008**, *19*, 165603.
147.A. Camposeo, I. Greenfeld, F. Tantussi, S. Pagliara, M. Moffa, F. Fuso, M. Allegrini, E. Zussman, D. Pisignano, Nano lett. **2013**, *13*, 5056-5062.
148.A. Arinstein, J*. Polym. Sci., Part B: Polym. Phys*. **2013**, *51*, 756-763.
149.K-H. Lee, K-W. Kim, A. Pesapane, H-Y. Kim, J. F. Rabolt, *Macromolecules* **2008**, *41*, 1494-1498.
150.C. Huang, S. Chen, D. H. Reneker, C. Lai, H. Hou, *Adv. Mater*. **2006**, *18*, 668-671.
151.S. C. Moon, R. J. Farris, *Polym. Eng. Sci.* **2008**, *48*, 1848–1854.
152.J. Najem, S-C. Wong, *ANTEC 2009 Plastics: Annual Technical Conference Proceedings,* **2009**, 2747-2756.
153.K. W. Kim, K. H. Lee, M. S. Khil, Y. S. Ho, H. Y. Kim, *Fiber. Polym*. **2004**, *5*, 122-127.
154.S. Moon, R. J. Farris, *Carbon* **2009**, *47*, 2829 –2839.
155.T. Kongkhlang, K. Tashiro, M. Kotaki, S. Chirachanchai, *J. Am. Chem. Soc*. **2008**, *130*, 15460-15466.
156.A. Zucchelli, M. L. Focarete, C. Gualandi, S. Ramakrishna, *Polym. Adv. Technol*. **2011**, *22*, 339-349.
157.R. Neppalli, C. Marega, A. Marigo, M. P. Bajgai, H.Y. Kim, S. S. Ray, V. Causina, *J. Mater. Res.* **2012**, *27*, 1399-1409.
158.L. Cheng, X. Zhou, H. Zhong, X. Deng, Q. Cai, X. Yang , *Mater. Sci. Eng., C.* **2014**, *34*, 262-269.
159.L. Liu, Y. Zhou, S. Pan, *J. Reinf. Plast. Compos*. **2013**, *32*, 823–834.
160.B. D. Schoenmaker, S. v. d. Heijden, S. Moorkens, H. Rahier, G. V. Assche, K. D. Clerck, *Compos. Sci. Technol*. **2013**, *79*, 35-41.
161.R. Neppalli, V. Causin, A. Marigo, M. Meincken, P. Hartmann, A. J. van Reenen, *Polymer* **2013**, *54*, 5909-5919.
162.S. Jiang, A. Greiner, S. Agarwal, *Compos. Sci. Technol*. **2013**, *87*, 164-169.
163.F. Meng, Y. Zhan, R. Zhao, X. Liu, *Eur. Polym. J.* **2012**, *48*, 74-78.
164.S. Jiang, H. Hou, A. Greiner, S. Agarwal, *Acs Appl. Mater. Inter*. **2012**, *4*, 2597-2603.
165.Y. Dong, T. Mosaval, H. J. Haroosh, R. Umer, H. Takagi, K-T. Lau*, J. Polym. Sci.* **2014**, *52*, 618-623.
166.Y. Sun, R. Shankar, H. G. Borner, T. K. Ghosh , R. J. Spontak, *Adv. Mater.* **2007**, *19*, 87-91.
167.U. Stachewicz, A. H. Barber, *Langmuir* **2011**, *27*, 3024-3029.
168.U. Stachewicz, C. A. Stone, C. R. Willis, A. H. Barber, *J. Mater Chem.* **2012**, *22*, 22935-22941
169.S. J. Hardman, N. Muhamad-Sarih, H. J. Riggs, R. L. Thompson, J. Rigby, W. N. A. Bergius, L. R. Hutchings, *Macromolecules* **2011**, *44*, 6461-6470.
170.E. Ozden, Y. Z. Menceloglu, M. Papila, *Acs Appl. Mater. Inter*. **2010**, *2*, 1788-1793.
171.J-S. Kim, D. H. Reneker*, Polym. Compos*. **1999**, *20*, 124-131.
172.M. M. Bergshoef, G. J. Vancso, *Adv. Mater*. **1999**, *11*, 1362-1365.

173.H. Fong, *Polymer* **2004**, *45*, 2427-2432.
174.G. Chen, H. Liu, *J. Appl. Polym. Sci*. **2008**, *110*, 641-646.
175.C. Tang, H. Liu, *Compos. Part A-Appl. S*. **2008**, *39*, 1638-1643.
176.S. O. Han, W. K. Son, J. H. Youk, W. H. Park, *J. Appl. Polym. Sci.* **2008**, *107*, 1954-1959.
177.W. Sun, Q. Cai, P. Li, X. Deng, Y. Wei, M. Xu, X. Yang, *Dent. Mater*. **2010**, *26*, 873-880.
178.R. Neppalli, C. Marega, A. Marigo, M. P. Bajgai, H. Y. Kim, V. Causin, *Eur. Polym. J*. ***2010***, *46*, 968–976.
179.B. Lu, G. Zheng, K. Dai, C. Liu, J. Chen, C. Shen, *Mater. Lett*. **2015**, *140*, 131-134.
180.M. Wu, Y. Wu, Z. Liu, H. Liu, *J. Compos. Mater*. **2012**, *46*, 2731-2738.
181.H. Liao, Y. Wu, M. Wu, X. Zhan, H. Liu, *Cellulose* **2012**, *19*, 111-119.
182.S. Lin, Q. Cai, J. Ji , G. Sui , Y. Yu, X. Yang, Q. Ma, Y. Wei, X. Deng, *Compos. Sci. Technol.* **2008**, *68*, 3322-3329.
183.C. Tang, M. Wu, Y. Wu, H. Liu, *Compos. Part A-Appl. S*. **2011**, *42*, 1100-1109.
184.H. Liao, Y. Wu, M. Wu, H. Liu, *Polym. Compos*. **2011**, *32*, 837-845.
185.Q. Chen, L. Zhang, M-K. Yoon, X-F. Wu, R. H. Arefin, H. Fong, *J. Appl. Polym. Sci.* **2012**, *124*, 444-451.
186.S. Jiang, G. Duan, H. Hou, A. Greiner, S. Agarwal, *Acs Appl. Mater. Inter*. **2012**, *4,* 4366-4372.
187.J. Chen, L. Lu, D. Wu, L. Yuan, M. Zhang, J. Hua, J. Xu , *Acs Sustain. Chem. Eng.* **2014**, *2*, 2102-2110.
188.L-S. Chen, Z-M. Huang, G-H. Dong, C-L. He, L. Liu, Y-Y. Hu, Y. Li, *Polym. Compos.* **2009**, *30*, 239-247.
189.M. Tian, Y. Gao, Y. Liu, Y. Liao, R. Xu , N. E. Hedin, H. Fong , *Polymer* **2007**, *48*, 2720-2728.
190.F. Meng, R. Zhao, Y. Zhan, X. Liu, *J. Mater. Chem*. **2011**, *21*, 16385-16390.
191.G. M. Bayley, M. Hedenqvist, P. E. Mallon, *polymer* **2011**, *52*, 4061-4072.
192.Z. Chang, *Mater. Sci. Forum.* **2011**, *688*, 41-44.
193.S. Jiang, G. Duan, J. Schöbel, S. Agarwal, A. Greiner, *Compos. Sci. Technol.* **2013**, *88*, 57-61.
194.R. Neppalli, C. Marega, A. Marigo, M. P. Bajgai, H. Y. Kim, V. Causin, *Polymer* **2011**, *52*, 4054-4060.
195.J. Zhang, H. Niu, J. Zhou, X. Wang, T. Lin, *Compos. Sci. Technol*. **2011**, *71*, 1060-1067.
196.D. Chen, R. Wang, W. W. Tjiu, T. Liu, *Compos. Sci. Technol*. **2011**, *71*, 1556–1562.
197.F. R. Lamastra , D. Puglia, M. Monti, A. Vella, L. Peponi, J. M. Kenny , F. Nanni, *Chem. Eng. J.* **2012**, *195-196*, 140-148.
198.E. Özden-Yenigün, Y. Z. Menceloğlu, M. Papila, *Acs Appl. Mater. Inter*. **2012**, *4*, 777-784.
199.R. Neppalli, V. Causin, E. M. Benetti, S. S. Ray, A. Esposito, S. Wanjale, M. Birajdar, J-M. Saiter, A. Marigo, *Eur. Polym. J*. **2014**, *50*, 78-86.
200.X-f. Wang, Z-M. Huang, L-s. Chen, *Fiber. Polym*. **2011**, *12*, 359-365.
201.H. J. Oh, H. Y. Kim, S. S. Kim, *J. Adhes*. **2014**, *90*, 787-801.
202.T. Guo, Z. Zhou, H. Guo, G. Xiao, X. Tang, M. Peng, *J. Appl. Polym. Sci*. **2014**, *131*, 41119.
203.M. Swart, R. T. Olsson, M. S. Hedenqvist, P. E. Mallon, *Polym. Eng. Sci*. **2010**, *50*, 2143-2152.
204.Y. Chen , D. Han, W. Ouyang, S. Chen, H. Hou, Y. Zhao, H. Fong, *Compos. Part B-Eng*. **2012**, *43*, 2382–2388.
205.C. Chen, M. Cho, J-D. Nam, Y. Lee, *Compos. Part A-Appl. S*. **2013**, *53*, 10-15.
206.R. Palazzetti, A. Zucchelli, C. Gualandi, M. L. Focarete, L. Donati , G. Minak, S. Ramakrishna, *Compos. Struct*. **2012**, *94*, 571-579.
207.X-F. Wu, A. L. Yarin, *J. Appl. Polym. Sci.* **2013**, *130*, 2225-2237.
208.R. Palazzetti, A. Zucchelli, I. Trendafilova, *Compos. Struct*. **2013**, *106*, 661-671.
209.L. Liu, Y. M. Liang, G. Y. Xu, H. S. Zhang, Z. M. Huang, *J. Reinf. Plast. Compos*. **2008**, *27*, 1147-1162.

210.S. Sihn, R. Y. Kim, W. Huh, K-H. Lee, A. K. Roy, *Compos. Sci. Technol*. **2008**, *68*, 673-683.
211.D. W. Y. Wong, L. Lin, P. T. McGrail, T. Peijs, P. J. Hogg, *Compos. Part A-Appl. S*. **2010**, *41*,759–767.
212.S. N. Yadav, V. Kumar, S. K. Verma*, Mater. Sci. Eng., B*, **2006**, *132*, 108–112.
213.A. Godara, L. Gorbatikh , G. Kalinka , A. Warrier, O. Rochez, L. Mezzo, F. Luizi, A. W. van Vuure, S. V. Lomov, I. Verpoest*, Compos. Sci. Technol*. **2010**, *70*, 1346–1352
214.H. Kishi, M. Kuwata, S. Matsuda, T. Asami, A. Murakami, *Compos. Sci. Technol*. **2004**, *64*, 2517–2523.
215.H. Ghiasi, K. Fayazbakhsh, D. Pasini, L. Lessard, *Compos. Struct*. **2010**, *93*, 1–13.
216.A. B. Pereira, A. B. de Morais, *Compos. Part A-Appl. S*. **2004**, *35*, 265–272.
217.A. B. Pereira, A. B. de Morais, A. T. Marques, P. T. de Castro, *Compos. Sci. Technol*. **2004**, *64*, 1653–1659.
218.S. K. Sharma, B. V. Sankar, *J. Reinf. Plast. Compos*. **1997**, *16*, 425-434.
219.G-C. Tsai, J-W. Chen, *Compos. Struct*. **2005**, *69*, 1–9.
220.L. Chen, P. G. Ifju, B. V. Sankar, *J. Compos. Mater*. **2005**, *39*, 1311-1333.
221.G. Tang, Y. Yan, X. Chen, J. Zhang, B. Xu, Z. Feng, *Mater. Des*. **2001**, *22*, 21-25.
222.W. E. Howard, T. Gossard, R. M. Jones, *AIAA J*. **1986**, *27*, 610-616.
223.O. O. Ochoa, W. S. Chan, *Key Eng. Mater*. **1989**, *37*, 285-303.
224.Y.A. Dzenis, D.H. Reneker, US patent, 6265333, **2001**.
225.Y. Dzenis, *Science* **2008**, *319*, 419-420.
226.K. Molnár, E. Kostáková, L. Mészáros, *Express Polym. Lett*. **2014**, *8*, 62-72.
227.S-F. Hwang, B-C. Shen, *Compos.Sci.Technol.* **1999**, *59*, 1861-1869.
228.Q. Chen, L. Zhang, A. Rahman, Z. Zhou, X-F. Wub, H. Fong, *Compos. Part A-Appl. S.* **2011**, *42*, 2036-2042
229.J. Zhang, T. Lin, X. Wang, *Compos. Sci. Technol.* **2010**, *70*, 1660-1666.
230.Q. Chen, Y. Zhao, Z. Zhou, A. Rahman, X-F. Wu, W. Wu, T. Xu, H. Fong, *Compos. Part B-Eng*. **2013**, *44*, 1-7.
231.G. Li, P. Li , C. Zhang, Y. Yu , H. Liu, S. Zhang, X. Jia, X. Yang , Z. Xue, S. Ryu, , *Compos. Sci. Technol*. **2008**, *68*, 987-994.
232.B. D. Schoenmaker, S. V. der Heijden, I. D. Baere, W. V. Paepegem, K. D. Clerck, *Polym. Test*. **2013**, *32*, 1495-1501
233.L. A. Carlson, R. B. Pipes, In Experimental Characterization of Advanced Composite Materials; Prentice-Hall, Englewood Cliffs: NJ, **1987**.
234.K. Shivakumar, S. Lingaiah, H. Chen, P. Akangah, G. Swaminathan, M. Sharpe, R. Sadler, *AIAA J*. **2009**, *47*, 1723-1729.
235.P. Akangah, S. Lingaiah, K. Shivakumar, *Compos. Struct*. **2010**, *92*, 1432-1439.
236.N. G. Yuna, Y. G. Wona, S. C. Kim, *Polymer* **2004**, *45*, 6953–6958.
237.G. Li, P. Li, Y. Yu, X. Jia, S. Zhang, X. Yang, S. Ryu, *Mater. Lett*. **2008**, *62*, 511-514.
238.P. Li, D. Liu, B. Zhu, B. Li, X. Jia, L. Wang, G. Li, X. Yang, *Compos. Part A-Appl. S.* **2015**, *68*, 72–80.
239.K. Bilge, E. Ozden-Yenigun, E. Simsek, Y. Z. Menceloglu, M. Papila, *Compos. Sci. Technol*. **2012**, *72*, 1639–1645.
240.K. Bilge, S. Venkataraman, Y. Z. Menceloglu, M. Papila, *Compos. Part A-Appl. S.* **2014**, *58*, 73–76.
241.K. Magniez, T. Chaffraix, B. Fox, *Materials* **2011**, *4*, 1967-1984.
242.J. Zhang, T. Yang, T. Lin, C.H. Wang, *Compos. Sci. Technol*. **2012**, *72*, 256-262.
243.K. Magniez, C. De Lavigne, B. L. Fox, *Polymer* **2010**, *51*, 2585-2596.
244.H. Saghafi, T. Brugo, G. Minak, A. Zucchelli, *Compos. Part B-Eng.* **2015**, *72*, 213-216.
245.H. Saghafi, R. Palazzetti, A. Zucchelli, G. Minak, *Eng. Solid Mech*. **2013**, *1*,85-90.
246.H. Saghafi, T. Brugo, G. Minak, A. Zucchelli, *Eng. Solid Mech*. **2015**, *3*, 21-26.

247.S. v. d. Heijden, L. Daelemans, B. D. Schoenmaker, I. D. Baere, H. Rahier, W. V. Paepegem, K. D. Clerck*, Compos. Sci. Technol.* **2014**, *104*, 66-73.
248.A. D. Kelkar, R. Mohan, R. Bolick, S. Shendok, *Mater. Sci. Eng., B*. **2010**, *168*, 85-89.
249.D. K. Shinde, A.D. Kelkar, *Int. J. Chem. Nucl. Metall. Mater. Eng*. **2014**, *8*, 54-60.
250.S. Hamer, H. Leibovich, A. Green, R. Intrater, R. Avrahami, E. Zussman, A. Siegmann, D. Sherman , *Polym. Compos*. **2011**, *32*, 1781-1789.
251.S. Hamer, H. Leibovich , A. Green, R. Avrahami, E. Zussman, A. Siegmann, D. Sherman, *Compos.Sci. Technol*. **2014**, *90*, 48–56.
252.H. Saghafi, A. Zucchelli, R. Palazzetti, G. Minak, *Compos. Struct*. **2014**, *109*, 41-47.
253.F. Bovicelli, H. Saghafi, T. M. Brugo, J. Belcari, A. Zucchelli, G. Minak, *Procedia Mater. Sci.* **2014**, *3*, 1316 – 1321.
254.E. J. Garcia, B. L. Wardle, A. J. Hart, *Compos. Part A-Appl. S*. **2008**, *39*, 1065–1070.
255.Q. Chen, W. Wu, Y. Zhao, M. Xi, T. Xu, H. Fong, *Compos. Part B-Eng*. **2014**, *58*, 43-53.
256.Q. Chen, L. Zhang, Y. Zhao, X-F. Wu, H. Fong, *Compos. Part B-Eng*. **2012**, *43*, 309-316.
257.R. Palazzetti, X. Yan, A. Zucchelli, *Polym. Compos*. **2014**, *35*, 137-150.
258.S. Alessi, M. D. Filippo, C. Dispenza, M. L. Focarete, C. Gualandi, R. Palazzetti, G. Pitarresi, A. Zucchelli, *Polym. Compos*. **2014.**
259.R Palazzetti, *J. Compos. Mater.* **2014**.
260.L. Liu, Z.-M. Huang, C.L. He, X. J. Han, *Mater. Sci. Eng. A,* **2006**, *435-436*, 309-317.
261.L. Liu, Z-M. Huang, G-Y. Xu, Y-M. Liang, G-H. Dong, *Polym. Compos*. **2008**, *29*, 285-292.
262.J-H. Park, P. V. Braun, *Adv. Mater*. **2010**, *22*, 496–499.
263.S. Sinha-Ray, D. D. Pelot, Z. P. Zhou, A. Rahman, X.-F. Wu, A. L. Yarin, *J. Mater. Chem.* **2012**, *22*, 9138-9146.
264.X-F. Wu, A. Rahman, Z. Zhou, D. D. Pelot, S. Sinha-Ray, B. Chen, S. Payne, A. L. Yarin*, J. Appl. Polym.* Sci. **2013**, *129*, 1383–1393.